An Introduction to Interfacial Engineering

March 29, 2009

An Introduction to Interfacial Engineering

G.J.M. Koper

Department of Chemical Engineering
Faculty of Applied Sciences
Delft University of Technology

VSSD

© VSSD
First edition 2007
corrected 2009

Published by VSSD
Leeghwaterstraat 42, 2628 CA Delft, The Netherlands
tel. +31 15 27 82124, telefax +31 15 27 87585, e-mail: hlf@vssd.nl
internet: http://www.vssd.nl/hlf
URL about this book: http://www.vssd.nl/hlf/d007.htm

All rights reserved. No part of this publication may be reproduced, stored in a retrieval system, or transmitted, in any form or by any means, electronic, mechanical, photocopying, recording, or otherwise, without the prior written permission of the publisher.

ISBN-13 978-90-71301-95-7

NUR 952

Key words: chemical thermodynamics

Preface

In 2004 the first course on Interfacial Engineering was given a the chemical engineering department DelftChemTech of Delft University of Technology. Before that time, there was some coverage with colloidal systems in courses on physical chemistry and a voluntary course on "disperse systems". The idea was to give a course that would deal with colloidal phenomena while giving a good perspective on technological applications. Hence the name Interfacial Engineering. The teaching goal of the course was set at a decent level: after studying the course, the students should be able to critically assess the relevant scientific literature.

This first course was developed simultaneously with prof. dr. Theo van de Ven (McGill University, Montreal), who was a visiting professor of the department at the time. A significant amount of course material was generated from which the students could study, but a textbook covering all topics of the course was not available. Over time, the idea developed to write one myself. The result of half a year writing text while teaching the course is what you are reading now. The book is still under construction. Many ideas have been put into this book and the coverage is not fully balanced yet. Also, the text will not be without flaws. Therefore, any suggestion or correction will be welcomed so that in a following print more accuracy will be attained.

The contents of the book can be roughly divided into two parts. The first part contains the basic knowledge required to deal with colloidal systems albeit that some technological issues are discussed. These are the chapters 1 - 5. With these chapters, there is a bundle of worked exercises, taken from the author's own experience and from other textbooks, that will be available upon request. The chapters 6 - 8 deal with technologies such as emulsification, film formation and flotation. In these last chapters some new fundamental issues are discussed where necessary but the emphasis is on the application.

In a half-semester course – of weekly 2 consecutive lecture hours – one chapter is discussed per week, sometimes together with some exercises. The last three chapters are discussed in conjunction with scientific papers from the contemporary literature. This teaches the students how to use their knowledge with published material and how to extract key information for a given process. Particular attention is paid on how to read a scientific paper, how to extract information from it, and how to evaluate its significance. A method has been developed to do this systematically. Subsequently, some calculations are made with the material presented in the paper where it does occur that another conclusion is drawn than in the paper. The exam for the students consists of the assessment

of a – small – scientific paper and some relevant calculations.

Most of the information in this book is not mine. It is the accumulated knowledge of the field and I acknowledge all contributors: there are too many to name and I feel indebted to them all. My role has been to make a selection of topics and to organize and discuss these in such a way as to teach chemical engineers the essentials about colloid science and its technological applications.

Finally, I thank all who have helped me writing this book and Delft University of Technology for their support. Last but not least I thank my wife and children for their patience: they had to suffer my absence during long evenings of working to finish this work.

Ger Koper,
Leiden, 5 March 2007.

Contents

Chapter 1

Introduction

1.1 Nature of the colloidal state

The challenge of Interfacial Engineering is the wide range of length scales that it deals with, see figure 1.1. On the one hand there are the molecules of which their typical length scale is in the Ångstroms. On the other hand there is the size of the mixing vessel or reactor of which the length scale is meters or more. In almost all practical situations, there is at least one particular length scale — the colloidal length scale — that is associated with the degree of dispersion in the system. This colloidal length scale is in the range of 10^{-9} – 10^{-3} m and encompasses the range that is currently exploited by the "nanoscientists".

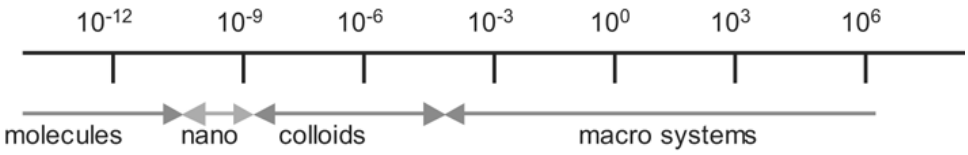

Figure 1.1 Length scales operative in Interfacial Engineering.

The term *colloid* stems from the greek word $\kappa o \lambda \lambda \alpha$ that means glue and refers to classical colloids as protein or gelatin solutions. Using a membrane, colloids can be distinguished from molecules in the classical experiment depicted in figure 1.2.

A *colloidal system* or *colloid* is an essentially multiphase — usually two-phase — system, such as paint or milk, in which one of the phases is dispersed in the other. In such systems the *colloidal particles* have at least one dimension in the colloidal range. A special class is formed by solutions of high polymers which are in fact molecular solutions but where the globules are nevertheless in the colloidal range. The two constituting phases can either be solid, liquid or gas and hence many types of colloids are possible, see table 1.1. In this table there is one entry, g $\subset$ G, that has question marks; consider this as a question to ponder ...

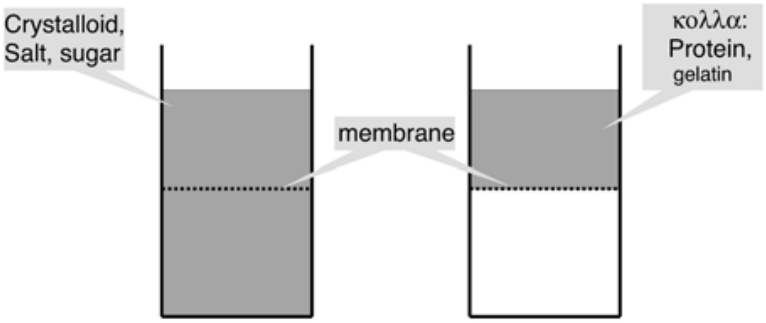

Figure 1.2 Classical experiment to distinguish colloids from molecular solutions.

Type (intern ⊂ extern)	Name	Examples
s ⊂ G	aerosol	smoke
l ⊂ G	aerosol	mist, hair spray
g ⊂ G	?	?
s ⊂ L	sol	ink, paint
l ⊂ L	emulsion	milk, mayonnaise
g ⊂ L	foam	shaving foam
s ⊂ S	solid dispersion	pearls, ruby glass
l ⊂ S	solid emulsion	ice cream, butter, bitumen
g ⊂ S	solid foam	marshmallows, PUR foam

Table 1.1 Possible combinations of phases to form colloids

The dispersions may form either spontaneously, such as protein solutions, after mixing or require significant energy input, such as the case with emulsions. In the first case, the dispersion is called *reversible* or *lyophilic*[1]. The other case is called irreversible or *lyophobic*[2].

An important aspect of colloidal systems is the specific surface. As an example, first consider the simple situation of a dispersion of spherical particles with uniform radius $a = 3$ nm. The *volume fraction* or *fill factor* is $\phi = 0.1$. The specific surface area is now given by

$$A_{sp} = \frac{3\phi}{a} \tag{1.1}$$

which in this particular case evaluates as

$$A_{sp} = \frac{3 \times 0.1}{3 \cdot 10^{-9}} \text{ m}^2/\text{ m}^3 = 10^8 \text{ m}^2/\text{ m}^3$$

[1]The term *lyophilic* means solvent-loving, which in the case of water becomes *hydrophilic*
[2]The term *lyophobic* means solvent-hating, which in the case of water becomes *hydrophobic*

In other words, a volume of only 1 mL of this dispersion has a surface area of 100 m^2, which is of the same order of magnitude as the surface area of a lecture room.

> The proof of the above expression is as follows. Let the number of particles in a volume V be N, then the total volume occupied by the particles is $V_d = 4\pi N a^3/3$ and the total surface area is $A_d = 4\pi N a^2$. Using that $\phi = V_d/V$ the specific area is obtained as
>
> $$A_{sp} = \frac{A_d}{V} = \frac{A_d}{V_d} \times \frac{V_d}{V} = \frac{3}{a} \times \phi$$
>
> which is the expression given in eq. 1.1.

Care has to be taken in the usage of the term specific area. The one usage, discussed above, is the specific area per unit volume of dispersion. Another usage is the specific area per unit mass of *dispersed material*.

1.2 Microscopic colloidal behavior

The experienced interfacial engineer has some simple tools at hand to distinguish a molecular solution from a dispersion. The phenomena described below are both fundamental in nature but very practical in their application.

1.2.1 Osmotic pressure

The classical experiment to measure molar masses of polymers is of very good use to colloid scientists as it can provide in a relatively simple way information about the mass as well as the size of the dispersed particles. The set-up requires a semi-permeable mem-

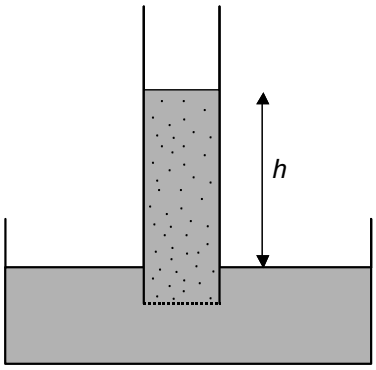

Figure 1.3 Osmotic pressure experiment.

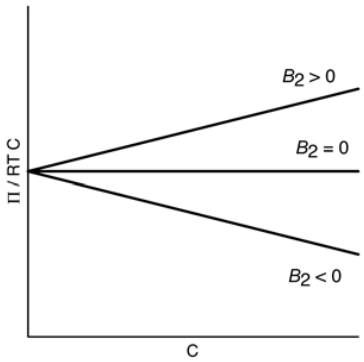

Figure 1.4 Analysis of osmotic pressure experiment, various second virial coefficient conditions.

brane that does not allow the dispersed particles to go from the vertical tube to the reservoir below, see figure 1.3. The height h is directly related to the osmotic pressure Π, due to the dispersion, by

$$\Pi = \rho g h$$

with ρ the mass density of the solvent and g the gravitational constant. Van 't Hoff's law relates this osmotic pressure to the mass concentration C of dispersed material by

$$\frac{\Pi}{RT} = \frac{C}{M}(1 + B_2 C + \ldots) \tag{1.2}$$

where the second virial coefficient B_2 has been added. The molar mass M of the dispersion is related to the particle mass M_p by

$$M = N_A M_p$$

with $N_A = 6.0 \cdot 10^{23}$ Avogadro's number. The second virial coefficient is related to the effective interaction volume of the dispersion. For hard spheres, the second virial coefficient is equal to

$$B_2 = 4\frac{V_p}{M_p}$$

with V_p the particle volume. But the second virial coefficient can also vanish which is equivalent to the situation at the Boyle temperature in gases: the repulsive and attractive interactions balance. For polymers such situation is called the *theta solvent conditions* and similarly in colloidal dispersions the situation is largely dependent on solvent conditions. In a good solvent, the virial coefficient is not negative. When the second virial coefficient is negative, attractive interactions dominate, sometimes leading to thermodynamically stable flocculation, see figure 1.4.

1.2.2 Brownian motion and diffusion

When a particle is forced to move through a liquid, the velocity v it acquires is proportional to the applied force F. This is essentially Stokes' law and it reads

$$v = \frac{F}{f} \tag{1.3}$$

The proportionality factor f is called the *friction factor* which for a sphere[3] is given by

$$f = 6\pi\eta a \tag{1.4}$$

with a the radius of the particle. The friction that the particle experiences in the liquid arises from the hydrodynamic momentum transfer which in itself is mediated by collisions of liquid molecules with the moving particle surface.

But there is an additional effect of these collisions. Even at rest, there is a fluctuating momentum transfer from the liquid molecules to the particle and as a consequence the particle exhibits irregular motion, the so called *thermal motion* or *Brownian motion*. The time average of the momentum transfer vanishes, but there is a noticeable effect on the position of the particle. In a given time lapse Δt the uncertainty in the center-of-mass position of the particle has increased by an amount

$$\Delta r = \sqrt{6D\Delta t} \tag{1.5}$$

The proportionality constant D in the above equation is the diffusion coefficient of the particles, which is related to its friction factor by the *Einstein relation*

$$D = \frac{k_B T}{f} \tag{1.6}$$

in which $k_B = 1.38 \cdot 10^{-23}$ J/K is the Boltzmann constant or molecular gas constant and T is the absolute temperature of the liquid. It is important to note that Brownian motion is a chance process and hence there is no way to predict the actual distance covered by a particle. The only statement one may make is that after a time lapse Δt there is a high probability to find the body within a sphere of radius $\sqrt{6D\Delta t}$. Colloquially one says: the particle has "diffused" over a distance $\sqrt{6D\Delta t}$.

It is easy to see that the Brownian motion of a tennisball will not be too impressive, but for a 3 nm sphere the diffusion coefficient is about $72 \cdot 10^{-12}$ m^2/s so that after a second "it diffuses" a distance of approximately 20 micrometer which is about 700 times its size!

Now, consider a liquid colloidal dispersion in a transparent vessel as in figure 1.5 where the dispersed phase has a higher mass density than the liquid. After some time, a density gradient will set in so that the dispersed phase is denser at the bottom of the vessel than at the top. In the extreme case all the dispersed mass is at the bottom, which is called *sedimentation*. The situation where the dispersed phase has a lower mass density is called

[3] Even though many (colloidal) objects are not spheres, one still uses expressions for spheres to obtain the correct order of magnitude in the absence of a more accurate value.

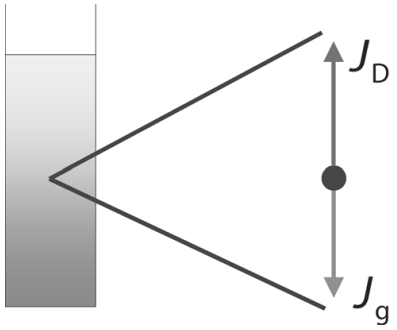

Figure 1.5 Sedimentation in a colloidal dispersion.

creaming because the density gradient is opposite. The density profile $c(z)$ has the same functional form as the barometric height distribution

$$c(z) = c(z_0)\exp\left\{-\frac{gV_p\Delta\rho}{k_BT}(z-z_0)\right\} \tag{1.7}$$

in which g is the gravitational constant, $\Delta\rho$ is the mass density difference between dispersed phase and continuous phase, and V_p particle volume.

> It is customary to derive the above expression using the Boltzmann distribution known from statistical thermodynamics. As an illustration that equilibrium phenomena are actually due to balancing fluxes, let us consider the particle flux due to gravity alone. The mass of one particle is $m_p = \Delta\rho V_p$ and hence the gravitational force on the particle is $F_z = m_p g = gV_p\Delta\rho$. The velocity that the particle will acquire due to this force is given by $v_z = F_z/f$ with f its friction factor. The total flux of particles moving with gravity is given by $J_z = cv_z$, where it is assumed that the particles do not hinder each other.
>
> Due to the movement of particles with gravity, a particle concentration gradient will develop. According to Fick's law, this will give rise to an opposite flux given by $J_D = -D\nabla c$.
>
> In stationary state — equilibrium — the two fluxes balance which leads to the differential equation
>
> $$\frac{dc}{c} = -\frac{gV_p\Delta\rho}{k_BT}dz$$
>
> of which the solution is given in equation 1.7.

For some systems, the particle density gradient is easily visible whereas for others spectroscopic techniques are required.

1.2.3 Tyndall effect and light scattering

Wherever there are optical density variations, there are refractive phenomena. In the case of colloidal systems the density fluctuations take place at length scales which are

comparable to the wavelength of visible light. Therefore, colloidal systems scatter visible light very much like a ray of sun in a dark room is visible through the light scattering dust particles in its pathway. A demonstration of this phenomenon is depicted in figure 1.6 where a "laser pointer" is used to send a beam of light through two vessels, one containing a colloidal dispersion and the other a pure solvent. A typical way to assess the light

Figure 1.6 Demonstration of the Tyndall effect. On the left side a colloidal dispersion and on the right side the pure solvent.

scattered by a colloidal solution is by means of a standard visible light spectrometer. Such an instrument measures the light loss along an optical path of length d through a calibrated cuvette containing the dispersion. According to Lambert-Beer's law the light loss leads to a transmission factor

$$T = \exp\{-(\kappa+\tau)d\} \tag{1.8}$$

with κ the absorption and τ the *turbidity*. Here, the case of light absorption is discarded because most – but not all – colloidal dispersions are "dielectric". It is noteworthy, however, that light scattering manifests itself as absorption in a spectrometer but also to the human eye. A good example is ruby glass which appears red to the observer even though there is no light absorption. One observes a color due to the fact that light of the other wavelengths is scattered in all directions and hence very little reaches the eye. In particular, this means that colloidal systems may show a different color upon reflection and on transmission, a phenomenon used in the famous Lycurgus cup[4].

For not too dense systems, the turbidity of colloidal dispersions is proportional to the concentration, i.e.

$$\tau = cS \tag{1.9}$$

[4]A picture movie and a description is available from the British Museum in London, see http://www.thebritishmuseum.ac.uk/science/lycurguscup/sr-lycugus-p1.html .

The proportionality constant is called the *scattering cross section S* which, for not too large and dense particles, is proportional to an optical contrast factor and volume squared

$$S \propto \left[\frac{n^2-1}{n^2+2}\right] V_p^2 \tag{1.10}$$

with n the relative refractive index. For larger particles the scattering cross section is a complex function of wavelength, scattering angle, refractive index and particle size which is fully described by the Mie theory[5]. An extremely useful consequence of the above equations is, that the turbidity of a colloidal suspension of given volume fraction is directly proportional to the product of volume fraction and particle volume and hence to particle size cubed, i.e. $S \propto \phi V_p = \phi a^3$.

1.3 Applications

1.3.1 Environmental sciences

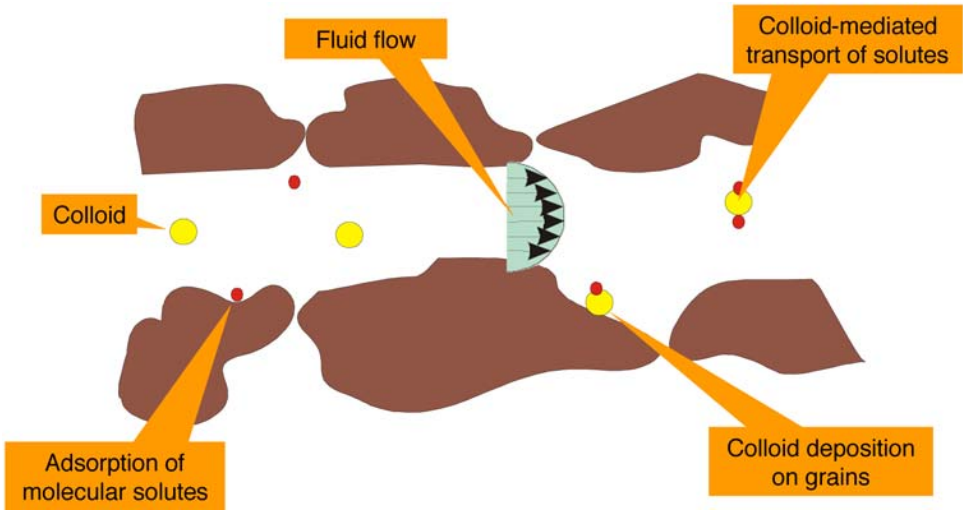

Figure 1.7 Colloidal phenomena in the environmental sciences.

Due to the strong attachment of chemicals such as heavy metals, radionuclides, pharmaceuticals to the solid phase of porous media it was for a long time assumed that the transport of these chemicals by the water phase would be extremely slow. Recent field- and laboratory-scale observations have shown that mobile colloidal particles such as microbes, humic substances, clays, and metal oxides, can act as pollutant carriers and thus

[5] see Bohren, C. F. and Huffman, D. R. *Absorption and Scattering of Light by Small Particles*. New York: Wiley, 1983. There are various web sites giving computational aid to evaluate the scattering cross section.

provide a much more rapid transport pathway for strongly sorbing contaminants, see figure 1.7. These observations have led to an enormous upsurge of colloid science in this field.

1.3.2 Liposomes as colloidal cargo carriers

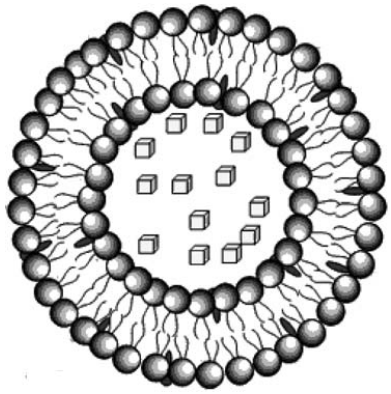

Figure 1.8 Liposomes as colloidal cargo carriers.

Whereas emulsions consist of one liquid phase dispersed into the other, such as oil in water, dispersions of liposomes allow for an aqueous phase to be dispersed in another aqueous phase. As such, liposomes are used as containers to transport drugs, vitamins or special proteins through the human body, see figure 1.8. In the colloid literature the word liposome is rarely found, the particular structure formed by surfactant molecules is called *vesicle* in that domain.

There are many fields in which liposomes are used or proposed for use, such as cosmetics, medicine and in the field of genetic engineering. In all cases, the main issue is to prevent the cargo from entering into the continuous phase where it might degrade for instance by oxidation. In other cases, direct exposure to for instance the blood circuit might activate anti-immune reactions before the target is reached. Novel systems have special receptors that allow targeted release of the cargo.

1.3.3 Sol-gel technology

The sol-gel process is a versatile solution process for making ceramic and glass materials. In general, the sol-gel process involves the transition of a system from a liquid sol into a solid gel phase. Applying the sol-gel process, it is possible to fabricate ceramic or glass materials in a wide variety of forms: ultra-fine or spherical shaped powders, thin film coatings, ceramic fibers, microporous inorganic membranes, monolithic ceramics and glasses, or extremely porous aerogel materials. An overview of the sol-gel process is

presented in a simple graphic work[6] depicted in figure 1.9.

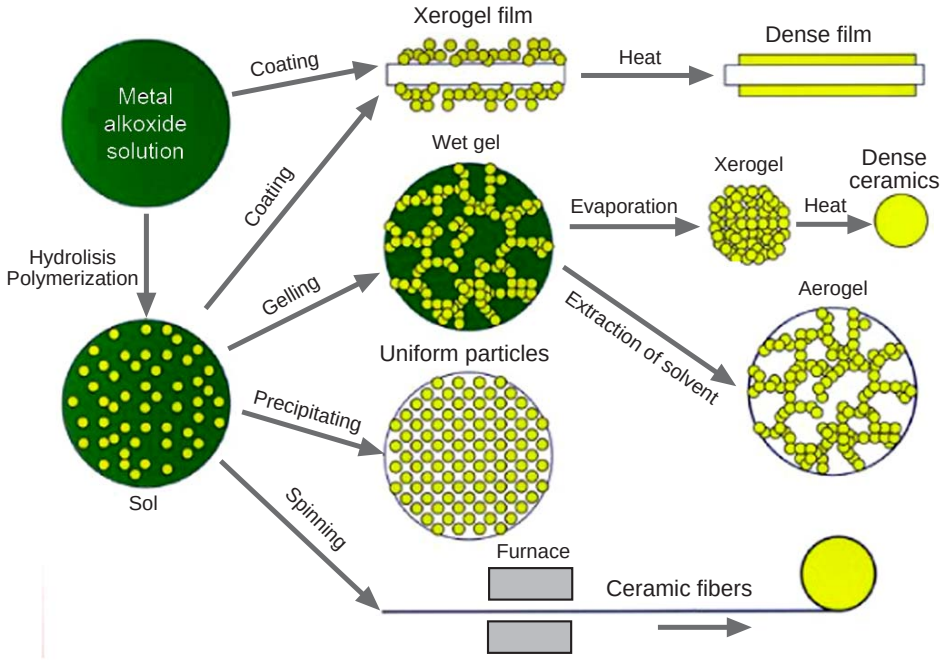

Figure 1.9 Various routes in sol-gel technology.

The starting materials used in the preparation of the sol are usually inorganic metal salts or metal organic compounds such as metal alkoxides. In a typical sol-gel process, the precursor is subjected to a series of hydrolysis and polymerization reactions to form a colloidal suspension, or a sol. Further processing of the sol enables one to make ceramic materials in different forms. Thin films can be produced on a piece of substrate by spin-coating or dip-coating. When the sol is cast into a mold, a wet gel will form. With further drying and heat-treatment, the gel is converted into dense ceramic or glass articles. If the liquid in a wet gel is removed under a supercritical condition, a highly porous and extremely low density material called "aerogel" is obtained. As the viscosity of a sol is adjusted into a proper viscosity range, ceramic fibers can be drawn from the sol. Ultra-fine and uniform ceramic powders are formed by precipitation, spray pyrolysis, or emulsion techniques.

1.3.4 Food technology

Traditionally, colloid science has evolved mainly from two technological areas: food processing and detergency. Many colloid experts, up till recently, could be found in industrial

[6] Adapted from http://www.chemat.com/

research laboratories. The applications in food processing are so numerous, that it is currently evolving as a popular branch of science[7].

[7] See the website http://khymos.org/ and for the dutch http://www.kokenchemie.nl

Chapter 2

Capillary phenomena

2.1 Thermodynamic stability

Dispersions are – more often than not – thermodynamically unstable, in other words the general tendency for a dispersion is to separate into the phases that it was originally composed of. This process is initiated by aggregation of the entities that form the dispersed phase. On these larger clusters or flocs of dispersed phase the dispersive effect of Brownian motion is much less than on the original entities and sedimentation or creaming initiates the process of phase separation.

The Gibbs energy G of a dispersion depends on temperature T, pressure p, mole numbers n_j of the various components, and surface area A. It reads

$$dG = -SdT + Vdp + \sum_j \mu_j n_j + \gamma dA \tag{2.1}$$

with V the volume of the dispersion, μ_j the chemical potential of component j, and γ the surface tension. The Gibbs energy mainly depends on two groups of contributions because pressure and temperature are usually kept constant. The term with the chemical potential accounts for solubility effects and in particular for the contributions of surface active components. The other term accounts for the larger Gibbs energy due to the larger surface area inside a dispersion. The fact that the total entropy of the system increases upon dispersion has no major effect here.

2.2 Surface free energy

From numerous experiments it is known, that the force F needed to pull a needle from a liquid surface – corrected for attaching liquid volume – is proportional to the length L of the needle, see figure 2.1, where the proportionality factor is a constant for a given liquid

$$F = 2\gamma L \tag{2.2}$$

The proportionality factor, apart from a factor 2, is called the *surface tension* γ of the liquid-air interface and its dimension is N/m.

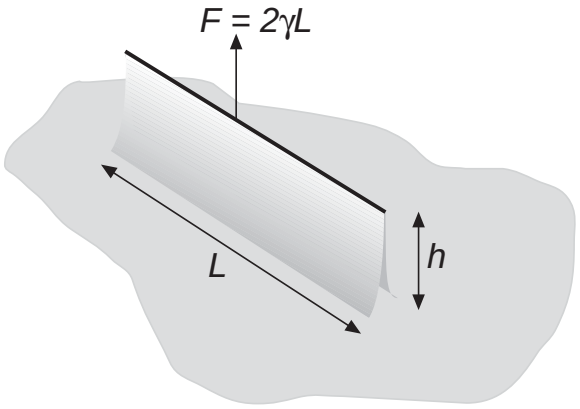

Figure 2.1 Pulling a needle from a liquid surface.

By pulling the needle a distance dh from the liquid, the surface area A of the liquid increases by an amount of $dA = 2Ldh$, the factor 2 arises because on either side of the needle a surface area Ldh is created. The work needed to bring this surface increase about is given by

$$dW = Fdh = \gamma dA \tag{2.3}$$

From this latter expression one deduces the dimension of the surface tension to be J/m^2 which is indeed equivalent to N/m.

As an example, consider a needle of 5 cm at the air-water interface. The surface tension of water is equal to 73 mJ/m^2 and so the force that is required to pull the needle from the surface is equal to 7.3 mN.

The origin of surface tension lies in the frustration of the molecules that are located in the surface. Consider figure 2.2 where the situation of a molecule at the surface (right panel) is compared to that of a molecule in the bulk (left panel). The molecule in the bulk is typically surrounded by z neighboring molecules where z is the coordination number. The total (negative) interaction energy of this molecule is given by

$$u_{bulk} = \frac{z}{2} w_{AA} \tag{2.4}$$

where w_{AA} is the interaction energy, due to van der Waals interactions , between a pair of molecules. At the surface, there is at least one unsatisfied bond so that the surface coordination number z_s is less than the bulk coordination number z. The interaction energy of a molecule at the surface is hence given by

$$u_{surf} = \frac{z_s}{2} w_{AA} \tag{2.5}$$

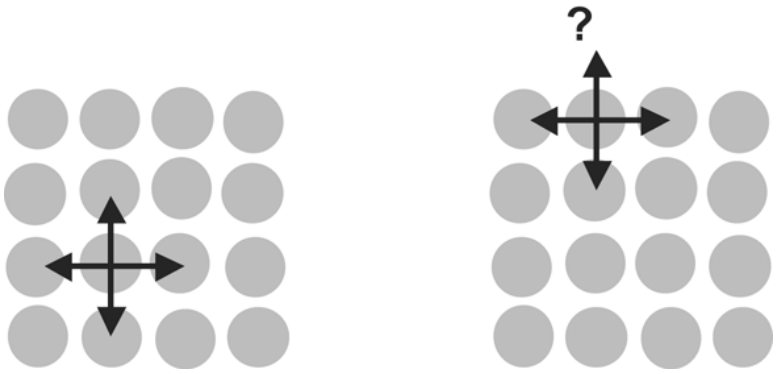

Figure 2.2 Left: molecule in the bulk, right: molecule at the surface.

The surface excess energy is now readily calculated to be

$$\gamma = \frac{u_{excess}}{\sigma} = \frac{z_s - z}{2\sigma} w_{AA} \tag{2.6}$$

where σ is the area that a single surface molecule occupies.

As an example, consider carbontetrachloride for which the vaporization enthalpy is given by $\Delta_{vap}H^{\ominus} = 29.7$ kJ/mol. From this vaporization enthalpy the typical energy between neighboring molecules is estimated to be

$$w_{AA} = -\frac{\Delta_{vap}H^{\ominus}}{N_A z/2} = -\frac{29.7 \text{ kJ/mol}}{6.0 \cdot 10^{23} \times 6/2 \text{ mol}^{-1}} = -1.6 \cdot 10^{-20} \text{ J} \tag{2.7}$$

where it is assumed that the typical coordination number is 6 for carbontetrachloride. This appears to be a relatively small number, but it still amounts to about -4 k_BT. The typical surface area per surface molecule is estimated from the typical distance between the molecules, which is for a fluid of molecular mass 154 g/mol and density 1.6 kg/dm^3 approximated by

$$d = \sqrt[3]{\frac{M}{\rho N_A}} = \sqrt[3]{\frac{154 \cdot 10^{-3}}{1.6 \cdot 10^3 \times 6.0 \cdot 10^{23}}} = 0.54 \text{ nm} \tag{2.8}$$

so that σ = 0.3 nm^2. Assuming that the surface coordination number of carbontetrachloride is one less than the bulk coordination number we arrive at an estimate for the surface tension of

$$\gamma = \frac{z_s - z}{2\sigma} w_{AA} = \frac{5-6}{2 \times 0.3 \cdot 10^{-18}} \times (-1.644 \cdot 10^{-20}) \text{ J/m}^2 = 27.4 \text{ mJ/m}^2 \tag{2.9}$$

which is to be compared to the tabulated value of 26.4 mJ/m^2. The above example demonstrates two facts

- The vaporization enthalpy, which indeed essentially consists of breaking all the bonds that molecules have in the liquid phase, provides for a good estimate of the interaction energy between molecules and hence for the surface tension.

- The picture of the "frustrated molecule" is essentially correct.

The experiment described above is in essence the principle according to which many methods for surface tension measurement work. Examples are the Wilhelmy plate method that uses a platinum plate and the Du Noüy ring method.

2.3 The Five Laws of Interfacial Engineering

The energy cost involved in the increase in surface area manifests itself in five specific ways. Each of these ways can be manipulated specifically and offers the possibility to control the process at hand.

2.3.1 Hamaker's law

The work per unit area that is needed to separate two identical surfaces by a distance h, the cohesion energy as depicted in figure 2.3, is given by

$$\frac{W}{A} = -\frac{A_H}{12\pi h^2} \tag{2.10}$$

with A_H the so called Hamaker coefficient. At closest separation h_{min}, which is of molecu-

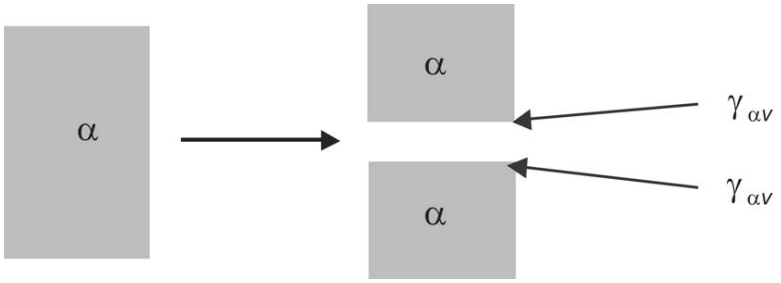

Figure 2.3 Work of cohesion.

lar size, this work is just twice the surface tension between the material and air (vacuum). Equating both results leads to a relatively easy way to estimate the Hamaker coefficient which can be summarized as

$$\frac{W}{A} = -\frac{2\gamma h_{min}^2}{h^2} \tag{2.11}$$

The above equation gives the (macroscopic) *van der Waals interaction* between two flat surfaces. For many geometries the van der Waals interaction has been calculated, for instance for two identical spheres of radius a and separation h it is given by[1]

$$W = -\frac{A_H a}{12h} \tag{2.12}$$

[1] See J. Israelachvili, *Intermolecular and Surface Forces*, Academic Press 1992, Chapter 11.

2.3.2 Young's law

When a droplet of liquid is put on a solid surface there are three interfaces, one between solid and liquid, one between solid and air (vapor), and one between liquid and air. Each of these interfaces will try to minimize its surface area. At the contact line, this leads to opposing forces as depicted in figure 2.4. The projection of the forces in the plane of the

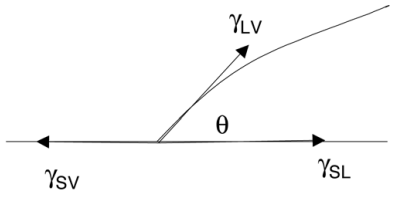

Figure 2.4 Contact angle of a drop on a surface.

solid surface gives rise to the force balance which is known as *Young's law*[2]

$$\gamma_{SV} = \gamma_{SL} + \gamma_{LV} \cos\theta \tag{2.13}$$

with θ the *contact angle*.

For a vanishing contact angle, the liquid spreads over the surface to completely wet it. In contrast, when the contact angle is 180^o the droplet lies on the surface without any flattened part except for the deformation due to gravity. For intermediate contact angles

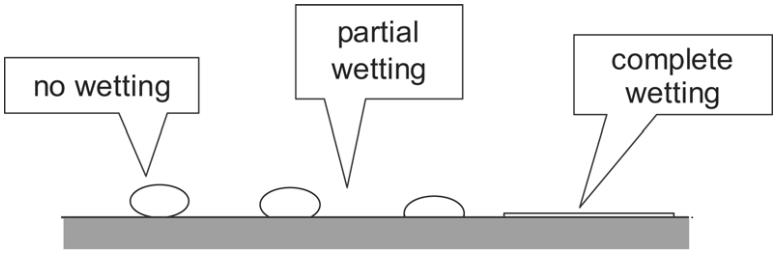

Figure 2.5 Various wetting situations.

one passes from completely wetting, through partial wetting to non-wetting as the contact angle changes from 0^o to 180^o. Measurement of the contact angle is often used to compare surface tensions of solid surfaces.

[2]For a solid or liquid drop on a liquid surface similar albeit more involved equations can be formulated.

2.3.3 Laplace's law

In many situations one encounters the case of droplets of one phase dispersed in another continuous phase, see figure 2.6. The consequence of the general tendency of the interfacial surface to become as small as possible has two consequences here. The one is that the droplet tries to acquire the minimal surface that is possible with the given volume of material, which results in the spherical form for liquid droplets in a fluid continuum. The other is, that a pressure difference $\Delta p = p_{in} - p_{out}$ between inside and outside develops that is commonly known as the *Laplace pressure*.

$$\Delta p = \frac{2\gamma}{a} \tag{2.14}$$

in which γ is the surface tension and a the radius of the droplet. A more elaborate form of

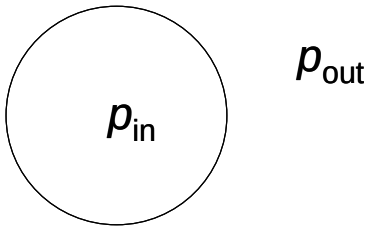

Figure 2.6 Droplet of one phase in another continuous phase.

Laplace's equation can be constructed using the local curvatures of a surface. A discussion of this more involved situation is deferred to a subsequent section. The Laplace pressure is significant for colloidal systems, for 1 μm droplets of water in air it amounts to 1.5 Bar.

> The proof of the statement that the sphere is the shape that has the minimal surface for a given volume is an interesting topic in mathematics. A simpler proof can be constructed using spherical harmonics as perturbations around the spherical form.
>
> In order to prove Laplace's law, we consider a sphere, as depicted in figure 2.6, with radius a. The surface area of a sphere is given by $A = 4\pi a^2$. A small change da in the radius of the sphere brings about a change in the surface area of $dA = 8\pi a da$ and the work that is involved in this change is given by $dW = \gamma dA = 8\pi\gamma a da$. The force, due to the surface tension, that opposes this change is therefore given by $F = -dW/da = 8\pi\gamma a$. In addition, there is the difference in pressure between the inside of the droplet and the exterior of the droplet that makes up the force balance
>
> $$(p_{in} - p_{out})4\pi a^2 - 8\pi\gamma a = 0$$
>
> from which one immediately derives equation 2.14.

Capillary rise

One frequently encountered example of Laplace' law is in connection with capillary rise, see figure 2.7 for a schematic sketch of the archetypal situation of a capillary of diameter

$2a$ in which liquid has risen to a height h above the liquid surface in contact with ambient pressure. In actual fact, there are two phenomena that are acting simultaneously. The one

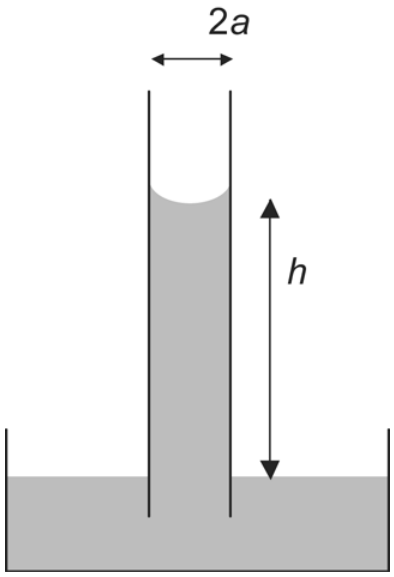

Figure 2.7 Capillary rise.

is the curvature of the liquid surface enforced by the contact angle of the liquid in contact with the solid surface and the ambient gas (vapor) phase. This curvature forces the liquid interface to be larger and this induces a force that tries to flatten the interface. Instead, this is the second phenomenon, the liquid level rises until the forces balance on either side of the curved surface. Hence, the Laplace pressure is balanced by the pressure due to the column of liquid. This leads to the capillary rise formula

$$h = \frac{2\gamma\cos\theta}{\rho g a} \tag{2.15}$$

In many cases, such as water in glass tubes, the contact angle vanishes and in many other cases this is assumed to happen in the absence of sufficient knowledge of the situation. Important to realize is, that the shape of the capillary is immaterial, it is only the diameter of the opening where the meniscus is formed that counts in the calculation.

As an example, consider the vessels in trees that at the top, the pores in the leaves, have a diameter of about 100 nm. These vessels can transport water until the height of the tree exceeds 146 m, which is indeed the height achieved by sequoias. The situation is of course much more involved than the simple picture of water in vessels where the contact angle is almost zero.

Washburn equation

When the capillary in figure 2.7 is just put in the liquid, the liquid level will start to move: the difference between the Laplace pressure and the hydrostatic pressure is then driving the upward flow of the liquid. For the situation where the hydrostatic pressure is not present or can be neglected, the Washburn equation describes the time evolution of the height h of the liquid in the capillary

$$\frac{dh^2}{dt} = \frac{\gamma}{2\eta} a \cos\theta \tag{2.16}$$

in which η is the viscosity of the liquid.

For small capillaries this flow will be laminar and the Poiseuille equation may be used, which relates the volumetric flow to the pressure gradient as

$$\frac{dV}{dt} = \frac{\pi a^4}{8\eta} \frac{\Delta p}{h}$$

with a the radius of the capillary and h the length of the liquid column over which the pressure difference Δp acts. Substituting $V = \pi a^2 h$ as the volume transferred at time t and the Laplace equation for the pressure across the capillary (neglecting hydrostatic pressure!) yields

$$\frac{dh}{dt} = \frac{\gamma}{4\eta} \frac{a}{h} \cos\theta$$

from which equation 2.16 follows after substituting $dh^2 = 2hdh$.

In porosimetry both the capillary rise equation and the Washburn equation are invoked to translate pressure versus transferred volume relations into a pore size distribution.

2.3.4 Kelvin's law

The formation Gibbs energy of a liquid droplet of radius a in a (supersaturated) vapor at pressure p is given by

$$\Delta G = -\frac{4\pi a^3/3}{V_L} RT \ln\left(\frac{p}{p^o}\right) + 4\pi a^2 \gamma \tag{2.17}$$

in which V_L is the molar volume of the liquid and p^o is the equilibrium vapor pressure at the given temperature. The pressure ratio is often termed the *degree of supersaturation*. It contains two terms, the first of which is associated with the pressure work (evaluated for a perfect gas) and the second with the work to create the interface. A graphical representation of this formation Gibbs energy is given in figure 2.8. For very small droplet sizes, the surface work dominates which leads to an initial increase of the formation Gibbs energy. For larger sizes the volume work dominates and leads to spontaneous droplet growth. The

maximum that is thus achieved is an *unstable equilibrium* situation which is described by the Kelvin equation

$$RT \ln\left(\frac{p}{p^o}\right) = \frac{2\gamma V_L}{a} \tag{2.18}$$

where the radius a is the *critical droplet size*.

The above treatment holds equally well for the situation of the development of solid phase formation in supersaturated solutions.

Nucleation

In a supersaturated vapor or solution the density fluctuations sometimes overcome the critical droplet size predicted by the Kelvin equation which leads then to the formation of a nucleus that is viable to grow further. In this picture, the formation Gibbs energy describes the energy barrier that embrionic nuclei have to overcome in order to grow. Similar to the situation for chemical reactions, one invokes the Arrhenius equation to relate the formation rate of nuclei to this energy barrier by

$$r \propto p^2 \exp\left(-\frac{\Delta G}{RT}\right)$$

where the proportionality constant is of the order of 10^7. In figure 2.9 the formation rate of water drops at 0 ^{o}C is plotted as a function of supersaturation. The prediction of the presented model using the formation Gibbs energy and the Arrhenius equation

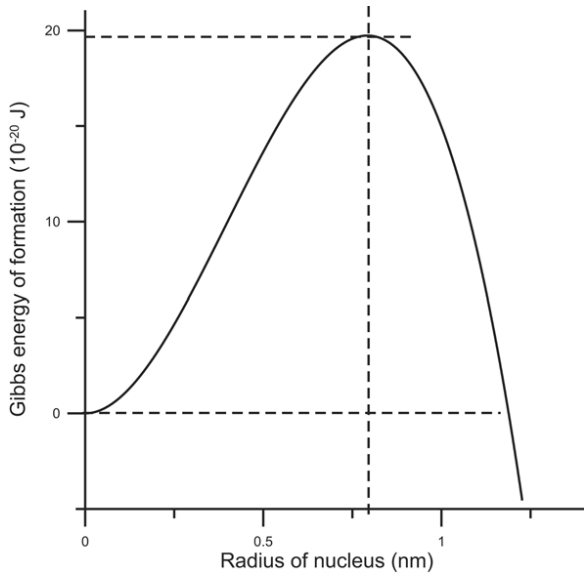

Figure 2.8 Formation Gibbs energy for a water drop in its vapor at 373 K and a supersaturation of 3.

accounts for the general observation that homogeneous nucleation sets in rather abruptly with pressure variation.

When in a supersaturated vapor or solution there are particles of another material, the wetting behavior of these particles largely determines nucleation behavior which becomes heterogeneous. When the particles are fully wetting and larger than the critical radius, there is no energy barrier for nucleation left. The partial wetting situation is well described by the equation

$$\Delta G_{max,hetero} = \Delta G_{max,homo} \frac{(2+\cos\theta)(1-\cos\theta)^2}{4} \tag{2.19}$$

where θ is the contact angle of the liquid with the particle material.

Droplet growth is described by the Rayleigh equation

$$a\frac{d^2a}{dt^2} + \frac{3}{2}\left(\frac{da}{dt}\right)^2 = \frac{1}{\rho_L}\left(p_{in} - p^o - \frac{2\gamma}{a} - \frac{4\eta}{a}\frac{da}{dt}\right) \tag{2.20}$$

with p_{in} the pressure inside the bubble and ρ_L the mass density of the liquid. Care should be taken in using this equation in the case of solutions, as it assumes that the concentration outside the droplet remains constant whereas usually depletion sets in close to the growing droplets.

The mechanisms described above allow for the formation of droplets of all kinds of sizes. This is in practice limited by a phenomenon called *Ostwald ripening* which states that the larger droplets will grow at the expense of the smaller droplets.

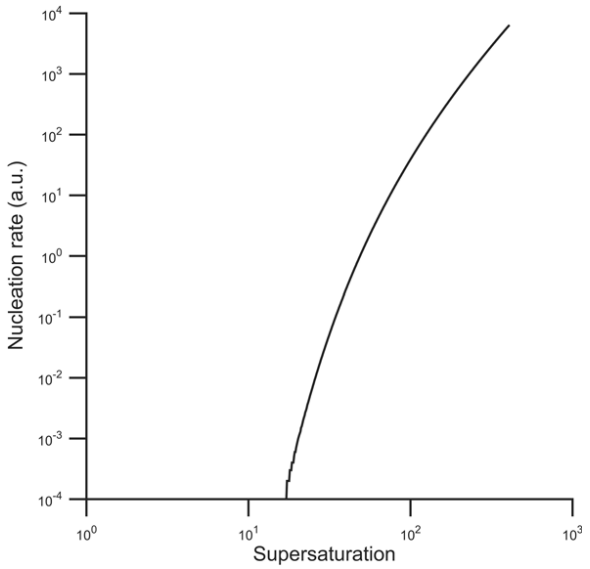

Figure 2.9 Formation rate of water drops at 0 °C as a function of supersaturation.

The mechanism of Ostwald ripening is easily understood if one considers two droplets of different size, the smaller having a larger Laplace pressure than the other one. If a connection would be brought about between the droplets, a mass flux would establish that depletes the smaller droplet completely. If only vapor or solution exists between the two droplets, the rate of Ostwald ripening is controlled by the diffusion of material between the droplets. The diffusion will go faster at higher concentrations (or pressures).

2.3.5 Gibbs' law

A closer look at the interface between two fluid phases reveals that at the molecular scale the interface is not abrupt but rather extends over a certain distance. In figure 2.10 this is illustrated with x the height coordinate. At heights $x << x_0$ there is phase α and for $x >> x_0$ there is phase β. Along the ordinate is plotted an arbitrary observable property P

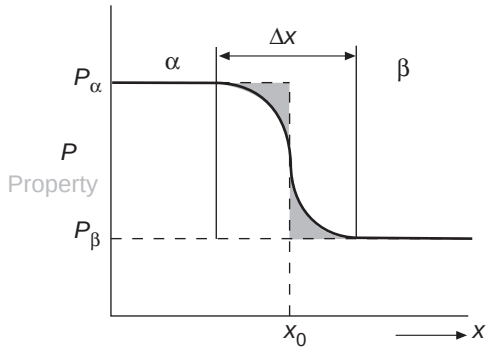

Figure 2.10 Illustration of the dividing surface and surface excess.

of the system such as the density. In phase α this property has the uniform value P_α and in phase β the uniform value is P_β. Around x_0, within a region of width Δx this property smoothly changes from the one value into the other.

For ease of calculations, one introduces a *dividing surface* that in figure 2.10 is arbitrarily put at the height $x = x_0$. It is subsequently assumed that the phase α extends all the way up till this dividing surface where it abruptly changes over into the phase β. The hatched areas in figure 2.10 mark the regions where the actual value for the property P deviates from the one that follows from the application of the dividing surface. The integral of this difference is the *surface excess* P^σ of the property across this interface

$$P^\sigma \equiv P - p_\alpha V_\alpha - p_\beta V_\beta \tag{2.21}$$

in which $p_i = P_i/V_i$. The value of the surface excess will depend on the choice of the location of the dividing surface. However, measurable quantities that are calculated using the concept of surface excess are independent of the location of the dividing surface. In addition, there is often a rational for the choice of a particular dividing surface, such as the

so called *equimolar surface* which is located in such a way that the molar concentration of one component, usually the solvent, vanishes.

It was Gibbs who for the first time declared the surface as an independent thermodynamic system, albeit with an extensivity less than that of the surrounding bulk phases. Just like for the bulk phases there is a thermodynamic relation for the Gibbs energy of this surface

$$dG^{\sigma} = -S^{\sigma}dT + \gamma dA + \sum_j \mu_j dn_j^{\sigma} \tag{2.22}$$

The intensive quantities, such as temperature and chemical potential, are considered to be uniform throughout the interface assuming of course equilibrium. From the above equation, Gibbs derived his famous adsorption equation that reads

$$\Gamma = -\frac{1}{RT}\frac{d\gamma}{d\ln(c/\tilde{c^{\ominus}})} \tag{2.23}$$

for a single component mixed with a solvent where the dividing surface is chosen to be the equimolar surface for the solvent. In this equation, $\Gamma = n^{\sigma}/A$ is the surface excess of the solute.

To derive the above Gibbs' adsorption equation, consider equation 2.22 for two components, a solvent and a solute. The dividing surface is chosen to be equimolar such that the surface excess of the solvent vanishes. The temperature is assumed to be constant, $dT = 0$. Under these conditions the equation 2.22 reduces to

$$dG^{\sigma} = \gamma dA + \mu dn^{\sigma}$$

Using Euler's equation for extensivity (not bulk but surface this time) yields

$$G^{\sigma} = \gamma A + \mu n^{\sigma}$$

and subsequent differentiation yields

$$dG^{\sigma} = \gamma dA + A d\gamma + \mu dn^{\sigma} + n^{\sigma} d\mu$$

Combined with the previous equation this yields the Gibbs Duhem equation for the surface

$$A d\gamma + n^{\sigma} d\mu = 0$$

One finds equation 2.23 using the definition of the surface adsorption $\Gamma = n^{\sigma}/A$ and

$$\mu = \tilde{\mu^{\ominus}} + RT\ln\left(\frac{c}{\tilde{c^{\ominus}}}\right)$$

with the standard chemical potential $\tilde{\mu^{\ominus}}$ given for the reference concentration $\tilde{c^{\ominus}}$.

In many cases, the specific area of a molecule at the interface is the more useful quantity. This specific area is defined as

$$\sigma = \frac{1}{\Gamma N_A} \tag{2.24}$$

where the division by Avogadro's number yields the result in area per molecule rather than per mole.

A special class of molecules are surfactants, who have the tendency to preferentially reside at the interface between a polar and a non-polar medium. This is due to their special structure of a lyophilic and a lyophobic part. In the following chapter it will be discussed how such molecules affect the surface tension of interfaces and how this can be analyzed using Gibbs' equation, see figure 3.3.

Chapter 3

Amphiphilic systems

A special class of molecules are amphiphilic molecules, which have the tendency to preferentially reside at the interface between a polar and a non-polar fluid. This is due to their special structure of a hydrophilic and a hydrophobic part. It is also called a surfactant because of its tendency to modify surface properties. In the following it will be assumed that the two fluids are either water and air or water and oil. Of course, the treatment will also hold for other fluids such as water and liquid carbon dioxide. The archetypal amphiphilic molecule is depicted in figure 3.1 in which one distinguishes the *hydrophobic* tail and the *hydrophilic* head group. Two commonly used examples of surfactant molecules are

Figure 3.1 Typical structure of an amphiphilic molecule.

depicted in figure 3.2. For both molecules it is the sulfonate head group that forms the hydrophilic part.

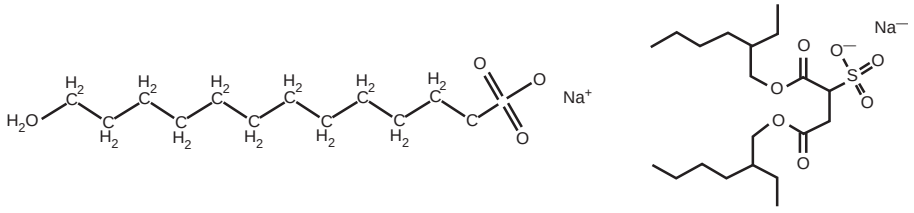

Figure 3.2 Two commonly used surfactant molecules: sodium dodecyl sulfonate (SDS, left) and sodium 1,4 bis (2-ethylhexyl) sulfosuccinate (AOT, right).

3.1 Classification of amphiphilic molecules

The classification of amphiphilic molecules according to head groups is as

- ionic, and subsequently subdivided into
  - anionic, such as the SDS molecule $(C_{12}H_{25}\text{-}O\text{-}SO^3)^-Na^+$ as shown in figure 3.2,
  - cationic, such as the cetyltrimethylammonium bromide $C_{16}H_{33}\text{-}N^+(CH3)_3Br^-$, or CTAB,
  - zwitterionic, such as dipalmitoyl phosphatidyl choline, or DPPC,
- nonionic, such as $C_{12}H_{25}\text{-}(O\text{-}CH_2\text{-}CH_2)_5OH$ pentaoxylethylene dodecyl ether which is commonly abbreviated by the pseudo formula C_mE_n with in this case $m = 12$ and $n = 5$.

The classification according to tail is

- single chain, such as SDS in figure 3.2,
- double chain, such as AOT in figure 3.2,
- or multichain, such as the triglycerides.

In addition to the relatively low molecular mass examples given above, there are many other molecules that demonstrate amphiphilic character. Amongst them are block copolymers and proteins.

3.2 Surface activity

Due to the adsorbtion[1] of amphiphiles at a fluid interface, various properties of the fluid as a whole are – sometimes drastically – modified. The most important influence is on the surface tension of fluid interface as illustrated in figure 3.3 in which the surface tension of aqueous SDS solutions is plotted versus concentration. The graph exhibits two linear regimes marked by A and B. In the first regime it is possible to establish a linear relationship, the slope of which one may use to calculate the adsorption as will be discussed later. Beyond this regime, there is a more or less abrupt change into another – again linear – regime indicated by B. In the latter regime, micelles are formed while the surface tension remains more or less constant. The crossover is hence called the *critical micelle concentration*. Micelles are aggregates of surfactants, that can come in many kinds as illustrated in figure 3.4. The driving force for aggregation is the need to create more interface. At the cmc the water-air interface is more or less saturated with surfactant molecules and the formation of micelles provides an alternative method to create more interface.

The graph in figure 3.3 is for an aqueous SDS solution and because the solution is relatively impure, the crossover between the two linear regimes is less abrupt than it would

[1] Note that the word absorption and adsorption only differ one letter but have completely different meanings.

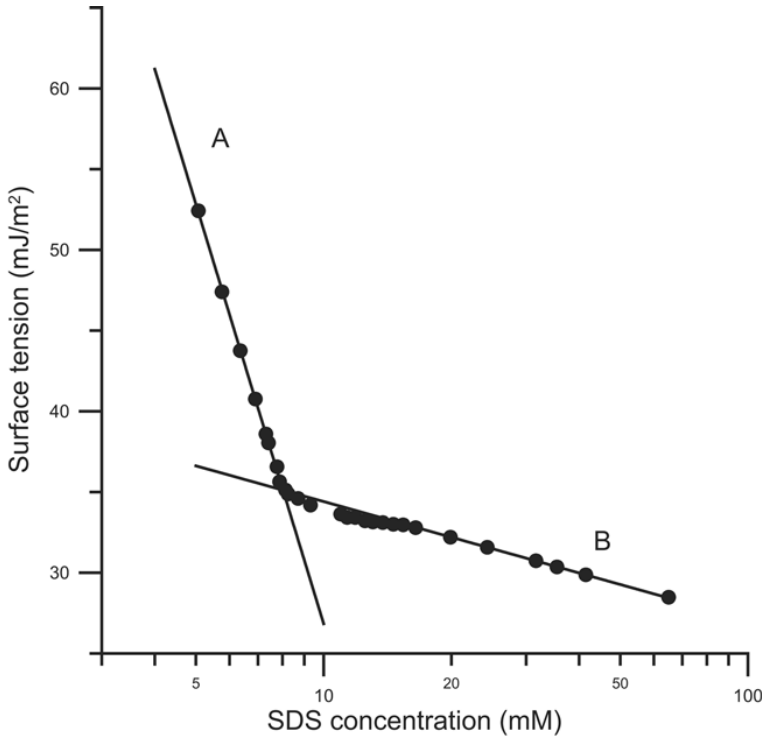

Figure 3.3 Surface tension of SDS versus concentration; see the text for further explanation.

be for a purer solution. Also, SDS is an ionic surfactant that fully dissociates in aqueous media. Hence, not only the surfactant molecules but also the counter ions will be located close to the interface. The Gibbs adsorption equation, equation 2.23, is easily adapted to this case and since there are as many counter ions as there are surfactant molecules this results in a simple factor of 2, so

$$\Gamma_{SDS} = -\frac{1}{2RT}\frac{d\gamma}{d\ln(c/c^{\ominus})} \tag{3.1}$$

This leads to a molecular surface area of 60 Å^2 as can be derived from the figure. However, when the same experiment would be performed in water with a sodium salt at an overwhelming concentration there would not be a surface excess for the counter ions in which case there is no factor 2.

3.3 Micellization

The shape of the micelles that are formed in surfactant solutions over the cmc are of special interest because, just like biological objects, they form spontaneously and they

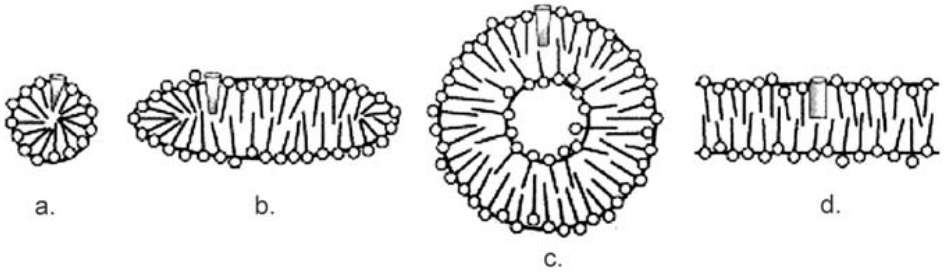

Figure 3.4 Various micellar aggregates: a. spherical micelle, b. wormlike micelle, c. vesicle, d. bilayers.

are commonly termed *self-organized structures*. Figure 3.4 presents an ordered sequence of possible micelle structures. The ordering is based on the "shape" of the surfactant molecule in the aggregate. The shape that a surfactant molecule takes in a particular environment depends strongly on the two solvents that form the interface. The ion type in the water phase and the ionic strength of the water determine largely the surface area that the molecule takes in the interface. As shown in the previous section, this surface area can be determined from interfacial tension measurements. The aliphatic tail makes up largely for the "length" of the surfactant where the degree of stretching depends on the solvent that it is immersed in. A rather "bad" solvent forces the chain to collapse more than a "good" solvent where the chain is more in the stretched configurations.

The spherical micelle is formed when the shape of the surfactant is a cone. More truncated cones form elongated – sometimes thread like – micelles and a cylindrical shape gives rise to relatively flat bilayers as is shown in figure 3.4. The curvature of the interface formed by the surfactant molecules changes from the spheres to bilayers rather significantly. Because of their shape, surfactant molecules assemble preferentially in interfaces with a particular curvature which is therefore called the *spontaneous curvature*.

3.3.1 Geometrical packing considerations

The number of surfactant molecules that go into a micelle is called the *aggregation number*[2] denoted by N_o. Because the surfactant molecules both make up for the surface of the micelle and for the volume, we can express this packing number in two different ways in the radius a of the micelle

$$N_o = \frac{4\pi a^2}{\sigma} = \frac{4\pi a^3}{3v}$$

where σ is the specific area and v is the molecular volume of the surfactant molecule. From these two equations one can find an expression for the radius of a micelle in terms

[2]Here and in what follows we shall assume that the size distribution of the micelles is relatively narrow. This, however, need not always to be true in which case N_o denotes the average aggregation number.

of molecular properties only

$$a = \frac{3v}{\sigma} \tag{3.2}$$

and if ℓ is the largest extension of the surfactant molecule one finds that spherical micelles can only be formed if

$$a \leq \ell \Rightarrow \frac{v}{\sigma\ell} \leq \frac{1}{3} \text{ for spherical micelles}$$

Similar arguments can be obtained for other micellar structures, such as

$$\frac{v}{\sigma\ell} \leq \frac{1}{2} \text{ for cylindrical micelles}$$

and

$$\frac{v}{\sigma\ell} \leq 1 \text{ for bilayers}$$

3.3.2 Micelle formation

The critical micelle concentration manifests itself in many physico-chemical properties as summarized in figure 3.5. The effect on surface tension has already been discussed before, but in almost any phenomenon the "transition" is visible. Many effects originate from the

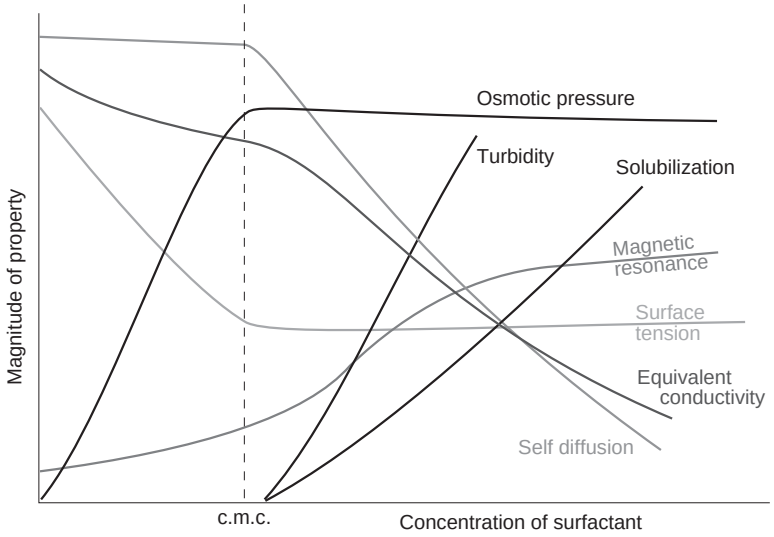

Figure 3.5 Manifestation of cmc in physico-chemical properties.

fact that above the cmc addition of an amount of Δn surfactant molecules only increases the number of free particles in the solution by a number $\Delta n/N_o$ with N_o the aggregation number. For the osmotic pressure for instance this gives a significant decrease in slope beyond the cmc.

Thermodynamics

The formation of micelles can be seen as a chemical equilibrium where N_o molecules of S react into one big entity S_{N_o} according to the equilibrium

$$N_o S \rightleftharpoons S_{N_o}$$

The equilibrium constant that is associated with this reaction is given by

$$K_{N_o} = \frac{[S_{N_o}]}{[S]^{N_o}} = \exp\left(-\frac{N_o \Delta_{mic} G}{RT}\right)$$

in which $\Delta_{mic}G$ is the formation free energy of a micelle per surfactant molecule which can be estimated as

$$\Delta_{mic} G \approx RT \ln\left(\frac{\text{cmc}}{\tilde{c}^{\ominus}}\right) \tag{3.3}$$

The above expression is derived from the definition of the equilibrium constant by taking the logarithm on either side and by dividing subsequently by the aggregation number which leads to

$$\frac{\Delta_{mic} G}{RT} = -RT\left\{\frac{\ln([S_{N_o}]/\tilde{c}^{\ominus})}{N_o} - \ln([S]/\tilde{c}^{\ominus})\right\}$$

When the added concentration of surfactant, i.e. $[S] + N_o[S_{N_o}] >>$ cmc, then the concentration of free surfactant concentration is approximately equal to the cmc, i.e. $[S] \approx$ cmc. At the same time, the concentration of micelles is relatively small compared to the cmc and the logarithm of that concentration divided by the aggregation number becomes negligibly small.

The transition that occurs around the cmc is, from a thermodynamic point of view, very much akin to what happens during phase transitions. For this transition to occur, the Gibbs energy of formation should be of the order of RT and therefore the enthalpy and entropy of formation compensate each other largely, see figure 3.6. From this figure one may observe that the heat of micellization is significant for most surfactants and in most cases the process is exothermic. Only in very few cases the process is endothermic. In addition, it should be kept in mind that there is a large influence of the solvent, for instance in the case of water it is the breaking of the water structure near the hydrophobic tails that brings the largest entropic effect.

Solubility

Micellization will only occur if the cmc is larger than the solubility of the surfactant. Furthermore, the micelles should be stable against flocculation. Flocculation, as shall be discussed in a later chapter, depends on the interaction between the micelles which in itself depends on the solubility of the surfactant in the solvent. For these two reasons, there is a certain temperature window within which micellization can occur.

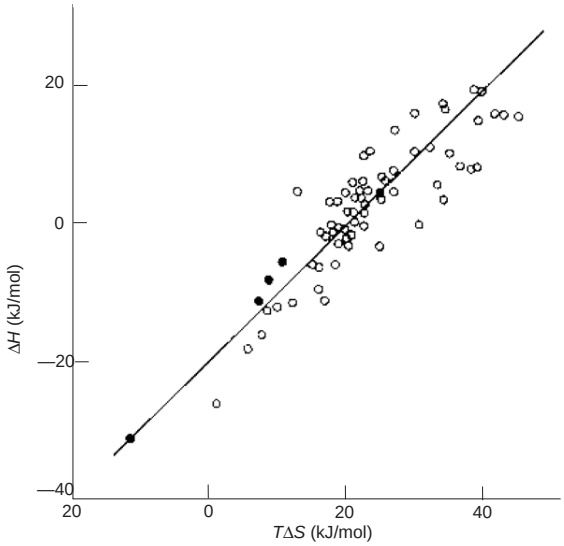

Figure 3.6 Enthalpy versus entropy of micelle formation for various surfactant molecules.

For ionic surfactant, it is usually only the surfactant solubility that significantly interferes with micelle formation, see figure 3.7. On the left side of the solubility curve is the regime where there is an equilibrium between dissolved surfactant molecules and a solid surfactant phase. On the right side there is only dissolved surfactant. The horizontal line is the cmc that varies slightly with temperature. Above this line and to the right of the solubility line is the regime where micelles are formed. The crossing point of the solubility curve and the cmc-line is called the *Krafft point*.

For nonionic surfactant, it is the interactions between the micelles that limit the regime where there is a homogeneous micelle solution, see figure 3.8. On the left side there is a regime between the single L_2-phase[3] and a two phase regime. The onset of this phase transition is the formation of flocs of micelles which gives rise to increased light scattering, hence the name *cloud point*. The larger flocs sediment or cream out of the solution to form a separate phase beyond this cloud point. Interesting to note is that this is a phase transition within a micellar phase, in which the micellar phase in itself has a transition from a homogeneous solution at low concentrations to a dispersed phase beyond the cmc.

Kinetics

One distinguishes two processes that dominate micelle formation. The one process is the exchange of single surfactant molecules according to the reaction scheme

$$S_N + S \rightleftharpoons S_{N+1}$$

[3]The L_2-phase denotes a droplet phase.

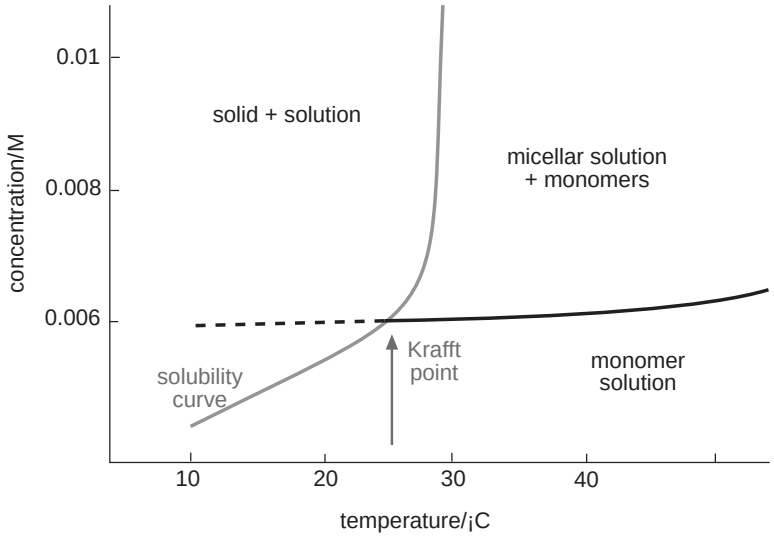

Figure 3.7 Solubility diagram for an ionic surfactant.

for which the typical time scale is microseconds. For SDS in water this *fast relaxation time* is equal to 15 μs. The other process is the association or dissociation of complete micelles according to the reaction scheme

$$N\mathrm{S} \rightleftharpoons \mathrm{S}_N$$

for which the typical time scale is milliseconds. For an SDS solution of 10 - 50 mM this *slow relaxation time* varies from 1.8 - 50 ms.

3.4 Solubilization and emulsions

Consider an aqueous surfactant solution above the cmc that is brought into contact with an oil phase. After some mixing, the aqueous solution will have taken up some or all of the oil, in other words the oil has been solubilized in the water phase. The *solubilization power* of a surfactant solution is a quantity that can be estimated on the basis of the specific area of the surfactant molecule, see for this the following section on microemulsions and the following chapter on emulsification.

One important application of the property of micelles to swell with a compatible internal phase is aquifer remediation, see figure 3.9. A micellar is injected near an oil spill and on a distinct distance, the solution is pumped up again. The idea being that the surfactant solution solubilizes the oil in the water which subsequently carries it away to the withdrawal well. The engineering problem that is to be considered is the transport time of the micelles compared to the residence time of the hydrocarbon molecules in the micelle. The micelles are transient in the sense that the surfactant molecules constantly exchange

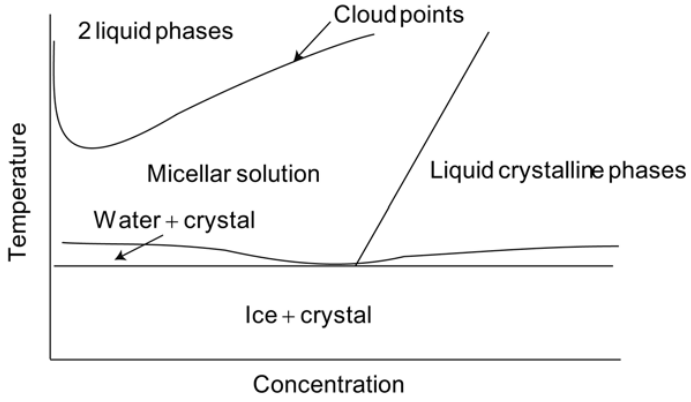

Figure 3.8 Solubility diagram for an nonionic surfactant.

between micelles and as such carry hydrocarbon molecules through the water phase. The residence time of hydrocarbons in a micelle can be estimated on the basis of its solubility in the aqueous phase and the residence time is found to scale inversely with the solubility, see table 3.1.

Probe	residence time (μs)	water solubility M
Anthracene	59	$2.2 \cdot 10^{-7}$
Pyrene	243	$6.0 \cdot 10^{-7}$
Biphenyl	10	$4.1 \cdot 10^{-5}$
Naphtalene	4	$2.2 \cdot 10^{-4}$
Benzene	0.23	$2.3 \cdot 10^{-2}$

Table 3.1 Residence time versus aqueous solubility for a particular surfactant enhanced aquifer remediation (SEAR) application.

The structure of *swollen micelles* is usually not much different from the nonswollen micelles, albeit that at high volume fractions of the dispersed phase the phase behavior of micelles is influenced by the presence of the dispersed phase so that also other structures may appear. The most commonly known structures are depicted in figure 3.10, which shows an oil swollen (normal) micelle in the right panel and a water swollen *reverse* micelle in the left panel. Other structures are depicted in figure 3.11. Swollen micelles are typically in the range of tenths of nanometers to tenths of microns.

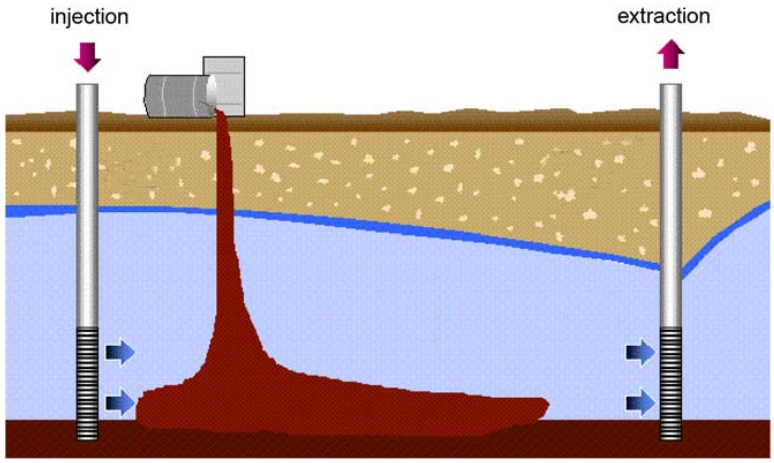

Figure 3.9 Surfactant enhanced aquifer remediation (SEAR).

3.5 Microemulsions

A special class of emulsions is formed by the so called *microemulsions* which in contrast to normal emulsions form spontaneously and are subsequently thermodynamically stable. Normal emulsions are not stable as can be understood from the Gibbs energy of formation of a droplet as depicted in figure 2.8. There is a droplet size where the Gibbs energy has an extremum, but this pertains to an unstable equilibrium and the droplet will either grow or shrink given the possibility.

Microemulsions typically have droplet sizes in the nanometer regime and hence the amount of surfactant needed to make such a system is relatively large. As a result the surface tension of the solution is very low and this is often claimed to be the main reason for the formation of a stable dispersion. But this is not true, as can be inferred from the discussion in the previous paragraph.

The origin of the thermodynamic stability of microemulsions lies in the bending elasticity of the surfactant layer that coats the microemulsion droplets. In order to understand this phenomenon consider figure 3.12 which depicts a curved surface. In any point of a surface there are defined two principal radii of curvature, R_1 and R_2 in figure 3.12, which are also termed principal curvatures[4] denoted by $C_1 = 1/R_1$ and $C_2 = 1/R_2$. To name a few examples: for spheres the two principal curvatures are the same and equal to the inverse radius, $C_1 = C_2 = 1/a$, for lamellae the principal curvatures are also the same but equal to 0. Bicontinuous structures are characterized by nonzero opposite curvatures, $C_1 = -C_2$.

Because of their molecular structure surfactant molecules tend to self assemble into surfaces with a well defined curvature, the spontaneous curvature. Hence, if the formation

[4]These are unambiguously defined of the two eigenvectors of the local curvature matrix, see for instance http://mathworld.wolfram.com/PrincipalRadiusofCurvature.html .

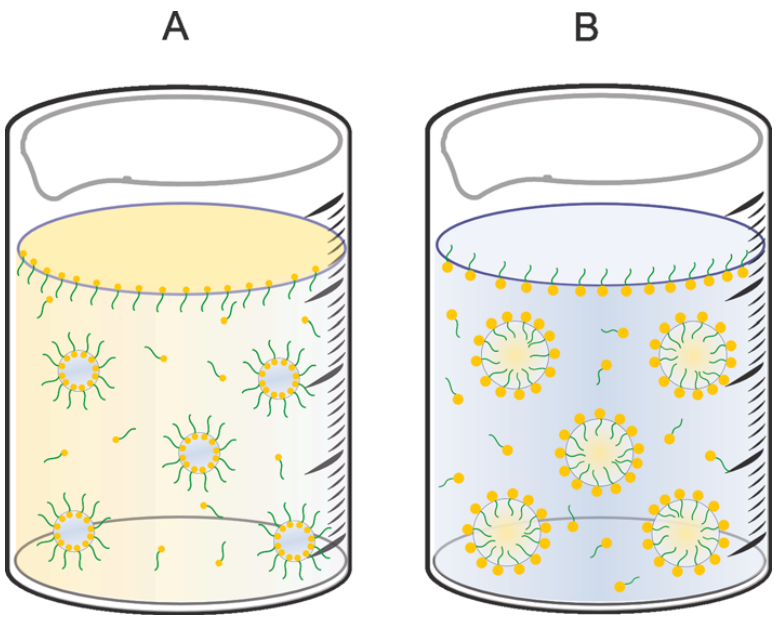

Figure 3.10 Reverse (left) and normal (right) swollen micelle.

Gibbs energy of a surface were plotted versus curvature one would find a minimum at this spontaneous curvature C_0. Because it is a minimum, an elastic force develops when such a surfactant surface is forced to a curvature different from this spontaneous curvature. The *bending elastic energy* associated with such a deformation is given as

$$G_{bending} = -\frac{\kappa}{2}(C - C_0)^2$$

in which κ is the bending elasticity coefficient of the surfactant layer. When the other contributions to the Gibbs energy of formation of a swollen micelle are small compared to the bending elastic contribution one may expect stable microemulsion formation. The

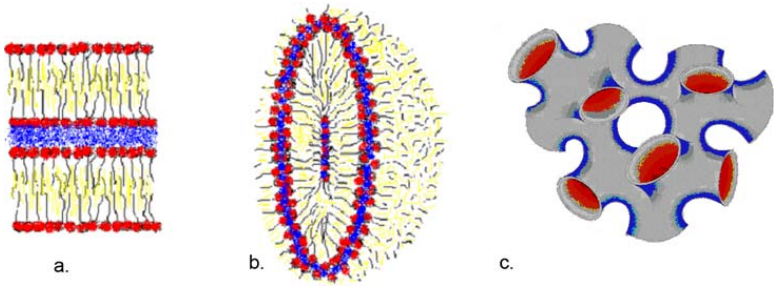

Figure 3.11 Various examples of swollen micelles.

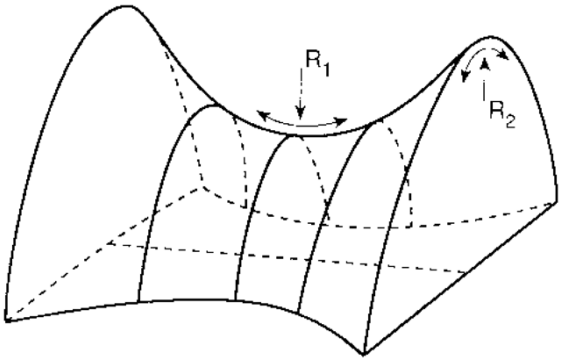

Figure 3.12 Radii of curvature on a curved surface.

total formation Gibbs energy of a microemulsion droplet is given by

$$\Delta G = -\frac{4\pi a^3}{3}\Delta p + 4\pi a^2\gamma + 8\pi\kappa\left(1-\frac{a}{a_s}\right)^2 \tag{3.4}$$

which is quite comparable to eq. (2.17) except for the bending elasticity term. In figure 2.8 the formation Gibbs energy for a droplet in its vapor is presented. Such a curve is reproduced in figure 3.13 together with the formation Gibbs energy for a droplet with a surfactant coating that renders bending elasticity[5].

The bending elasticity parameters C_0 and κ are strongly dependent on solubility so that temperature, ionic strength, and hydrocarbon composition have a significant effect. The phase diagrams of micromulsion systems are therefore very rich and worth a study in itself, see figure 3.14 for an example. This particular example is in the low surfactant regime relatively symmetrical. In point A there are oil droplets in water that, upon increase in surfactant and oil become spherical, point B. Upon systematic exchange of water to oil at constant surfactant content the system changes over to an inverted cylindrical micellar system in B'. Inbetween the system passes throguh irregular bicontinuous structures. Lowering the surfactant and water concentration further leads to spherical water-in-oil droplets, A'.

Nanoparticle synthesis

An often encountered microemulsion phase is the droplet phase, which can either be oil-in-water or water-in-oil. The droplet size in these systems is directly related to the composition of the microemulsion and given by

$$a \approx \frac{3v}{\sigma} w_o \tag{3.5}$$

where W is the molar dispersed phase to surfactant ratio.

[5]Further details can be found in the review by M. Borkovec in Adv Colloid Interf Sci 37 (1992) 195-217.

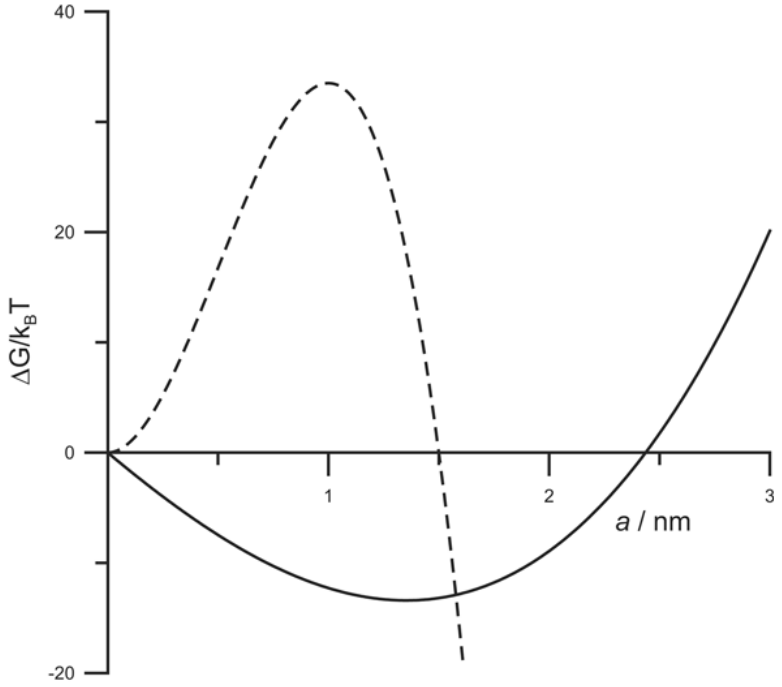

Figure 3.13 Formation Gibbs energy of a droplet without (dashed line) and with (continuous line) curvature free energy.

To derive the above relation, consider as an example a water-in-oil microemulsion. The droplet volume is given by

$$V_d = \frac{4\pi a^3}{3} = N_w v_w$$

with a the droplet radius, N_w the number of water molecules inside one droplet and v_w the molecular volume of water. For the surface area of one droplet one finds

$$A_d = 4\pi a^2 = N_s \sigma$$

with N_s the number of surfactant molecules in the surface and σ the specific area of one surfactant molecule. The radius of the droplet can be expressed in terms of the droplet volume and surface area as

$$a = \frac{3V_d}{A_d} = \frac{3v_w}{\sigma}\frac{N_w}{N_s}$$

The second fraction of number of water molecules over number of surfactant molecules is equal to the molar water to surfactant ratio. In this calculation, the surfactant contribution to the radius of the microemulsion droplet is neglected, therefore the above equation is actually an approximation of which the trend is correct.

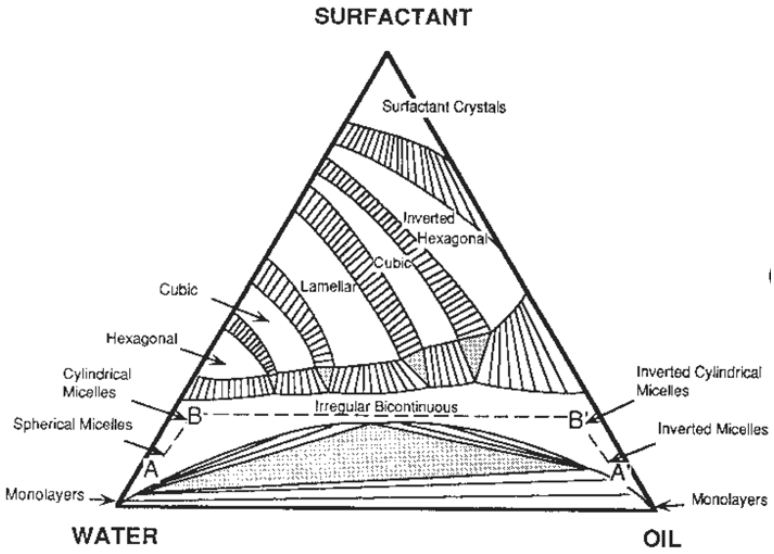

Figure 3.14 Typical microemulsion phase diagram.

This interesting size control that is feasible with microemulsion droplets has led to numerous applications, one of which is the synthesis of nanoparticles. There are a few schemes possible, but the simplest is that one chooses two soluble salts A and B that upon mixing will form an insoluble salt that if just mixed in water would readily precipitate. One prepares two water-in-oil microemulsions, one with salt A and one with salt B. Upon subsequent mixing, the A-ions will slowly but surely mix with the B-ions inside the microemulsion droplets and locally form small salt particles. Another scheme is graphically depicted in figure 3.15. If well controlled, a monodispersed nanoparticle solution emerges that remains well dispersed provided that the particle size does not become too big.

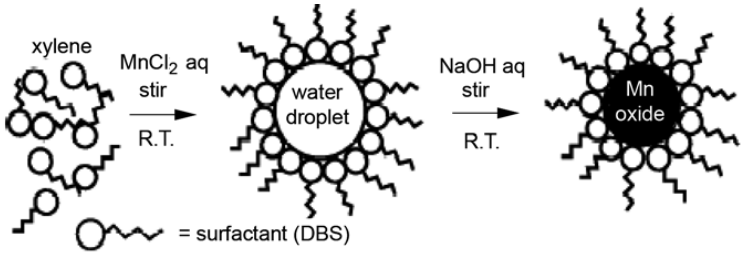

Figure 3.15 Scheme for nanoparticle synthesis in droplet phase microemulsions using anionic sodium dodecylbenzensulfonate (DBS) at room temperature.

Chapter 4

Colloidal interactions and flocculation

A major concern in the field of Interfacial Engineering is colloidal stability. Indeed there is a relatively small class of thermodynamically stable systems, such as the microemulsions discussed in the previous section. But the majority of colloidal systems are *kinetically* stabilized. Referring back to chapter 1 where various classifications were mentioned of colloidal systems, the kinetically stable systems are termed *lyophobic colloids* whereas the thermodynamically stable systems are called *lyophilic colloids*. Obviously, it is the kinetically stabilized systems that will be dealt with in this chapter.

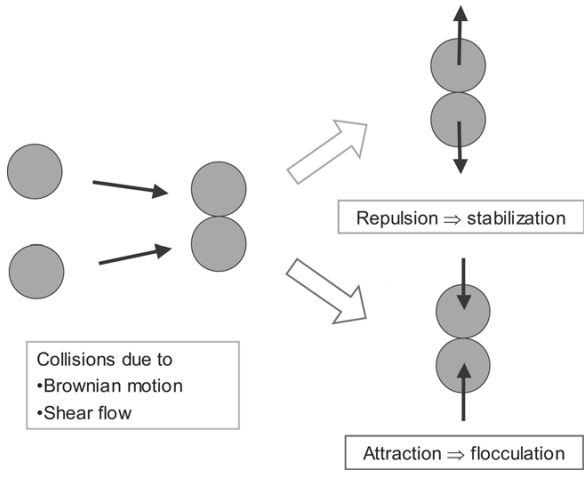

Figure 4.1 Schematic representation of the flocculation process.

In a colloidal system, the particles move because of Brownian motion and external forces, such as shear; see figure 4.1. Once in a while, two particles collide and then it

depends on the interaction between the particles whether they will stick together or will separate again. Due to external forces, particles may also separate also due to Brownian motion albeit that in the latter case this is usually a minor effect.

The process that sticks together particles continues and with time larger and larger *flocs* or *aggregates* are formed. The larger a floc, the slower it diffuses. Also its effective mass density changes which in the end leads to creaming or sedimentation. In the case of liquid-liquid dispersions, the sticking together of drops can also lead to the merging of the droplets, a process commonly termed *coalescence*.

4.1 Flocculation kinetics

As discussed above, the collisions between particles may either arise from Brownian motion, in that case leading to *perikinetic* flocculation[1], or from external forces, leading to *orthokinetic* flocculation.

In the following, it will be assumed that the particles stick once they have collided. This is often the case when only van der Waals forces act between the particles: due to the short length scale over which these forces range the particles behave as *sticky balls*. In section 4.3 the more general colloidal interactions are taken into account.

Let us denote that number concentration of single particles by c_1, the number of doublets by c_2, the number of triplets by c_3, etc. Then, rate equations can be written down for the time evolution of the various concentrations from simple mass balances

$$\begin{aligned} \frac{dc_1}{dt} &= -\frac{1}{2}k_{11}c_1^2 - k_{12}c_1c_2 + \ldots \\ \frac{dc_2}{dt} &= +\frac{1}{2}k_{11}c_1^2 - k_{12}c_1c_2 + \ldots \\ &\vdots \end{aligned}$$

with k_{ij} rate constants. The time evolution of the particle concentration can be analyzed by means of a digital computer, see figure 4.2. The initial concentration of single particles is denoted by c_0 and the total concentration of independent entities is given by

$$c = \sum_{k=1}^{\infty} c_k$$

For an analysis of the initial rate of flocculation the first rate equation is sufficient, so

$$\frac{dc}{dt} = -\frac{k}{2}c^2$$

where k denotes the rate constant of flocculation. The solution of this equation is found to be

$$c(t) = \frac{c_0}{1 + \frac{k}{2}c_0 t}$$

[1] The word *coagulation* is also used to denote flocculation.

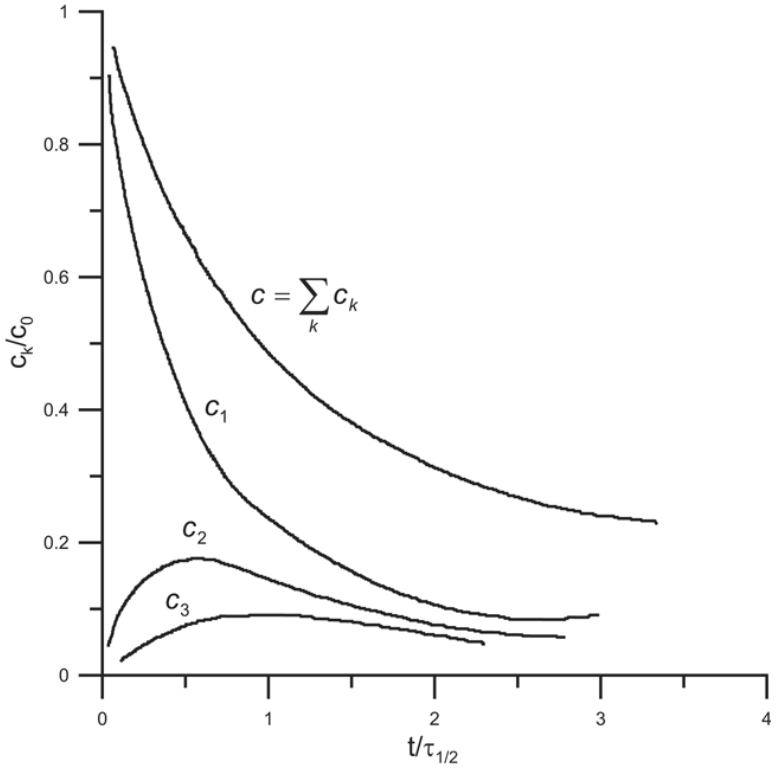

Figure 4.2 Concentration evolution during a flocculation process.

and the *flocculation half time* is given by

$$\tau_{1/2} = \frac{2}{kc_0} \tag{4.1}$$

This outcome was to be expected because the higher the particle concentration, the more probable are the collisions and the shorter the *flocculation time scale*; see also figure 4.2.

The time scale for perikinetic flocculation is given by

$$\tau_p = \frac{1}{8\pi Dac_0} \tag{4.2}$$

and it is independent of particle size because the diffusion coefficient for a particle is inversely proportional to particle size, see section 1.2.2. However, the concentration that is used in this equation is a number concentration. If instead one would use a concentration that is proportional to the total dispersed volume such as the mass concentration, then this introduces a strong particle size dependence.

The derivation of the above expression for perikinetic flocculation is due to Smoluchowski who used the following simple picture, see figure 4.3, where the target sphere of radius a is gray. Around the target sphere is a larger *collision sphere* of radius $2a$.

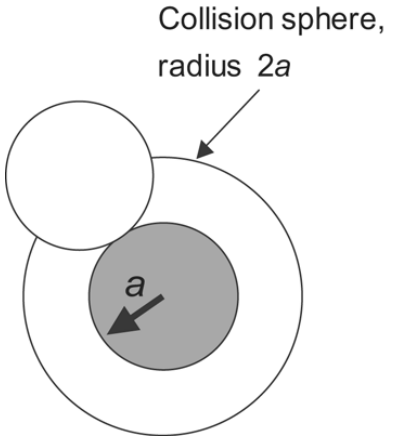

Figure 4.3 Sphere (gray) with collision sphere.

All other spheres that enter this collision sphere will flocculate with the target sphere. Consider now the situation where the particle concentration far away from the target sphere is given by c_0 and that the particle concentration at the surface of the collision sphere is 0 which is meant to indicate that once a particle has collided with the target particle it is removed. Due to the particle concentration difference, a particle flux develops that is given by

$$J = -D_{rel}\left(\frac{\partial c}{\partial r}\right)$$

where the relative diffusion coefficient is twice the particle diffusion coefficient because the relative displacement between two independently moving particles is given by

$$\langle (x_1 - x_2)^2 \rangle = \langle x_1^2 \rangle - 2\langle x_1 x_2 \rangle + \langle x_2^2 \rangle = 4Dt$$

Using mass conservation, one obtains

$$\frac{\partial c}{\partial t} = -D_{rel}\frac{1}{r^2}\frac{\partial}{\partial r}\left(r^2\frac{\partial c}{\partial r}\right)$$

For steady state, assuming the concentration c_0 fixed, the solution of this differential equation with the above described boundary conditions is

$$c = c_0\left(1 - \frac{2a}{r}\right)$$

The rate of flocculation is now calculated as the number of particles that diffuse into the collision sphere, so

$$\left(\frac{\partial c}{\partial t}\right)_{r=2a} = 4\pi(2a)^2 D_{rel}\left(\frac{\partial c}{\partial r}\right)_{r=2a} = 16\pi D a c_0$$

where $D_{rel} = 2D$ has been substituted. Comparing this with the flocculation rate equation one deduces that the rate coefficient for perikinetic flocculation is $k = 16\pi Da$ and equation 4.2 follows.

For orthokinetic flocculation one finds likewise[2]

$$\tau_o = \frac{3}{16Ga^3c_0} \tag{4.3}$$

and contrary to perikinetic flocculation, there is a strong particle size dependence if number concentration is kept constant and not if volume fraction is kept constant.

The above two cases are called the fast flocculation time scales, because in actual fact one tries to decrease the flocculation rate by introducing repulsive colloidal interactions between the particles. The ratio of the actual flocculation time scale and the fast time scale is called the *stability ratio*. The art of colloidal stabilization is to find methods to tune the stability ratio such that is achieves acceptable values under all practically possible conditions.

4.2 Colloidal interactions

This section is intended to give an overview of colloidal interactions that are used to stabilize disperse systems. It does not provide a detailed and fundamental treatment albeit that references to the relevant literature are given. Of old, the DLVO-interactions[3] enjoy more attention than the steric interactions whereas in practice their relevance is quite comparable. Therefore, this section devotes roughly the same amount of attention to both kinds of interactions.

4.2.1 Van der Waals interactions

The origin of the van der Waals interactions is in the distribution of electrons around the nuclei of the molecules. It is intrinsically quantum mechanical in nature, but a simple picture may be sketched based on the classical Bohr model of atoms and molecules. Consider first a mono-atomic molecule such as Argon. The nucleus represents the center of mass of the positive charges in this molecule. The center of mass of all the negative charges, the electrons, on average coincides with the center of mass of the positive charges. The electrons, however, orbit the nucleus and as a consequence their center of mass fluctuates around the nuclear center of mass. This gives rise to a fluctuating dipole that radiates an electromagnetic field. The electron clouds around molecules in the neighborhood respond to this fluctuating dipole and themselves radiate an electromagnetic field that is partly correlated with the received field. The net average of this fluctuating dipole - fluctuating dipole interaction is attractive. For more involved molecules there are also

[2] See T.G.M. van de Ven, *Colloidal Hydrodynamics*, Academic Press 1989; eq. 5.21 with $q = 1$.

[3] The abbreviation stands for the four names of Derjaguin, Landau, Verweij and Overbeek who developed the theory for the combination of van der Waals and electrical interactions, see P.C. Hiemenz and R. Rajagopalan, *Principles of Colloid and Surface Chemistry*, Marcel Dekker 1997; Chapter 11.

contributions from vibrational motions inside the nuclei and even rotational motions of the molecules as a whole. A detailed description of van der Waals forces can be found in the book by Jacob Israelachvili[4].

To find the van der Waals interaction between surfaces or between spherical particles, summation rules are invoked[5]. For spheres of radii a_1 and a_2 of a material α in a medium β, the van der Waals interaction can be written as

$$w(h) = -\frac{A_{\alpha\beta\alpha}}{6h}\frac{a_1 a_2}{a_1 + a_2} \tag{4.4}$$

which reduces to the previously given equation (2.12) for the case of identical spheres. The importance of this expression is that the van der Waals interaction between spheres varies inversely with the separation and is proportional to the "average" radius.

The strength of the interaction is determined by the Hamaker coefficient $A_{\alpha\beta\alpha}$. As has been discussed in section 2.3.1, its value can be related to the interfacial tension of the material. In general one finds, that for particles of the same material α that are dispersed in a liquid β the Hamaker constant is always positive because

$$A_{\alpha\beta\alpha} \approx \left(\sqrt{A_{\alpha\alpha}} - \sqrt{A_{\beta\beta}}\right)^2 \geq 0$$

but that for particles of different materials α and γ it could be negative since

$$A_{\alpha\beta\gamma} \approx \left(\sqrt{A_{\alpha\alpha}} - \sqrt{A_{\beta\beta}}\right)\left(\sqrt{A_{\beta\beta}} - \sqrt{A_{\gamma\gamma}}\right)$$

An example is poly(methyl methacrylate) or PMMA-particles in water, for which the Hamaker constant is $7.11 \cdot 10^{-20}$J whereas the Hamaker constant for the interaction between PMMA-particles and air bubbles in water is attractive, it is $-1.23 \cdot 10^{-20}$J.

4.2.2 Electrical double layer forces

A surface in contact with an electrolyte, see figure 4.4 (left), may acquire a surface charge by several mechanisms. One of the most frequently occurring mechanisms is the dissociation of surface groups and another mechanism is the specific adsorption of some ion type. With all mechanisms, the effect is that there are immobile ions at or in the surface and mobile ions in the electrolyte. The system as a whole is neutral, so that there is a balance between the *counter ions* and the surface charge. In addition, the electrolyte may contain more ions of different kinds that charge compensate amongst themselves.

The organization of the counter ions will be such that the Gibbs energy is minimized, which implies that (i) the surface charge is compensated on the shortest possible length scale and (ii) the effect of repulsion between the ions is minimal to minimize the enthalpy, and (iii) the ions are as much dispersed as possible to maximize the entropy. The presence of other ions assists in two ways (i) by intermingling positive and negative ions the effect of interactions between the ions is balanced and (ii) more ions allow for more distributions that maximize the entropy. The organization of the ions near the surface leads to an

[4] J. Israelachvili, *Intermolecular and Surface Forces*, Academic Press 1992, Chapter 6.
[5] J. Israelachvili, *Intermolecular and Surface Forces*, Academic Press 1992, Chapter 11.

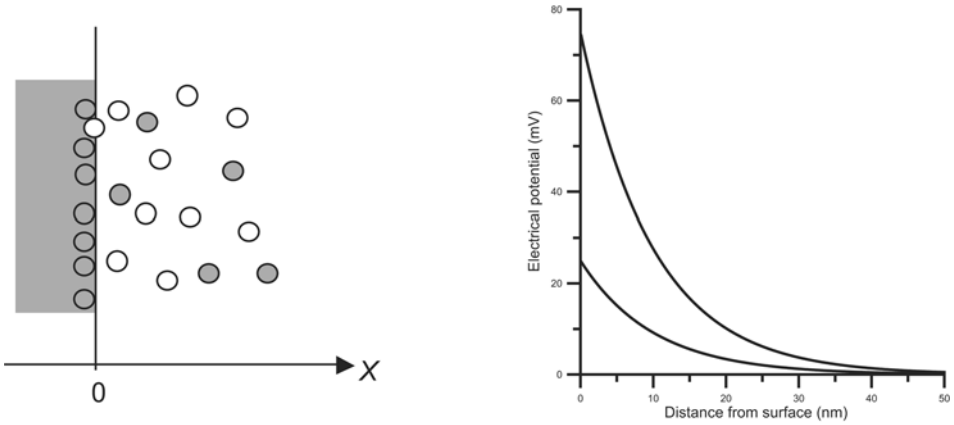

Figure 4.4 Charged surface in contact with an electrolyte (left) and electrical potential in the liquid (right) in which both a high and a low surface potential case at the same ionic strength are shown.

electric potential ϕ as depicted in figure 4.4 (right). The resulting electrical potential is well approximated by

$$\phi(x) = \phi_{\text{eff}} e^{-\kappa x} \tag{4.5}$$

where x is the distance from the surface. There are two characteristics of this potential that need to be discussed. The first is the exponential decay dictated by the inverse Debye length scale

$$\kappa = \sqrt{\frac{e^2}{\varepsilon_0 \varepsilon k_B T} I} \approx 3.23 \cdot 10^9 \sqrt{\frac{I}{c^{\ominus}}} \ \text{m}^{-1} \tag{4.6}$$

with $c^{\ominus} = 1$ M. The other constants in the above equation are $e = 1.60 \cdot 10^{-19}$ C the proton charge, $\varepsilon_0 = 8.85 \cdot 10^{-12}$ C^2/(Jm) the dielectric permittivity of vacuum, ε the relative dielectric permittivity of the solvent (about 80 for water), $k_B = 1.38 \cdot 10^{-23}$ J/K Boltzmann's constant, and T absolute temperature. The ionic strength is defined as

$$I = \frac{1}{2} \sum_j z_j^2 \frac{c_j}{c^{\ominus}} \tag{4.7}$$

in which c_j is the concentration of ion type j far away from the charged surface and z_j is the valency of ion type j. Some values of the Debye screening length are given in table 4.1. The above equation summarizes the experience that the more ions there are in the system, the more effective their *screening* effect. This screening is essentially the same as in ionic solutions where ions of the one kind organize themselves around ions of the other kind so as to minimize the electric fields that arises because of their presence. The ionic distribution in front of the surface effectively formes a *diffuse double layer* with a thickness that scales with the Debye screening length.

[NaCl]	κ^{-1}
M	nm
10^{-7}	960
10^{-4}	39.4
10^{-3}	9.6
1	0.3

Table 4.1 Some values of the Debye screening length for a 1-1 salt such as NaCl.

The second characteristic of the potential is the effective surface potential ϕ_{eff}. In figure 4.5 the relation between the effective potential and the actual surface potential as can be determined by for instance potentiometric titration. The picture clearly shows, that for low actual potentials, the effective potential and the surface potential are equal. For high actual potentials, the effective potential levels of to a constant value, $4k_BT/e$ in the case of a simple 1-1 electrolyte solution. The explanation for this behavior lies in the ionic distribution. For low surface potentials the diffuse double layer effectively screens the surface charge, but for high potentials the attraction between the free ions and the surface charge would become too high if not a significant amount of the counter ions resides very close to the surface. This *charge condensation* is a very local effect close to the surface, so that further away from the surface the effective charge that is felt in the double layer and beyond is as if the larger part of the surface charge is not present. Hence the term *effective surface potential*.

The effective surface potential follows from the solution of the Poisson-Boltzmann equation for a flat interface[6]. The full solution for z-z electrolyte reads

$$\tanh\left(\frac{ze\phi}{4k_BT}\right) = \tanh\left(\frac{ze\phi_d}{4k_BT}\right)\exp\{-\kappa(x-d)\}$$

where d is some point away from the surface where the potential is ϕ_d. Under rather mild assumptions, this result can can be cast in the form

$$\phi = \frac{4k_BT}{ze}\tanh\left(\frac{ze\phi_d}{4k_BT}\right)\exp\{-\kappa(x-d)\}$$

One typically assumes – largely because more detailed information on the structure of electrified interfaces is not available – that for $d \approx 0$ the electrical potential is equal to so-called ζ-potential and to the electrochemical potential determined by for instance potentiometric titration. One then obtains what is called above the effective potential

$$\phi_{\text{eff}} = \frac{4k_BT}{ze}\tanh\left(\frac{ze\zeta}{4k_BT}\right)$$

in terms of the surface or zeta-potential.

[6] See R.J. Hunter, *Introducton to Modern Colloid Science*, Oxford 1992.

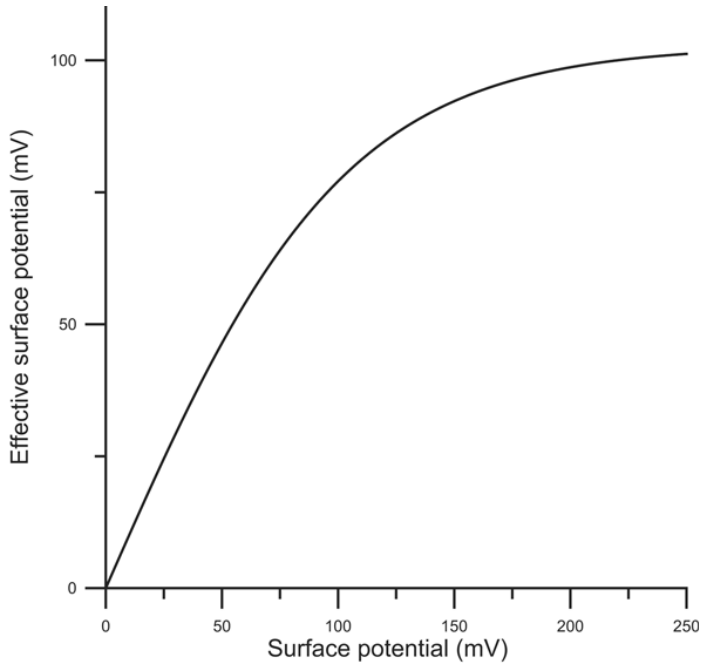

Figure 4.5 Effective potential as a function of surface potential.

The relation between the surface charge and the surface or *zeta*-potential is rather involved[6]. For not too large surface potentials it reads

$$\sigma = \varepsilon_0 \varepsilon \kappa \zeta \tag{4.8}$$

where κ is the Debye screening length. The surface charge of a particle is a quantity that can be measured by recording its motion under the influence of an electric field. By means of such electrophoretic measurements one hence obtains the *zeta potential* of the surface. More information on this and similar methods can be found in the books of Bob Hunter, one of the pioneers of the technique[7].

4.2.3 DLVO potential

When the two charged particles approach one another within the range of the electric potential, which means that the separation between the surfaces is less than a few times the Debye screening length, repulsive electrical interactions arise with a strength that increases with distance. At closer separation, the attractive van der Waals interactions become noticeable. The resulting interaction potential is depicted in figure 4.6. This potential is approximately described by the following equation

$$w(h) \approx -\frac{Aa}{12h} + 2\pi a \varepsilon_0 \varepsilon \phi_{\text{eff}}^2 e^{-\kappa h} \tag{4.9}$$

[7] R.J. Hunter, *Foundations of Colloid Science*, Oxford 2001.

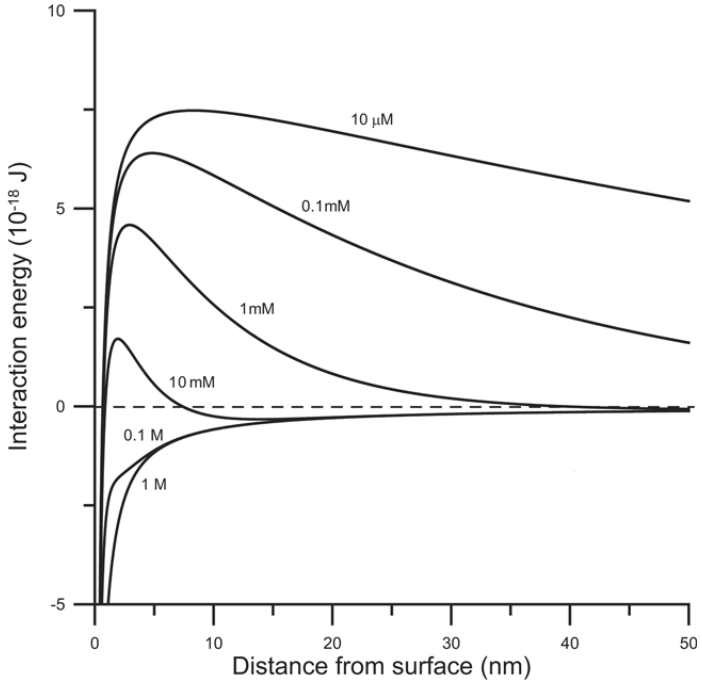

Figure 4.6 DLVO potential for particles of 0.5 μm with a zeta-potential of 75 mV and a Hamaker coefficient of $1.4 \cdot 10^{-19}$ *J in a 1-1 electrolyte.*

where

$$\phi_{\text{eff}} = \frac{4k_BT}{ze} \tanh\left(\frac{ze\zeta}{4k_BT}\right)$$

with ζ the actual surface potential and h the separation between the particle surfaces. The characteristics of the DLVO-potential are as follows:

- For low ionic strength values, the potential is purely repulsive and exhibits an energy barrier that prevents particles to enter the attractive regime.
- For high ionic strength values, the potential is purely attractive.
- For intermediate ionic strength values the energy barrier is not too large and there may even be a *secondary minimum* in which particles may temporarily be trapped.

One of the main achievements of Verweij and Overbeek has been to show, that with this potential the empirical *Schulze-Hardy rule* that the critical salt concentration beyond which flocculation sets in, the critical coagulation concentration (ccc), scales with the valency of the ions as

$$\text{ccc} \propto \frac{1}{z^6} \tag{4.10}$$

4.2.4 Steric interactions

All particles and even molecules occupy some space that cannot be occupied or penetrated by other particles or molecules. This is called the *excluded volume* of a particle or molecule. In gases it is the high temperature value of the second virial coefficient that in essence is the mutually excluded volume of the gas molecules. Completely analogously, the second virial coefficient of the osmotic pressure of a particulate solution is determined by the mutually excluded volume of the particles. The cause of these so called steric interactions lies in the Born-repulsion of molecules that in themselves originate in the *Pauli exclusion principle* that states that electronic shells cannot be occupied by more than one electron with the same spin. In the following two different manifestations of steric interactions will be discussed, namely depletion interaction and adsorbed layer interaction.

Depletion interaction

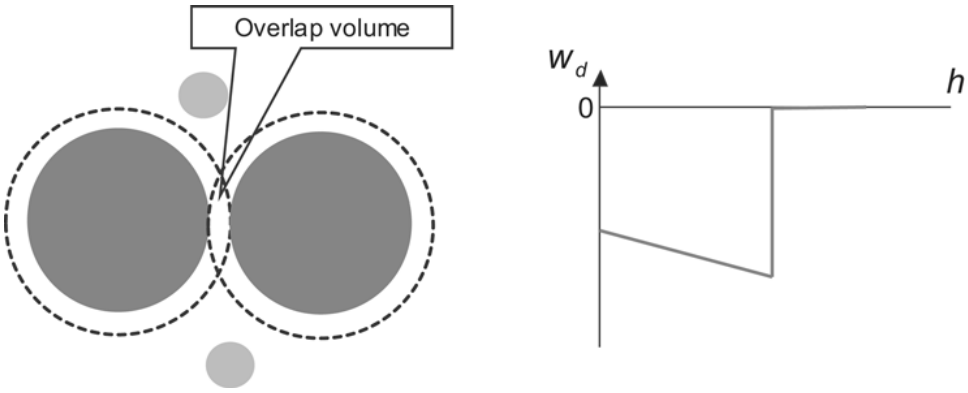

Figure 4.7 Two colloidal particles in a bath of small particles (left) and depeletion interaction potential (right).

Consider figure 4.7 which depicts two large colloidal particles in a bath of small particles. Around the colloidal particles a shell is drawn within which the centers of the small colloidal particles cannot penetrate. As long as the separation h between the big particles is larger than the diameter d of the small particles, the small particles may collide from all sides with the big particles. Since any collision on one side of the big particles is equally probable as a collision on the opposite side, the big particles will not experience a net force in one particular direction. However, when the separation $h < d$ the small particles can not enter the *overlap volume* v_o. This implies that small particle collisions on the opposite side of the big particle is not "compensated" by collisions from the side where now is the overlap volume. The net effect of this is, that the big particles will experience a force that brings them together. In terms of the osmotic pressure Π_s of the dispersion

due to the small particles the *depletion interaction potential* w_d can be written as

$$w_d = \begin{cases} -\Pi_s v_o & \text{for} \quad h < d \\ 0 & \text{otherwise} \end{cases} \tag{4.11}$$

and has the simple form depicted in the right panel of figure 4.7.

The osmotic pressure of a colloidal dispersion is, very much like that of a molecular solution, given by

$$\Pi = RTc$$

with c the (molar) concentration of the dispersion, see also equation(1.2). It derives from an equilibrium between the dispersion and pure solvent.

Adsorbed layer interaction

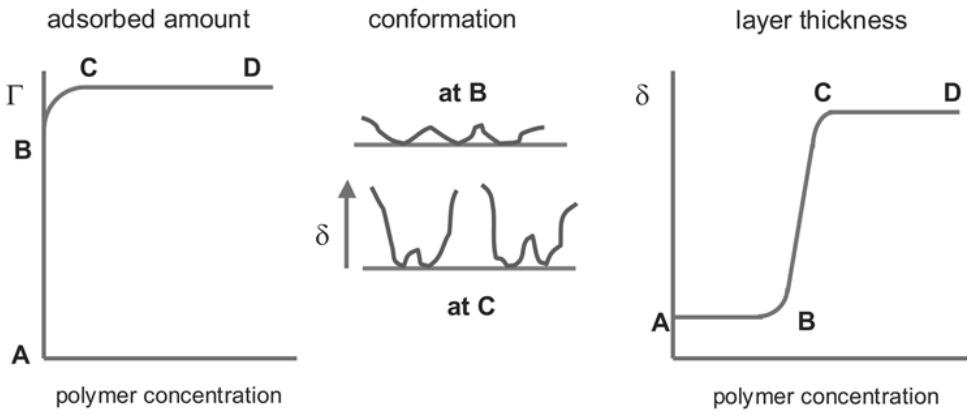

Figure 4.8 Adsorbed polymer layer properties.

Polymers may be made to adsorb on surfaces, being either flat surfaces or particle surfaces. Whether polymers will adsorb or not depends on the polymer-surface interactions and on the solvent. Many times one uses polymers with ionizable groups, so called polyelectrolytes, that are selected such that they preferentially bind to surface groups. In figure 4.8 the typical aspects of polymer adsorption are depicted[8]. In the most left picture is the graph of surface adsorption Γ versus polymer concentration. The right most picture depicts the polymer layer thickness as a function of concentration and in the middle are sketches of what the polymer conformations are at varies points.

[8]Much more information on polymer adsorption is available in the monograph by T. Cosgrove, G. J. Fleer, M. A. Cohen Stuart, J. M. Scheutjens, B. Vincent, *Polymers at Interfaces*, Springer 1999.

A-B At low concentrations there is barely polymer adsorption and those polymers that are adsorbed spread out over the surface at will. For a given polymer, there is a competition between the adsorbed polymer segments and those in solution. In other words, there is a balance between the enthalpy gained with the adsorbed segments and the entropy gained with the segments that are free in solution.

B-C At B the adsorption reaches a maximum in the sense that polymers adsorbed in the *flat* conformation occupy all of the available surface. There can be much more polymers on the surface, but then the conformation needs to change from the *flat* state to the *standing* state. This is why the layer thickness increases so drastically going from B to C compared to the increase in adsorption.

C-D In this regime the surface gets more and more saturated which is hardly noticeable on the adsorption or on the layer thickness. For all practical purposes the surface can be considered as full.

The quality of the solvent plays an important role in this respect which is expressed in the Flory polymer-solvent interaction parameter χ. For $\chi > 0.5$ the solvent quality is good and the polymer conformations are extended. In the other case, for $\chi < 0.5$ the solvent quality is considered to be bad which leads to compact conformations.

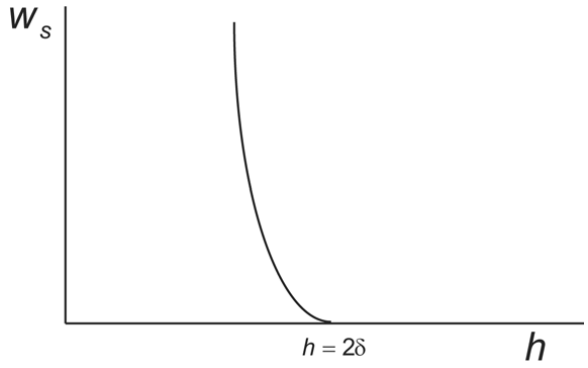

Figure 4.9 Adsorbed polymer layer interaction.

Now consider two particle surfaces that are not fully saturated with adsorbed polymer, see figure 4.9. When the separation is larger then twice the polymer layer thickness there is no interaction noticeable. Upon closer separation, the polymer layers are touching. This gives rise to a repulsive interaction when the solvent is also a good solvent for the polymer, because the polymer segments start to interpenetrate which leads to a loss of entropy. When the solvent quality is bad, the interaction is attractive. With polymer adsorption it is well possible to tune the interaction between colloidal particles. There are some pitfalls that one has to beware of

- If the solvent is too good, adsorbed polymers extend fat into the solvent and in fact polymers may *bridge* between two particles. This phenomenon leads to weak flocculation.
- Free polymer coils in the solution may lead to *depletion flocculation* because of the above described attractive depletion interactions.

In order to circumvent the problems mentioned above, one often chooses the more expensive block co-polymers with which one may tailor the one block to the adsorption on the surface and the other block to the optimal solvent behavior.

4.3 Colloidal stability

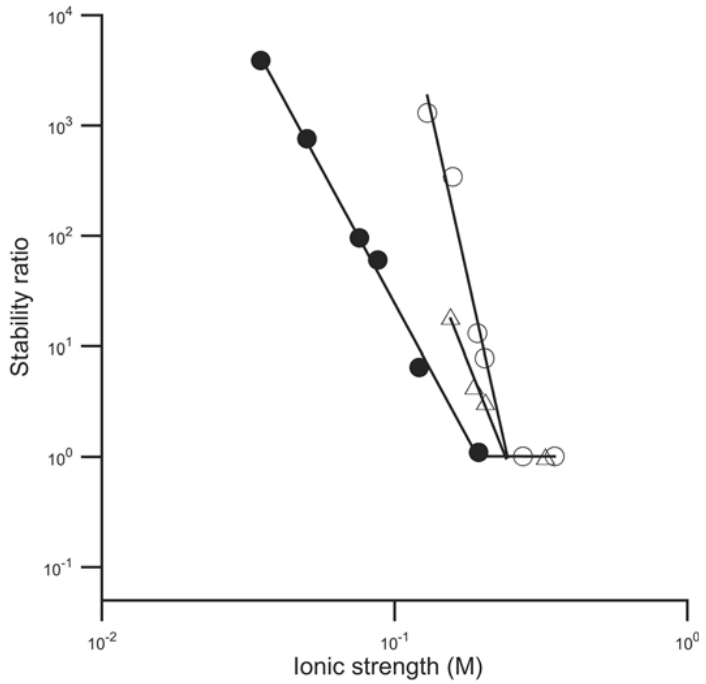

Figure 4.10 Stability ratio of AgI sols with KNO_3 as electrolyte for different particle sizes.

The colloidal interactions described in the section 4.2 above may be used to manipulate the stability of the suspension. The fastest flocculation time scale τ_{fast} is described in section 4.1. Manipulation of the colloidal interactions in such a way that the interactions become (partly) repulsive leads to a longer flocculation time scale τ_{slow}. The ratio between these two time scales is the *stability ratio*

$$W = \frac{\tau_{slow}}{\tau_{fast}}$$

This stability ratio may be studied, experimentally as well as theoretically, and yields graphs as in figure 4.10 for the case of electrostatic stabilization. Along the abscissa is plotted the ion concentration of the salt or the ionic strength. For each of the salts there is a line that has a break at a specific concentration beyond which the stability ratio equals 1: in other words where the flocculation is fast as it can be. Clearly, beyond this *critical coagulation concentration* (ccc) the stabilizing features of the electric double layer have disappeared. This is understood from the DLVO-theory as discussed above. What is also shown is that the valency of the salt strongly influences the ccc which is approximately verifying the Schulze Hardy rule, see equation 4.10.

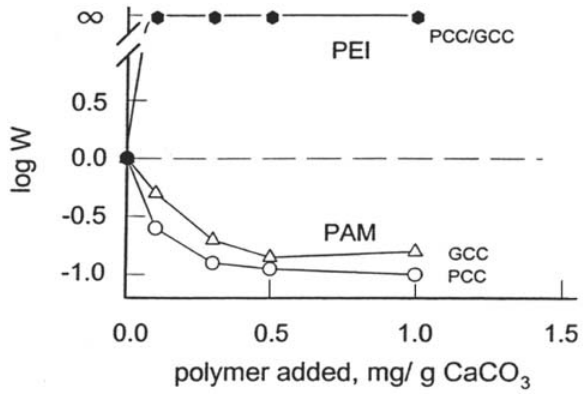

Figure 4.11 Stability ratio of ground (GCC) and precipitated (PCC) $CaCO_3$ sols with indicated polyelectrolytes.

Another case of a stability diagram is given in figure 4.11 where the amount of polyelectrolyte added to calcium carbonate particles is varied. It is seen that poly(ethylene imine) (PEI) is effective whereas poly(acryl amide) (PAM) is not. Here, the aim is to flocculate the calcium carbonate particles and the conclusion is then that PAM does the job pretty good. The reason is not so clear, probably bridging flocculation induced by the PAM is responsible for a flocculation time scale that is even slightly faster then without polymer layer. The reason why the adsorption of PEI leads to stable dispersions is possibly due to its very high charge density.

4.3.1 Kinetic stability

The above discussion was restricted to what could be called *thermal stability*. In the presence of external forces, different situations may arise depending on the interaction potential and on the strength of the external force. A special case is when the interaction potential has two minima, such as the DLVO potential. In that case weak flocculation, where particles adhere in the secondary minimum, and strong flocculation, with particles adhering in the primary minimum, may occur. In figure 4.12 an example is given where at very low stirring rates the particles are weakly flocculated. For intermediate stirring rates

they become stable and then flocculate again at higher shear rates because the particles, by the collisions induced by the stirring, are forced to adhere in their primary minima. Extreme, usually unattainable, stirring rates may redisperse the system again.

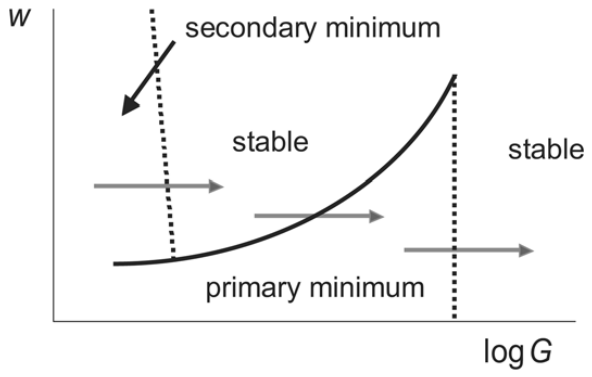

Figure 4.12 Stirring a dispersion might cause flocculation or redispersion!

Chapter 5

Rheology of dispersions

The term *rheology* stems from the greek as is reflected by the statement *panta rei* which is claimed to be due to Herakleidos who lived from 535 till about 480 BC. Indeed, the idea is that everything flows given the time of observation. Also mountains, which is already in Deborah's song in the Book of Judges in which one may find the line *The mountains flowed from before the LORD, even that Sinai from before the LORD God of Israel*. The name of Deborah is forever connected to this branch of science by the Deborah number to be discussed in the next section.

5.1 Deformation and flow

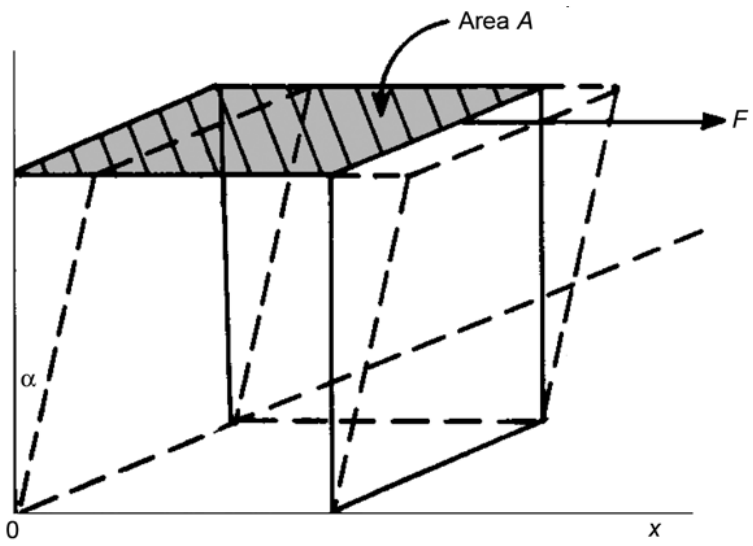

Figure 5.1 Solid-like behavior: elastic deformation

Consider a block of material, such as the rubber used in erasers, that is sheared as in figure 5.1. The stress acting on the surface is given as the force per unit area, in the figure this is $\sigma = F/A$. Due to this stress, the material will deform slightly which is measured by the angle α in the figure. The deformation is reversible in the sense that once the force is removed, the material assumes its original shape. The strain due to this stress is the displacement of the top surface with respect to the bottom surface relative to the height and is therefore simply the tangent of the deformation angle $\gamma = \tan\alpha$. In the case of ideal elastic behavior, the material behaves purely as a Hookean spring and the shear modulus is the proportionality factor between the stress and the induced strain

$$S = \frac{\sigma}{\gamma} \tag{5.1}$$

In the case of shearing forces, the force is applied in the plane of the surface. If the force is applied perpendicular to the surface, one applies *tensile stress* and the associated elasticity modulus is called *Young's modulus*[1].

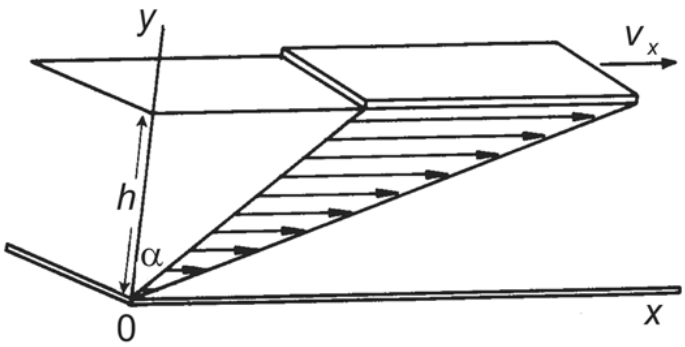

Figure 5.2 Fluid-like behavior: viscous flow

Consider now a fluid that is held between two surfaces as depicted in figure 5.2. If a shear force is applied on the top surface a linear velocity gradient develops in the fluid such that the fluid close to the surfaces take on the velocity of the surface itself. The shear rate is defined as the time rate of change of the deformation of the liquid as

$$G = \frac{d\tan\alpha}{dt} = \frac{1}{h}\frac{dx}{dt} = \frac{dv_x}{dy}$$

If the force is removed, the movement of the surface also stops but it does not restore itself. In other words, the deformation of the fluid is irreversible. The ratio of the applied

[1] Yet another situation arises when a hydrostatic pressure is exerted on a liquid. The change in local density due to a local hydrostatic pressure is described by the bulk modulus. Under conditions where one analyzes colloidal dispersions, the liquids may be considered incompressible and hence the bulk modulus of liquids is ignored.

shear stress and the induced shear rate is – for ideal viscous or *Newtonian* behavior – defined as the viscosity of the fluid

$$\eta = \frac{\sigma}{G} \tag{5.2}$$

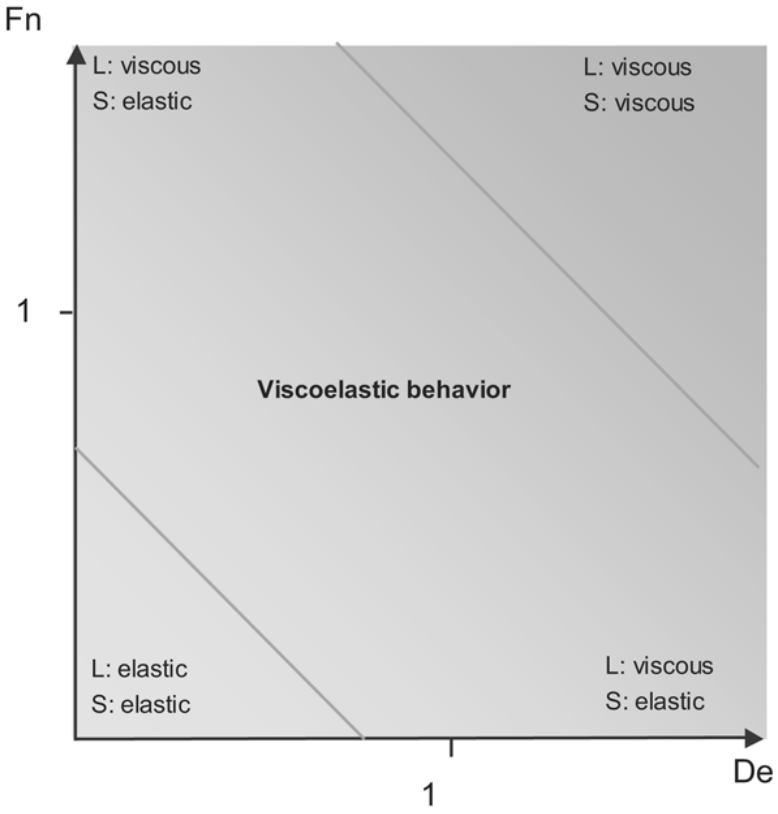

Figure 5.3 Flow behavior characterized by two dimensionless groups.

The above described elastic and viscous response are idealized and in practice neither of the two is always realized for the same system. For instance, water flows as we are used to if mildly moved . However, when we try to apply a quick impulse the response is much more elastic as everyone that has landed the wrong way after trying to dive into a swimming pool from some height found out. On the other hand, glass is typically responding elastically to forces. However, it does flow as can be seen on longer time scales. There are two characteristic numbers that can be used to identify the response of systems to forces. The Deborah number, defined by

$$\mathrm{De} = \frac{t_{\mathrm{relax}}}{t_{\mathrm{obs}}}, \tag{5.3}$$

compares the timescale of the system to the observation time and the force number compares the applied force to the internal forces

$$\mathrm{Fn} = \frac{F_{\mathrm{ext}}}{F_{\mathrm{int}}} \tag{5.4}$$

In figure 5.3 the plane spanned by these two characteristic numbers is sketched. Let us first consider the regime where the observation time is much longer than the internal relaxation times. Then for sufficiently strong forces compared to the internal forces, the system will respond viscous both in the case of fluids and solids. When the applied force is weak compared to the internal forces a solid may, because of its structure, still respond elastically but a fluid will respond viscous. For force and Deborah numbers around 1 both fluids and solids will show *viscoelastic* behavior: neither fully liquid-like nor fully solid-like. These systems will flow under sufficient stress but will recover also after the application of the force.

Both the shear modulus and the viscosity are material properties which are tabulated for most simple materials and fluids. For more complex systems such as polymer melts or liquid crystalline systems, constitutive equations are available which allow for an accurate evaluation of the viscoelastic behavior. A standard classification of the various flow types that are encountered is given in figure 5.4. The Newtonian behavior is what is typically

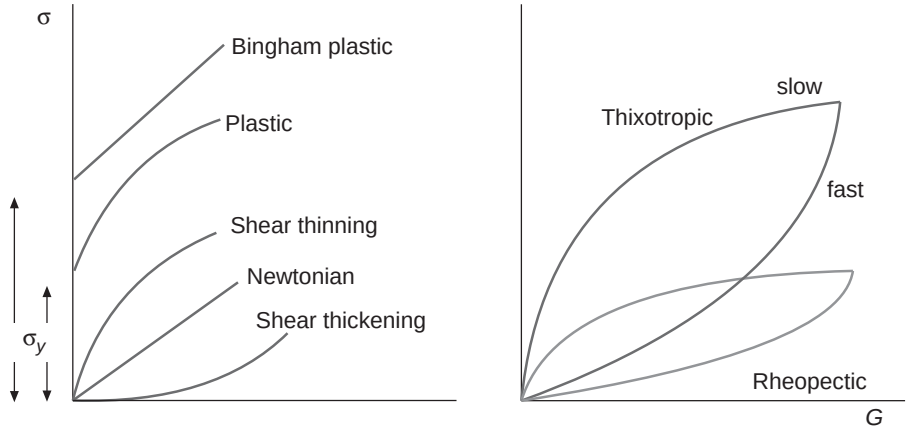

Figure 5.4 Typical flow behaviors and their rheograms.

assumed for as the standard behavior for fluids under standard conditions. The viscosity is assumed to be constant and independent of shear rate as in eq. 5.2. For more complex fluids, the viscosity is dependent on the shear rate, which is empirically described by the constitutive equation

$$\sigma = \eta G^n$$

Clearly, when the coefficient $n = 1$ the Newtonian behavior is recovered. For $n < 1$ the flow is called shear thinning and for $n > 1$ it is called shear thickening. In addition to

the effectively shear dependent viscosity, one may encounter a *yield stress*: largely flow behavior but some elastic part that is reflected by an internal stress that needs to be overcome before the system starts to flow. The *Bingham equation* is an empirical formula to model this type of flow behavior and reads

$$\sigma = \sigma_B + \eta G$$

in which σ_B is the yield stress. Apart from these two characterizations, non-linear viscosity and yield stress, other time-dependence may develop which are generally termed thixotropic and rheopectic behavior. The flow diagram in figure 5.4 sketches the corresponding rheograms.

5.2 Viscosity measurement

Viscosimetry is a standard experiment to characterize colloidal dispersions. In the following section the various contributions to the viscosity of a colloidal dispersion will be discussed, below follows a brief discussion of the most typical instruments used.

5.2.1 Ostwald viscometer

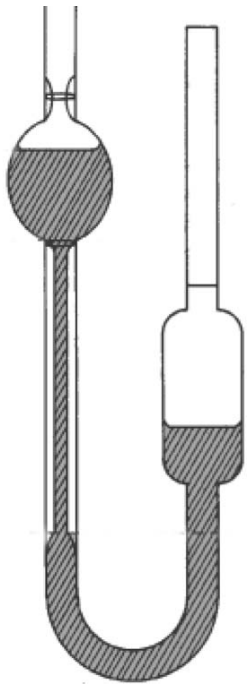

Figure 5.5 Ostwald or capillary viscometer.

The Ostwald or capillary viscometer[2], see figure 5.5 for a sketch, is based on the fact that a more viscous liquid takes longer to flow through a capillary than a less viscous liquid does. The flow of a viscous liquid through a capillary is described by the Poiseuille equation

$$Q = \frac{\pi a^4}{8\eta}\frac{\Delta p}{L}$$

in which Q is the amount of liquid passing through the capillary per unit time, a is the capillary radius, L the length of the capillary, and Δp the pressure difference across the capillary that is usually brought about by gravity and hence proportional to the mass density of the fluid ρ. So, for an unknown fluid the viscosity can be determined from

$$\eta_x = \eta_{\text{ref}}\frac{t_x\rho_x}{t_{\text{ref}}\rho_{\text{ref}}}$$

provided that some reference fluid has been used to calibrate the instrument. Automated equipment is nowadays available that does a number of experiments from which the flow through time t is computed as an average with standard error. In fact, this method immediately determines the kinematic viscosity η/ρ rather than the viscosity itself.

One of the largest problems that is often mentioned in conjunction with this instrument is the fact that the shear rate varies across the capillary. Varying the capillary diameter allows one to assess the importance of this dependence. Another, more severe problem – in particular with automated instruments – is the evaporation of the liquid. In the case of colloidal dispersions this implies that the fill factor of dispersed materials slowly increases during a series of experiments. Depending on the system studied, this can be accounted for in a usually trivial manner.

5.2.2 Couette viscometer

The Couette viscometer, see figure 5.6, basically consists of two concentric cylinders with a small gap in between. The outer cylinder is driven and the torque is measured on the inner cylinder. Due to the small gap, the gradient in the shear rate across the gap is small and approximately given by

$$G \propto \frac{\omega R}{d}$$

where ω is the angular frequency with which the cylinder is driven, R is the average diameter of the cylinders and d the gap width. The viscometer can be operated in two modes, at constant shear rate and at constant shear stress. Frequently encountered problems with this instrument are due to flow in the annulus which is the closing ring at the bottom side and instabilities when rotating the inner cylinder with a stationary outer cylinder.

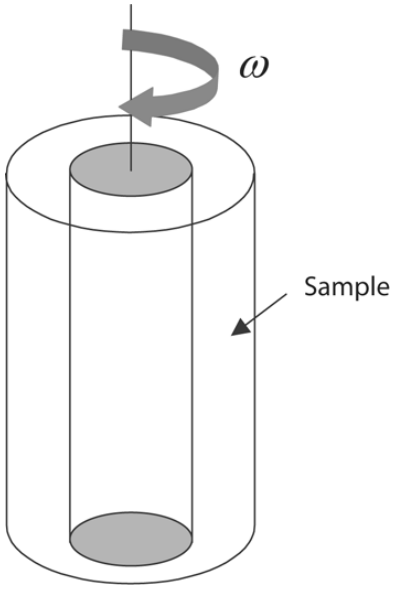

Figure 5.6 Couette viscometer.

5.2.3 Cone and plate viscometer

The cone and plate viscometer, see figure 5.7, is designed in such a way that the shear rate is constant over the whole volume

$$G = \frac{\omega R}{h} = \frac{\omega}{\tan \alpha}$$

In most commercial instruments, the cone is rotated at a fixed angular velocity ω and the torque is measured on the plate. Temperature control is relatively easy on this instrument, but evaporation of the solvent is a significant problem that can sometimes only be overcome by using a "water seal".

[2] An often encountered brand name, is Ubbelohde viscometer.

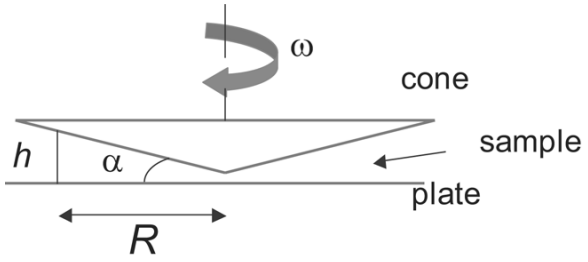

Figure 5.7 Cone and plate viscometer.

5.2.4 Falling ball viscometer

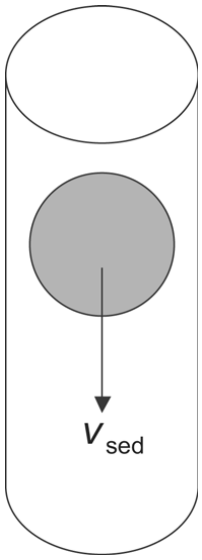

Figure 5.8 Falling ball viscometer.

In industrial practice, it is often not convenient to use delicate instrumentation and a more robust technique is called for. One of the simplest of those is the falling ball viscometer where one just registers the time it takes for a ball to sink in a vessel of given height. The *sedimentation velocity* is given by

$$v_{\text{sed}} = k_c \frac{g m_{\text{eff}}}{6\pi\eta a} = k_c \frac{2ga^2\Delta\rho}{9\eta}$$

in which $\Delta\rho$ is the mass density difference between ball and fluid, a is the ball radius, and g the gravitational constant. The factor k_c is a correction factor for wall effects. For large vessel diameters it tends to unity.

5.3 Dilute stable dispersions

Dispersed particles in a shear flow rotate and thereby disturb the flow field in their immediate vicinity. This constitutes a contribution to the dissipation that is proportional to the volume of the dispersed particle and the number density of particles. This is the basic understanding behind the well-known Einstein relation for the viscosity of a dilute dispersion

$$\eta = \eta_o \left(1 + \frac{5}{2}\phi\right) \tag{5.5}$$

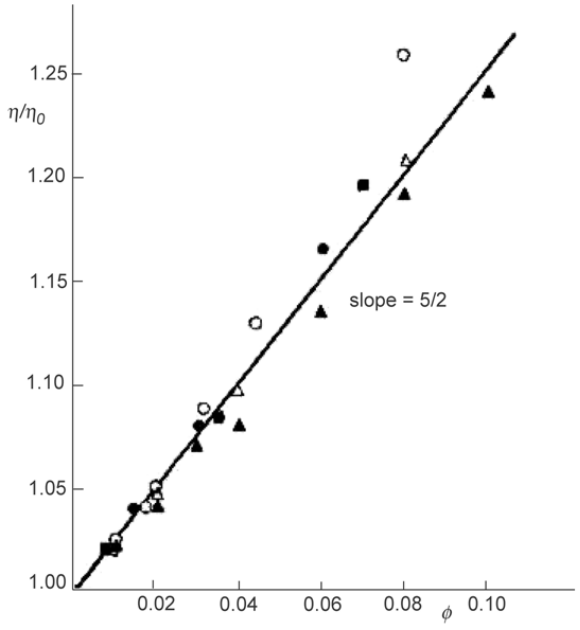

Figure 5.9 Relative viscosity versus colloid volume fraction.

in which η_o is the viscosity of the solvent. The specific viscosity, defined by

$$\eta_{sp} \equiv \frac{\eta - \eta_o}{\eta_o}$$

is obviously $5\phi/2$ and the *intrinsic viscosity*[3] defined by

$$[\eta] = \lim_{\phi \leftarrow 0} \frac{1}{\phi} \frac{\eta - \eta_o}{\eta_o}$$

is $5/2$.

For higher fill factors, the viscosity deviates from the "ideal" Einstein relation and this is generally accounted for by a "virial expansion" as

$$\eta = \eta_o \left(1 + \frac{5}{2}\phi + b\phi^2 + \ldots\right) \tag{5.6}$$

For relatively low values of the shear rate, Batchelor[4] found for the second virial coefficient a value of $b = 6.2$. This number contains both hydrodynamic and colloidal interaction effects.

[3]Other definitions are around where volumetric concentrations or mass concentrations are involved, the general idea remaining the same.

[4]See T.G.M. van de Ven, *Colloidal Hydrodynamics*, Academic Press 1989; sec 5.2.1.

5.3.1 Electroviscous effects

In many cases, dispersed particles carry a surface charge and the ions around the particle surface influence the flow field. This affects an increase of the intrinsic viscosity of particles which for thin double layers is given by

$$[\eta] = \frac{5}{2} + \frac{6\varepsilon^2\zeta^2}{K\eta_o a^2}$$

in which K is the specific conductivity of the dispersion, ε its dielectric permittivity, ζ the surface potential due to the surface charge, η_o the solvent viscosity, and a the particle radius.

In a similar way, the interactions between colloidal particles are affected by ions near the particle surfaces and this has its influence on the second virial coefficient b, an effect that is strongly dependent on the ionic strength of the dispersion.

5.3.2 Dependence on flow type

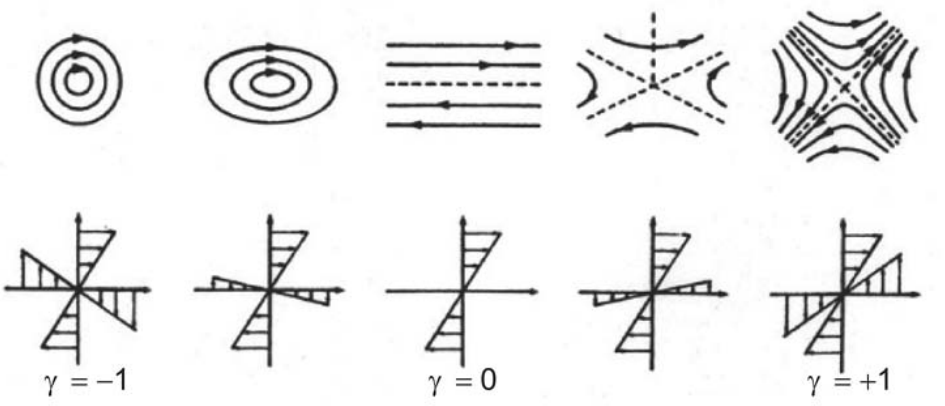

Figure 5.10 Classification of flow types; see text for further details.

What is usually called simple shear flow, and what is realized in for instance a capillary, is really a superposition of two more elementary flow types. The two are pure rotational flow and elongational flow, see figure 5.10 with $\gamma = -1$ and $\gamma = 1$ respectively. In figure 5.11 the effect of these two flow types on the second virial coefficient is depicted.
At high shear rates the flow becomes non-newtonian; shear thinning in simple shear flow and shear thickening in elongational flow. The crossover is given by the translational Péclet number, $\mathrm{Pe} = Ga^2/D$ with gives the balance between the shear flow and the Brownian motion. For $\mathrm{Pe} = \infty$ Brownian motion is absent.

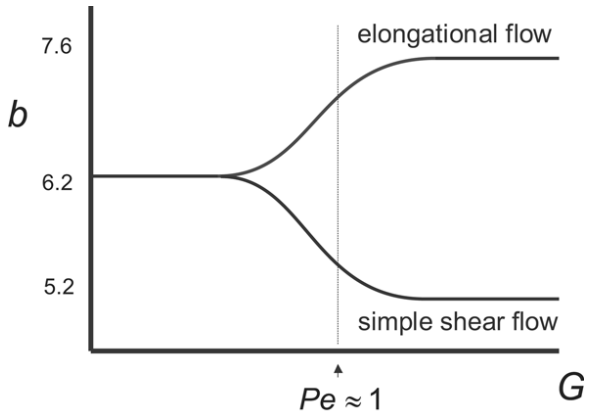

Figure 5.11 Effect of flow type on second virial coefficient.

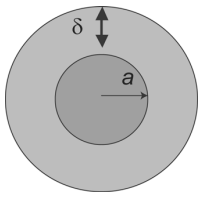

Figure 5.12 Coated particle.

5.3.3 Coated particles

A coating, such as an adsorbed polymer layer, makes the dispersed particles larger. As an approximation, reasonable when the thickness of the coating layer δ is much smaller than the particle radius a, one only takes the first correction term linear in the layer thickness leading to

$$[\eta] = \frac{5}{2}\left(1+3\frac{\delta}{a}\right)$$

5.3.4 Deformable droplets

So far, only nondeformable droplets have been dealt with. So called soft droplets deform in shear flow as is sketched in figure 5.13. To a good approximation, the effect of the deformation on the intrinsic viscosity is only a function of the ratio r of the viscosities of the internal phase to the external phase, i.e.

$$[\eta] = \frac{5r+2}{2(1+r)}$$

For bubbles, where the internal viscosity is a few orders of magnitude less than the external viscosity, the intrinsic viscosity is close to unity. For solid spheres, with the internal

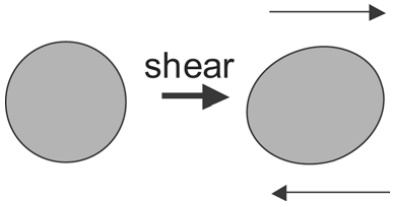

Figure 5.13 Deformable droplet in shear flow.

viscosity approximating infinity, the intrinsic viscosity is equal to the perfect sphere value $5/2$.

5.4 Dense stable dispersions

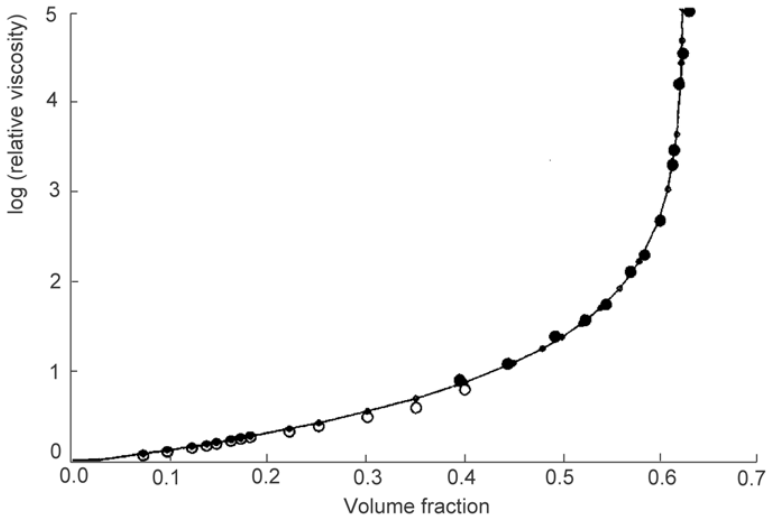

Figure 5.14 Krieger-Dougherty.

The viscosity of dispersions has a very characteristic viscosity - volume factor relationship, see figure 5.14. The viscosity varies relatively smoothly with volume fraction up to a critical value, which corresponds for many systems to the close packed volume fraction ϕ_c, beyond which it rises very steeply. There are many relationships available that describe this behavior qualitatively, but the experimental verification of such a relationship is extremely difficult. One of these relations has some fundamental basis and this is the

reason why it is advocated here. It is the Krieger-Dougherty relation

$$\eta = \eta_o \left(1 - \frac{\phi}{\phi_c}\right)^{-\frac{5}{2}\phi_c} \tag{5.7}$$

The value of volume fraction for close packing ϕ_c for hard spheres is about 0.63. The reason for this sudden increase of the viscosity is the fact that due to the shear flow the particles are rotating. When the particles are approaching each other, the two particle surfaces move in opposite directions causing a strong shear field between them. This gives rise to an enormous dissipation which is reflected by the (effective) viscosity.

Variable	change in variable	effect on viscosity
particle concentration	increase	increase
particle size	increase	no effect
particle size distribution	increase	decrease
particle shape	less spherical	increase

Table 5.1 Effect of dispersion properties on viscosity.

It is to be expected that all kinds of aspects of dispersions have their effect on the viscosity. This is only partly so, as demonstrated by the table 5.1. The most striking effect is the independence of particle size which is another characteristic of dispersion rheology.

5.5 Flocculating suspensions

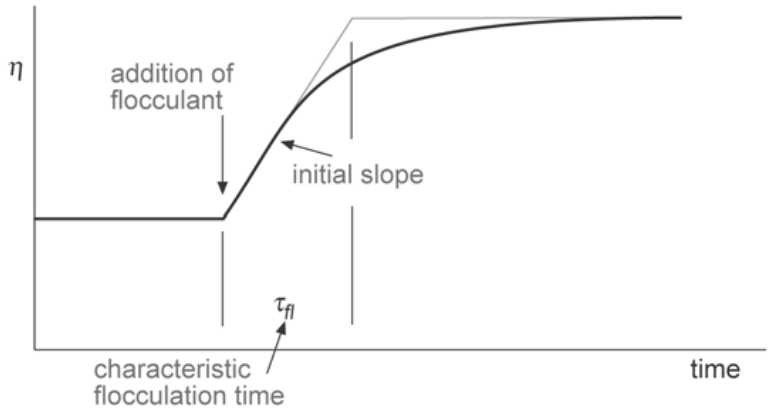

Figure 5.15 Flocculation experiment.

The viscosity of a dispersion is often used to monitor flocculation, see figure 5.15. Upon addition of a flocculant, such as salt in the case of electrostatically stabilized dispersions,

one observes an increase of the viscosity. There are two observables to interpret (1) the timescale of the viscosity variation and (2) the change in magnitude of the viscosity. As discussed above, at constant volume fraction one would not expect a change in viscosity upon flocculation. That this is nevertheless the case is due to the fact that in a floc there is entrapped solvent. This solvent is 'immobile" in the sense that it is no longer contributing to the momentum transfer in the fluid. Therefore, the effective volume of the cluster is larger than the total volume of the constituting particles and hence there is a viscosity increase. Hence the timescale of flocculation can be obtained from the experiment as well and should be analyzed according to what has been discussed in the previous chapter.

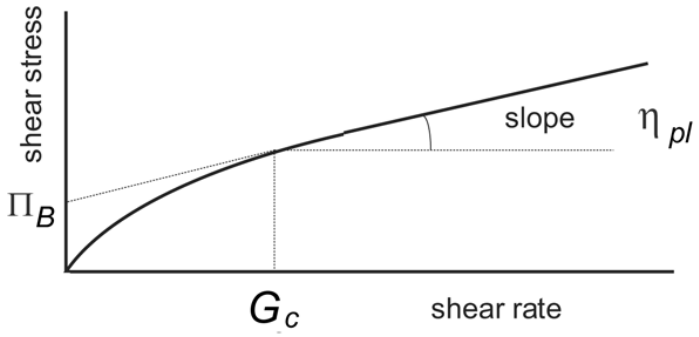

Figure 5.16 Rheology of a flocculating dispersion.

Shearing a flocculating suspension gives rise to interesting flow behavior, see figure 5.16. In a flocculating system there is a balance between the formation of flocs, either due to flow or to Brownian motion, and the break-up of flocs which is largely due to flow but can also be brought about by Brownian motion. The rheogram depicted in figure 5.16 is made such that each point is a stationary state of the dispersion. At very high shear rates one may assume that most flocs are ruptured and the viscosity, the slope of the flow curve, represents basically the viscosity of the dispersion of "free" particles. At low shear rates, large elastically responding flocs are present in the system which make up for the "Bingham"-like behavior of the system.

The above rheogram can in principle be analyzed with what is called the "elastic floc model". This model does predict values for the plastic viscosity, the yield stress and the critical shear rate. More refined models are currently being developed and it is to be expected that our understanding of this complex problem will evolve quickly.

Chapter 6

Emulsification

Making an emulsion is a simple thing to do, it is just mixing two immiscible fluids together with some kind of stabilizing agent. Many people do it daily as a routine exercise in the kitchen. The mixing should result in a dispersion of the one liquid into the other. Control over the droplet size and the stability is much harder to achieve and this is where the art of emulsification comes in. Here we shall only discuss some basic aspects of this art[1].

6.1 Relevant physicochemical quantities

The two immiscible fluids can of course be any kind, but for the sake of simplicity they will be called here oil and water. In that case, two types of emulsion are possible: oil-in-water (o/w) or water-in-oil (w/o). The volume fraction of the dispersed phase typically ranges from 0 to 50% although higher volume fractions are possible. In the latter case the continuous phase actually forms thin lamellae between large globules of dispersed phase. Another possibility is the formation of droplets into droplets, so called double emulsions, or even further dispersed.

The emulsion droplet size distribution is usually relatively broad and therefore it is important to specify exactly what kind of average droplet size is given. In most cases this is the so called *Sauter mean* diameter which is defined as

$$D_{32} = \frac{\int_0^\infty x^3 f(x)dx}{\int_0^\infty x^2 f(x)dx} \tag{6.1}$$

where f denotes the droplet size distribution. The advantage of this usage is that the

[1]This chapter is largely based on publications by Pieter Walstra: Chapter 2 entitled *Emulsion Formation*, in *Modern Aspects of Emulsion Science*, ed. B.P. Binks, RSC, Cambridge 1998, and chapter 11 entitled *Formation of Emulsions and Foams* of *Physical Chemistry of Foods* by Pieter Walstra, Marcel Dekker, New York 2004.

specific area of the emulsion droplets is easily computed as

$$A_{sp} = \pi \int_0^\infty x^2 f(x) dx = \frac{6\phi}{D_{32}} \tag{6.2}$$

with ϕ the dispersed phase volume fraction.

6.2 Mechanical action

6.2.1 Methods

There are various methods available to make emulsions. Some require very little energy and others much more. The low energy methods use supersaturation or chemical energy to create the droplets in a continuous medium. Supersaturation is for instance used to make the CO_2 bubbles in fizzy beverages. An alternative is to use calcium carbonate and citric acid to make carbonated lemonade. The latter case is an example of the use of chemical energy. A modern technique, that does not require much energy either, is membrane emulsification. This will not be discussed here.

The most common techniques, of old, use mechanical action: stirring, beating, homogenizing or cavitation. These forces are used to break up larger drops to smaller drops. The forces can be subdivided into two kinds: frictional or shear forces that act along the surface of the drops and inertial forces that act perpendicular to the drop surface. Most of the time, turbulent flow is needed although there are many examples where the flow remains laminar.

6.2.2 Weber number

In order to rupture a drop of a given radius a, the Laplace pressure has to be overcome. The Weber number, in case of laminar flow often called the *capillary number*, compares the external stress σ_{ext} to the internal stress as

$$\text{We} = \frac{\sigma_{\text{ext}}}{\Delta p/2} = \frac{\sigma_{\text{ext}} a}{\gamma} \tag{6.3}$$

with γ the interfacial tension between the continuous and the dispersed medium. Take, as an example, a droplet radius of 0.5 μm, an interfacial tension of 10 mJ/m^2 then the balancing stress equals $2 \cdot 10^4$ Pa. The break-up of such a droplet requires a pressure gradient ($\Delta p \propto \sigma/a$) of 10^{10} Pa which is difficult to achieve. The critical Weber number We_{cr}, where the transition from no break-up to break-up occurs is usually of order 1.

6.2.3 Regimes

The types of forces acting on emulsion droplets can be subdivided into two classes. The one class is the frictional forces or shear forces. These act parallel to the droplet surface and are proportional to the velocity gradient G of the flow field as $\eta_c G$ in which η_c is the

Regime	LV	TV	TI
Re flow	$<\sim 2000$	$>\sim 2500$	$>\sim 2500$
Re drop	< 1	< 1	> 1
σ_{ext}	$\sim \eta_c G$	$\sim \varepsilon^{1/2}\eta_c^{1/2}$	$\sim \varepsilon^{2/3} d^{2/3}\rho^{2/3}$
d	$\sim \frac{2\gamma \mathrm{We}_{cr}}{\eta_c G}$	$\sim \frac{\gamma}{\varepsilon^{1/2}\eta_c^{1/2}}$	$\sim \frac{\gamma^{3/5}}{\varepsilon^{2/5}\rho^{1/5}}$

Table 6.1 Various flow regimes and their emulsion action. Here ε is the power density inserted in the system.

viscosity of the continuous phase. The other class is the inertial forces that act perpendicular to the droplet surface. These are proportional to the divergence $\nabla \cdot \vec{v}$ of the local flow field.

The flow field is laminar for Reynolds numbers less than approximately 2000 and turbulent for Reynolds numbers over 2500. Two Reynolds numbers can be discriminated, one that is related to the flow itself,

$$\mathrm{Re} \equiv \frac{v\ell\rho_c}{\eta_c}$$

with ℓ the relevant dimension of the vessel or tube and ρ_c the mass density. In addition, the droplet Reynolds number needs to be considered where the relevant length scale ℓ is the droplet size. When the droplet Reynolds number is larger than unity, inertial forces are dominant. Using the above considerations, one may discriminate three regimes, see table 6.1 Laminar/viscous forces (LV) where the break-up is due to the viscous forces in a flow field. Turbulent/viscous forces (TV) and turbulent inertial forces (TI).

Laminar flow

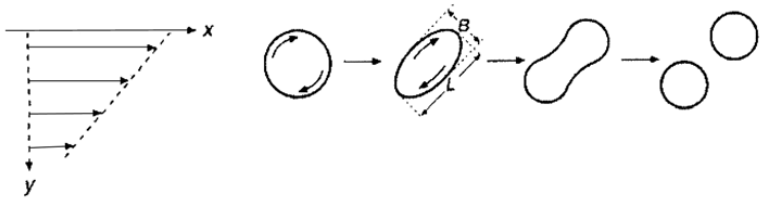

Figure 6.1 Simple shear flow.

As discussed in the previous chapter, see figure 5.10, simple shear flow is but one of the many types. In fact, flow types vary from pure rotational flow to pure elongational flow. In figure 6.1 the situation for simple shear flow is depicted. Due to the rotational

component in the flow, the droplets rotate. The fluid inside the drop also rotates in addition to being deformed. The relative deformation is defined as (see figure 6.1)

$$e = \frac{L-B}{L+B} \tag{6.4}$$

For small Weber numbers the deformation is simply equal to $e =$We and as soon as the critical Weber number is overcome, the droplet ruptures. In the case of elongational flow,

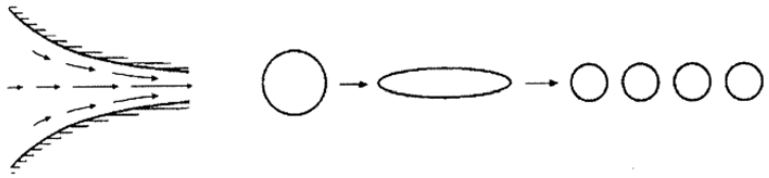

Figure 6.2 Elongational flow.

there is no rotation and the deformation takes place until the Rayleigh instability causes the break-up in two or more droplets, see figure 6.2.

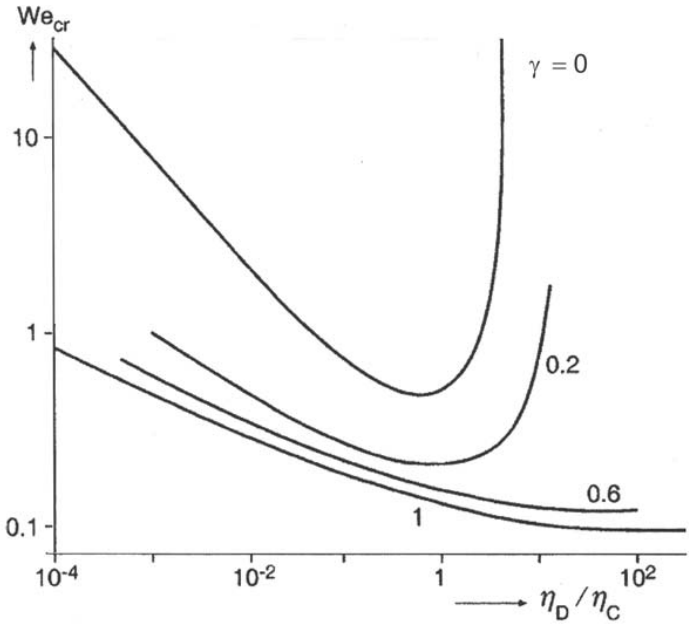

Figure 6.3 Critical Weber number as a function of viscosity ratio (dispersed phase over continuous phase) and flow type. For $\gamma = 0$ the flow type is simple shear and for $\gamma = 1$ the flow is purely elongational.

In figure 6.3 the critical Weber number is given as a function of flow type and the ratio of the viscosities of the dispersed phase and the continuous phase. Consider first the case

of simple shear flow which is the curve labeled $\gamma = 0$ in figure 6.3. For dispersed phase viscosities larger than 4 times the continuous phase viscosity, the drops are not broken-up at all. This is due to the fact that the deformation of the droplet takes more time than is available within the time needed for the droplet to make half a revolution in the flow field. Also for very small dispersed phase viscosities, such as encountered in foams, the critical Weber number becomes very large. This is because the drops deform in very long threads that do not rupture anymore.

In elongational flow, which is the curve labeled $\gamma = 1$ in figure 6.3, there is no internal rotation of the drop and elongation is the prime process. The Rayleigh instability than dominates and droplet break-up is relatively independent of viscosity ratio.

Turbulent flow

For turbulent flow, there are no exact expressions available. The flow is usually described by means of the Kolmogorov theory which yields scaling relations at the most. Flow is described in terms of eddies at varies length scales: eddies in eddies. The Kolmogorov theory provides a relation between the eddies of a particular length scale and the associated kinetic energy therein. In addition, it provides for a relation between the length scale and the life time of the eddy. The results can be found in the table 6.1.

6.2.4 Emulsification machines

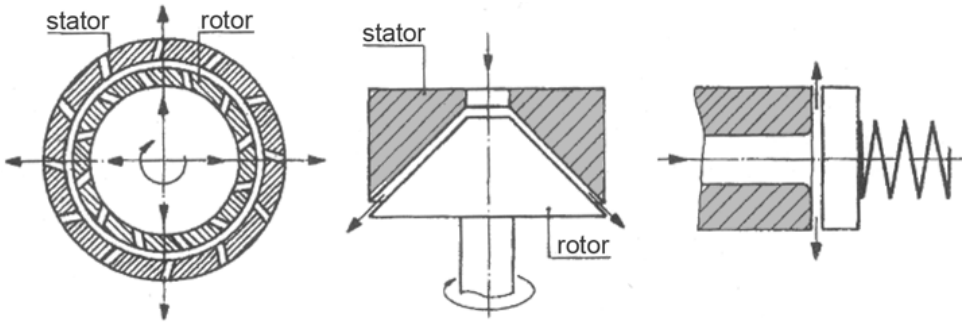

Figure 6.4 Relevant part of emulsification machines. From left to right: high intensity stirrer, rotor-stator systems, and high pressure homogenizer.

In figure 6.4 the relevant parts of the three most frequently used emulsification machines are depicted. From left to right these are the high intensity stirrer such as the *Ultra Turrax*, the rotor-stator machines known as *colloid mills*, and the high pressure homogenizers, the *whistles* that essentially consist of a valve. The first two instruments largely are, very inefficiently, creating extremely high shear fields and fluids can be mixed as well as emulsified with these machines. This is not the case with the homogenizers, where the fluids need to be premixed: only larger droplets can be ruptured to small droplets.

6.2.5 Complications

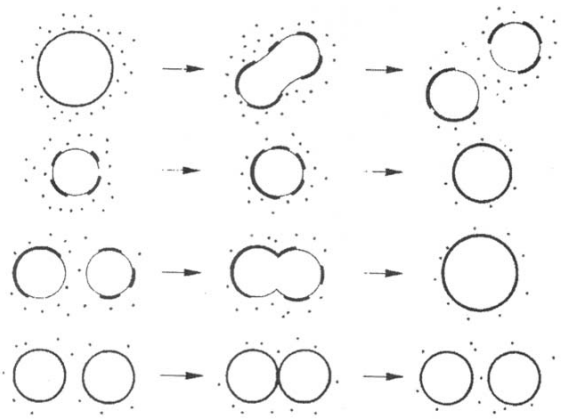

Figure 6.5 Droplet creation and break-up take many steps and can take many routes.

Despite the many theoretical aspects that are known about emulsification, the larger part of the science is empirical. A few aspects can be mentioned to illustrate the shortcomings of the theoretical knowledge.

- In none of the equations for the turbulent regime enters the viscosity of the dispersed phase. Nevertheless, it is a fact that this can have a dramatic influence and the cause is simply that, as in the laminar case, both the deformation stress and the timescale are determined by the dispersed phase viscosity.
- The power density is almost never homogeneous in the system. A good example is the impeller where the highest shear rates are only achieved at the tips.
- The droplet formation involves many steps, see figure 6.5, and for a detailed analysis information about the dynamics of the interface is needed as well.

6.3 Surfactant action

The primary role of surfactant in emulsified systems is claimed to be the lowering of the interfacial tension that leads to easier droplet break-up and a lower energy requirement. This is of course true, but it is certainly not the complete story. This is illustrated by figure 6.6 where the specific surface area and the achieved droplet size, in the TI-regime, are plotted. According to the information in table 6.1, the droplet size should be proportional to the surface tension as $\gamma^{0.6}$. According to the graph in figure 6.6 the trend is indeed there, but the variation with surfactant concentration shows that more needs to be explained.

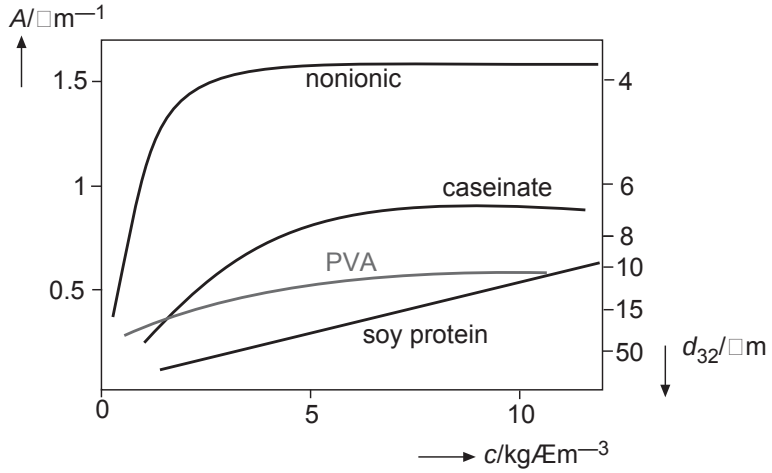

Figure 6.6 Specific surface area versus surfactant concentration. The plateau values for the interfacial tensions are 3, 10, and 20 mJ/m^2 for the nonionic, caseinate and PVA respectively.

6.3.1 Dual role

There are indeed two main roles that the surfactant has to play. The most important one is the prevention of recoalescence. When two newly formed droplets meet before having equilibrated their surface load of surfactant, there is a strong tendency to recoalesce. This is dependent on the relation between the time scale of re-collision and the one of equilibration. The effect is stronger for lower bulk concentration of surfactant. The other role is that of colloidal stability which is usually achieved by means of electrical stabilization in the case of ionic surfactants in an oil-in-water emulsion and by the surfactant tails, causing steric hindrance, in the case of water-in-oil emulsions.

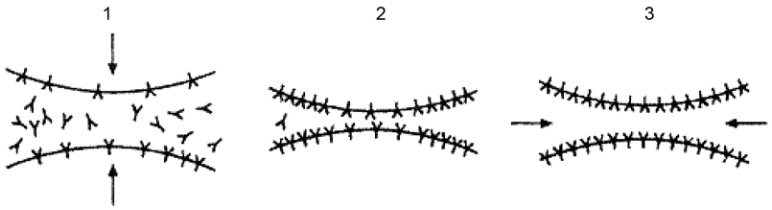

Figure 6.7 Schematic illustration of the mechanism of recoalescence prevention; see text for further details.

The prevention of recoalescence needs some further explanation which is given in figure 6.7. Assume that the droplets are just formed and have not yet attained their full surfactant loading. When two such droplets approach each other, the liquid in between is squeezed

out (1). This removes most of the free surfactant from the gap but also forces the surfactant in the surface away from the gap (2). This prevents the equalization of the surfactant loading of the surface from the liquid side and creates a gradient in the surfactant along the surface and a counterflow, known as the *Marangoni effect*, develops along the droplet surfaces to equalize the surfactant distribution along the surface. The liquid close to the droplet surface is dragged along into the gap thereby effectively causing a repulsion between the droplets (3).

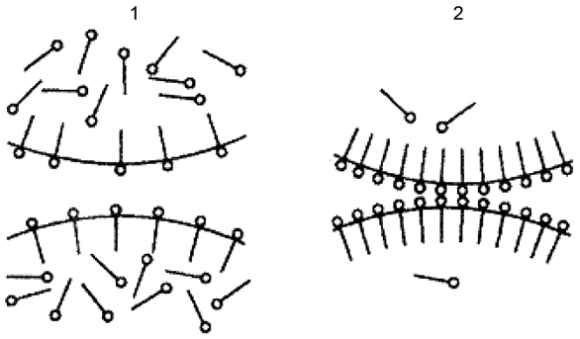

Figure 6.8 Schematic illustration of the ineffectivity of recoalescence prevention when the surfactant is in the dispersed phase.

When the surfactant is not dispersed in the continuous phase but in the dispersed phase, the above described mechanism does not work as is schematically depicted in figure 6.8. In that case, there does develop a gradient in the surface loading but it is replenished from inside the droplets without causing a significant Marangoni effect.

6.3.2 Bancroft's rule

The fact that the stabilization against recoalescence is only available in dispersions with an excess surfactant in the continuous phase leads to Bancroft's rule that states that stable emulsions can only be formed when the surfactant is preferentially in the continuous phase. The Hydrophile-Lipophile-Balance (HLB) is a number, tabulated for many surfactant molecules, that specifies this preference. Values between 3 and 6 refer to surfactants that preferentially form micelles in the oil phase and values between 8 and 18 in the water phase.

A more reliable method is the determination of the partition coefficient of a surfactant for a particular system of immiscible liquids. The experiment is relatively easy performed and yields exactly the information that is required for the combination of the two immiscible liquids and the surfactant. For water/oil systems, Schott's correlation can often be used which relates the partioning coefficient $K_{w/o}$ to the solubility δ_o of the surfactant in the oil,

$$K_{w/o} = -30.92 + 2.429\delta_o$$

The determination of a partitioning coefficient can be tricky, especially for commercial surfactants which tend not to be too pure, see figure 6.9. Only for extremely low con-

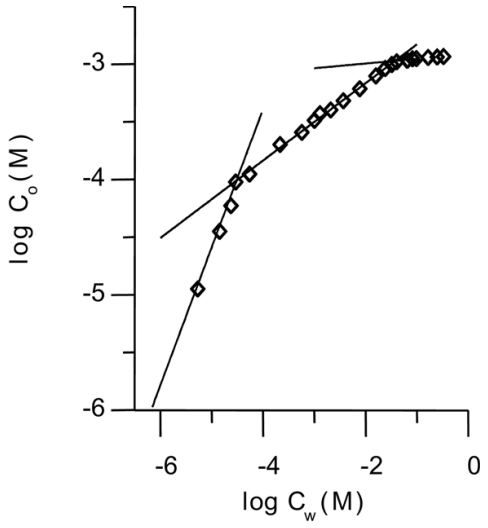

Figure 6.9 Determination of the partioning coefficient for a commercial surfactant.

centrations the correct slope is achieved that yields the prevailing partitioning coefficient. The intermediate "slope" is merely due to a distribution in tail lengths of the surfactant at hand.

Chapter 7

Adsorption and film formation from suspensions

Adsorption or deposition of particles from colloidal suspensions is used to form particulate films that upon aging cure into a homogeneous film. The most common application is latex paints. Since the ban on organic solvents for professional and household paints, the development of new paint formulations introduced more suspension paints that upon application first form a particulate film that is subsequently cured.

7.1 Adsorption

There are various models available to describe adsorption. Below we describe two that are based on relatively straightforward assumptions. There are, however, many more involved models available in the literature.

7.1.1 Langmuir equation

The simplest way to describe adsorption is by means of the Langmuir equation. It involves an adsorption term and a desorption term and hence should be used for reversible situations. One version of the Langmuir equation is

$$\frac{d\Gamma}{dt} = k_a c - k_d \Gamma \tag{7.1}$$

with Γ the adsorption, c the bulk concentration and k_a and k_d the adsorption and desorption rate coefficients respectively. However, there are more involved equations that take saturation of the adsorption collector into account. A characteristic aspect of the Langmuir adsorption equation is that it does not include interactions between adsorbed particles.

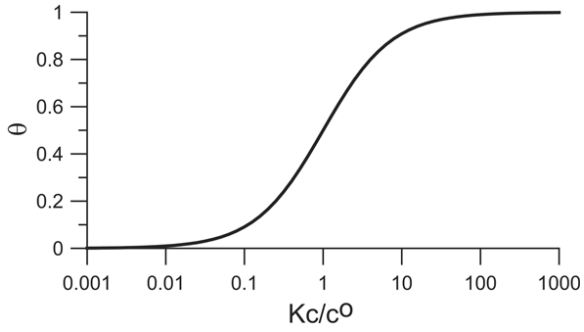

Figure 7.1 Langmuir adsorption isotherm.

The equilibrium solution of the above equation renders the *Langmuir adsorption isotherm* that we here give in terms of the surface coverage θ which is defined as the occupied surface area over the total available surface area. It reads

$$\theta = \frac{Kc/c^{\ominus}}{1+Kc/c^{\ominus}} \tag{7.2}$$

in which $c^{\ominus}$ is the standard concentration. The canonical graph of the Langmuir adsorption isotherm is depicted in figure 7.1. For relatively low concentrations, the surface coverage varies linearly with concentration and for very high concentrations the surface coverage saturates to 1. Exactly for $Kc/c^{\ominus} = 1$ the surface coverage equals $\theta = 1/2$ which also marks the region where the surface coverage varies most steeply with concentration.

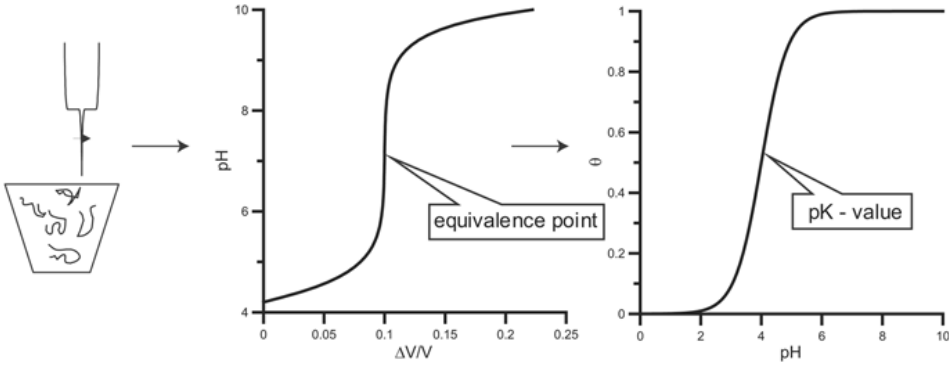

Figure 7.2 The Henderson-Hasselbalch equation and potentiometric titration.

The Langmuir isotherm comes in many guises. The alternative form is the Henderson-Hasselbalch equation for potentiometric titration, see figure 7.2. This equation comes in

two forms

$$\theta = \frac{1}{1+10^{-pH+pK}} \tag{7.3}$$

where θ is the degree of protonation and with $pK = \log K$ and

$$10^{-pH+pK} = \frac{\theta}{1-\theta} \tag{7.4}$$

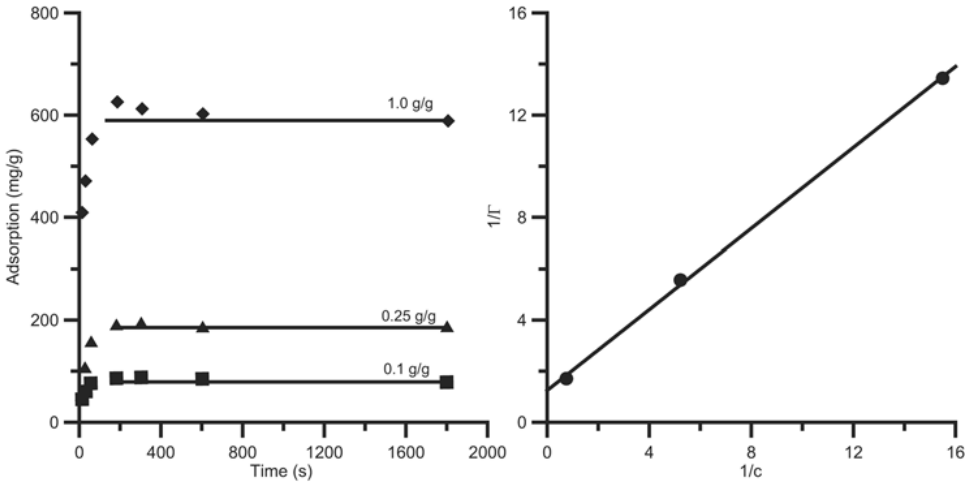

Figure 7.3 Adsorption of calcium carbonate particles on pulp fibers.

An example of the application of the Langmuir isotherm is given in figure 7.3 where the calcium carbonate particle loading of pulp fibers is given versus the bulk concentration[1]. On the right side the Lineweaver-Burk plot or double reciprocal plot is given of the stationary values of the adsorption. From the slope and the Y-axis cut-off value one obtains the equilibrium constant and the maximum adsorption.

7.1.2 Brunauer-Emmett-Teller (BET) model

A trivial extension of the Langmuir model that still does not take interactions with neighboring adsorbed particles into account is the BET-model. In principle, the model allows for multiple adsorption layers to be formed but in a very primitive way. It could well be called the random pile model as it allows each site to be loaded with 0, 1, 2, or more particles independent of its neighbors. But this simplicity makes the model analytically tractable and that is why it is so popular. It is often used in gas adsorption studies to find the monolayer coverage of an arbitrary surface. It is not of practical use to particle deposition. More information on this model can be obtained from standard physical chemistry textbooks.

[1] See J Pulp Paper Sci. 25 (1999) 81-83.

7.1.3 Frumkin-Fowler-Guggenheim model

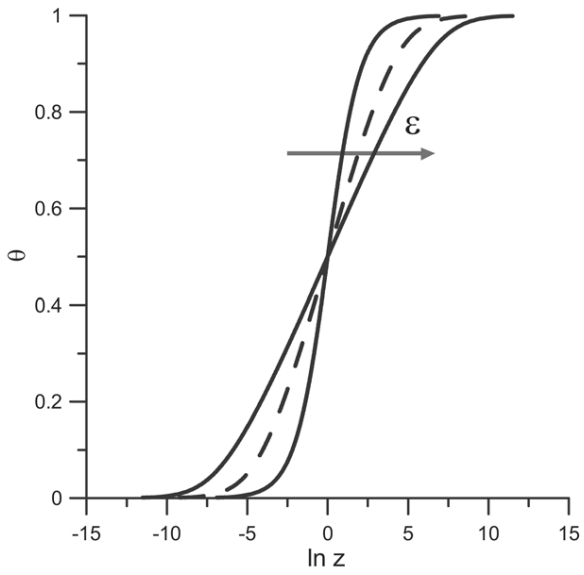

Figure 7.4 Example of a Frumkin-Fowler-Guggenheim isotherm.

The main drawback of the Langmuir model is the total neglect of interactions between adsorbed particles. An exact treatment of these interactions is not feasible, but a mean-field approximation is possible. The isotherm is described by

$$z = \frac{\theta}{1-\theta} 10^{\theta \varepsilon c} \tag{7.5}$$

in which z is the fugacity of the bulk solution that varies roughly proportional to the concentration. The mean field pair interaction energy E is given by the scaled parameter $\varepsilon = E/kT \ln 10$. When $\varepsilon = 0$ one recovers the Langmuir isotherm. For positive values of the pair interaction parameter the isotherm flattens and for negative values it becomes steeper. For too negative values, phase separation occurs.

7.2 Irreversible adsorption

So far, reversibility has been assumed which means that both adsorption and desorption take place on experimental time scales. When desorption does not take place at comparable time scales as adsorption, the behavior is categorized as irreversible. In figure 7.5 a cartoon is made of the two extreme situations. On the left side, the reversible case is depicted. When the bulk concentration over the surface is changed, the surface coverage follows within a reasonable time. On the right side, the irreversible case is shown where a decrease in bulk concentration does not lead to any change in surface coverage.

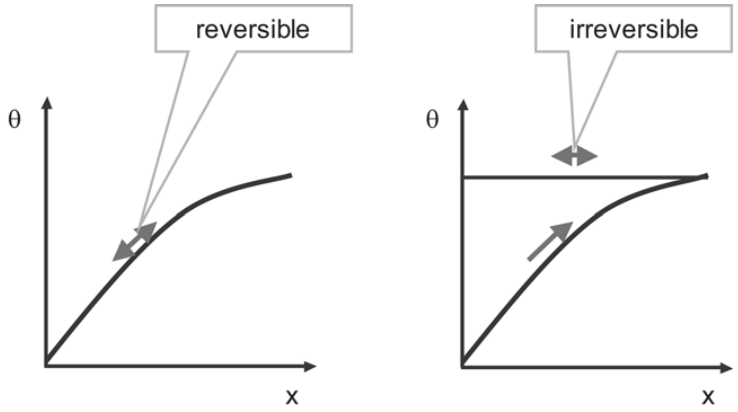

Figure 7.5 Reversibility and irreversibility.

In comparison to molecules, the binding forces of particles to a surface can be quite significant so that desorption is typically a slow process. This implies that in the case of particle adsorption, the behavior is largely irreversible which renders the above isotherms useless. Nevertheless, these models are often used to describe the data in the absence of better candidates. The fact that the models were originally conceived for reversible adsorption plays no role.

In that respect one has to be careful with the usage of the word *isotherm*. Indeed, the adsorption processes are often performed at constant temperature so that from that point of view the word is appropriate. However, the implied assumption of equilibrium is incorrect: most if not all of the times the adsorption is irreversible.

7.2.1 Random Sequential Adsorption model

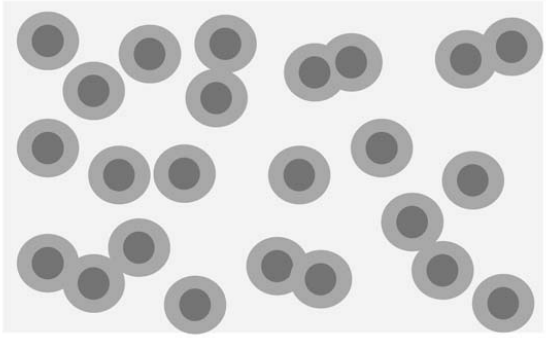

Figure 7.6 RSA configuation of soft spheres.

One of the most popular models to discuss irreversible adsorption is the Random Sequential Adsorption (RSA)-model of Jens Feder[2]. It is usually defined by its rules as if it were a game

- Particles are deposited sequentially,
- the first step of an adsorption trial consists in choosing an adsorption site,
- if the position of the incoming particle does not overlap with an adsorbed particle, it is irreversibly fixed.

For hard spheres this is all there is to define and statistical analysis can be used to obtain the theoretical predictions. Various quantities can be calculated of which the *jamming limit* is the most frequently used. For RSA the jamming limit is found to be $\theta_\infty = 0.547$. It is important to note, that the particle configurations that are obtained by the RSA model are in no way identical to the corresponding equilibrium situation.

Many variations on the RSA model are devised but the one for socalled *soft* particles is important here. The softness arises from the charged surface and the finite ionic strength. This can be modeled[3] by enlarging the particles to a radius that can be calculated from the surface charge and the ionic strength. Some overlap within the soft sphere is possible; a typical configuration is shown in figure 7.6.

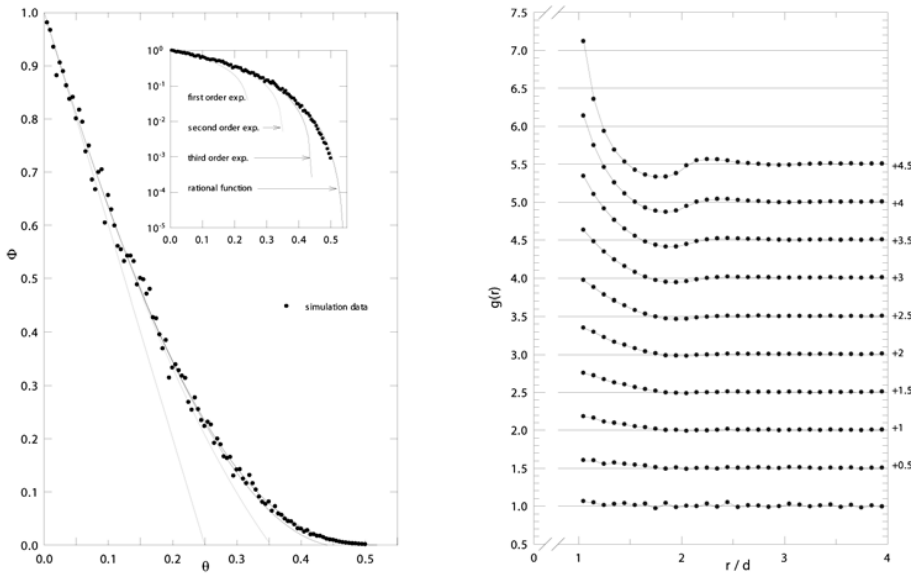

Figure 7.7 Available surface function and pair correlation function for RSA. The pair correlation function (right panel) is given for coverages from0 to 0.5 in steps of 0.05 .

[2] See J. Feder, I. Giaever, J. Colloid Interf. Sci. 78 (1980) 144.

[3] See Adamczyk, Z., and Warszynski, P., Adv. Colloid Interface Sci. 63 (1996) 41.

The probability with which a particle can be deposited on a surface depends on the amount of surface that is accessible to the depositing particle. This can be calculated to some extend analytically and furthermore can be evaluated by numerical simulations. The *available surface function* $\Phi(\theta)$ gives the fraction of available surface as a function of surface coverage θ. In figure 7.7 a graph is given of this function[4]. Another quantity that is available for numerical simulation as well as for analytical evaluation is the *pair correlation function* $g(r)$. It is the conditional probability of finding a position a distance r away from another particle. Clearly, the size of the particle is important for the evaluation of the pair correlation function and in figure 7.7 it is shown how this function behaves as a function of the relative distance r/d with d particle diameter. At low surface coverage the pair correlation function does not show any structure, but at high values there is and there is clear depletion next to the a particle and a slight excess a little further away. This implies that the organization of the adsorbed particles is far from crystalline which is another signal that the obtained structures are not equilibrium structures.

So far, experimental verification of the above results is hard to attain. Larger particle deposition can be studied by light microscopy but then the particles are usually too heavy to have purely random deposition. Other non-invasive microscopic techniques require excessive handling of the samples which always changes the structure to a certain extend. For practical purposes, the RSA-model yields quite useful results such as the jamming limit and the information on the structure of the adsorbed layer.

7.3 Adsorption kinetics

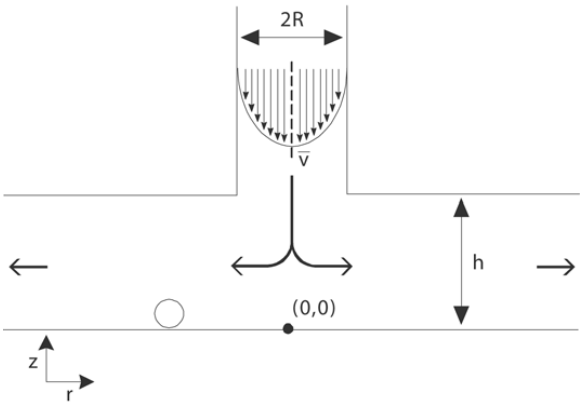

Figure 7.8 Stagnation point flow geometry.

Flow patterns in the neighborhood of a collector can be decomposed into two contributions. The one is parallel laminar flow as occurs between two parallel plates. The other

[4]See also Schaaf P, Voegel JC, Senger B Annales de Physique 23(6) 1998.

is *stagnation point flow*. In figure 7.8, an experimental set-up is sketched to study particle adsorption in stagnation point flow. The suspension is guided towards the collector surface by means of a tube of radius R in which the flow is laminar. The flow lines will be radially symmetric around the axis of the inlet tube that crosses the collector plane in $(0,0)$. There is no flow exactly in the stagnation point, but there is beyond.

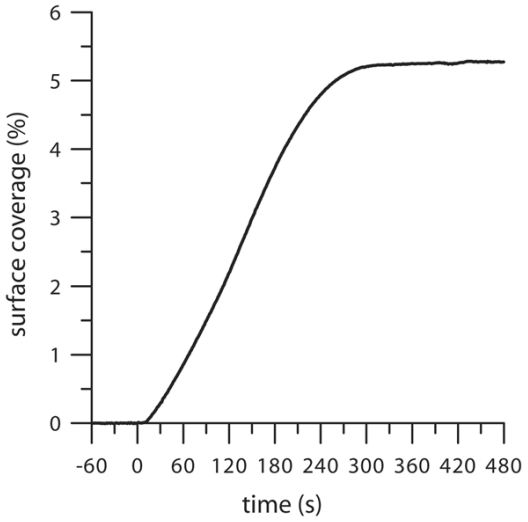

Figure 7.9 Typical adsorption kinetics experiment.

The mobility of particles in the close neighborhood of a surface differs from the mobility in the continuum fluid. Also, when particles approach a collector surface there are specific particle-surface interactions. One in particular is omnipresent: the Van der Waals interaction. These two complications render an analysis of the adsorption process in the neighborhood of collector surfaces complicated. Levich has circumvented the problem by assuming that the mobility near collector surfaces is unperturbed and that when a particle arrives at the surface it is adsorbed[5]. Within this so called *Levich approximation* the initial adsorption rate is given by

$$\left.\frac{d\Gamma}{dt}\right|_{t=0} = kc_b \tag{7.6}$$

with

$$k = 0.776(\nu D^2 \alpha \mathrm{Re})^{1/3} R \tag{7.7}$$

where ν is the kinematic viscosity of the dispersion, D the diffusion coefficient of the particles, α a flow parameter that is to be calculated for the specific geometry , and c_b the concentration of the dispersion. A typical example is given in figure 7.9. The adsorption rate remains surprisingly constant up to the saturation level, this is almost always the case.

[5]See See T.G.M. van de Ven, *Colloidal Hydrodynamics*, Academic Press 1989.

One often finds, that the saturation level is not really constant but that a slight increase with time persists.

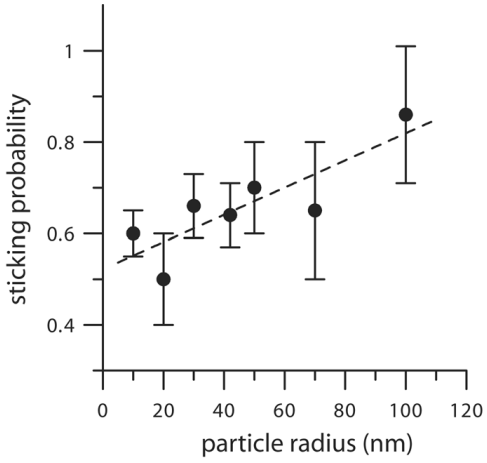

Figure 7.10 The sticking probability for particle adsorption onto a heterogeneous surface.

Despite the encouraging result that the linearity of equation 7.6 is almost always found, the proportionality constant often deviates from the predicted value. As an example see figure 7.10 where the *sticking probability*, which effectively is the ratio between the observed adsorption rate and the product kc_b, is plotted versus particle radius for a surface that has been rendered heterogeneous by means of pre-adsorbed dendrimers[6].

7.4 Film formation from suspensions

7.4.1 Particulate suspensions

Following the application of a particulate suspension onto a surface, a few processes take place depending on the particle properties. When the particles are relatively "hard", i.e. when the internal viscosity is very high, the process can be described as particle deposition. An example is the film formation by latex paint particles which actually largely consists of polymer particles and filler particles. After application, the particles adsorb onto the surface and at the same time the solvent, usually water, evaporates. After some time a close packed particle layer is formed over the surface and inbetween there is solvent. When the temperature is above the *minimum film formation temperature* (MFT) the particles will deform under the action of the capillary pressure to allow more water to evaporate. Then, the solvent film between the particles becomes small enough to rupture and more solvent disappears from the film. When the temperature is above the *glass temperature* T_g of the polymer and the polymer chains interpenetrate to form a homogeneous

[6] See R.C. van Duivenbode en G.J.M. Koper, J Phys Chem B 105 (2001) 11729-11736.

film. Depending on circumstances, the final drying of the film can be so fast, that solvent gets entrapped in the film. In the case of water, this makes the film very sensitive to temperature variations.

7.4.2 Emulsions

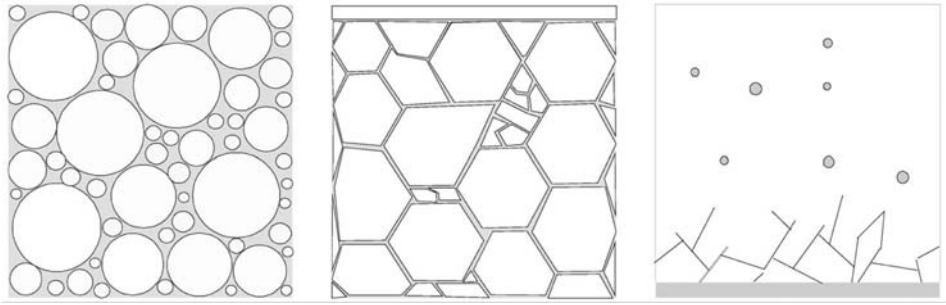

Figure 7.11 Schematic representation of the film formation process. The left figure represents the initial emulsion, the middle figure represents the bi-liquid foam with oily skin and the right figure represents the final stage where the (o/w) emulsion inverts into a (w/o) emulsion.

When the viscosity of the particles is relatively low, such as for alkyd emulsion paints, one actually has an emulsion that after evaporation of the larger portion of the continuous phase inverts. After inversion the film is alkyd continuous with entrapped water pockets. The alkyd chains cross link by means of an oxidation reaction and in this way a homogeneous film is formed. Also here, film formation may be so rapid that water gets entrapped in the film.

The film formation process typically involves three regimes, see figure 7.11[7]. Immediately after application, there is fast evaporation of "free water", where the initially already dense emulsion is further drained of water until a *bi-liquid foam* is formed. The kinetics is determined by the rate at which water evaporates. In this regime, the surfactant/water/surfactant membranes between the oil droplets gradually become thinner and the initially whitish film becomes transparent. Due to the water gradient, this manifests itself as a front propagating through the film from the top to the bottom. This regime ends when the membranes at the top of the film are drained so much that the oil droplets coalesce and an oil layer is formed on top of the film. This oil layer limits further water evaporation significantly. In the second regime, drainage of the thin membranes between the oil droplets occurs. The draining water diffuses through the oily top layer and evaporates from the top of the film. The transport of the drainage water to the top of the film is now rate limiting and mass loss is linear in time, which can be explained by water diffusion through a growing interfacial barrier layer. Also because of this, the water gradient in

[7] See F. Bouchama *et al*, Colloids and Surfaces A 210 (2002) 129-135.

the film is very small and the bi-liquid foam dehydrates almost homogeneously. The third drying regime starts when the bi-liquid foam ruptures. This is the actual phase inversion that takes place when most of the water has evaporated. The remaining water and surfactant is turned into micelles so that the remaining structure is a water-in-oil emulsion. If the water droplets are very small, the resulting structure might actually be a microemulsion which is thermodynamically stable. In the situation where density fluctuations are rather long-lived, which is probably the case in dense emulsions the phase inversion results in islands of hydrophilic material. The rate at which this rupture and concurrent coalescence of the droplets can take place depends on the micellization rate of the forming water-in-oil emulsion. There is virtually no water evaporation taking place in this regime.

Chapter 8

Flotation

Flotation is a separation process. Gas is blown through a suspension from which valuable or waste components specifically bind to gas bubbles. The attachment of particles to the gas bubbles results in aggregates of lower density than the suspension, which rise to the suspension surface. There the particles can be collected. The separation takes place according to density differences, but the characteristic of this separation process is the different abilities of various particle kinds to attach to the bubble surface.

8.1 Flotation Conditions

Figure 8.1 Two-step procedure to find the work of attachment of a colloidal particle to a gas bubble.

Energy is needed for the bubble-particle attachment. The attachment energy required to build a particle-bubble aggregate can be calculated distinguishing two attachment steps, see figure 8.1. In the first step, energy is needed to deform the bubble in order to make attachment of the particle possible. A single bubble has a spherical surface, which is the lowest energy state of the bubble. When the particle encounters the bubble, the bubble slightly deforms which results in a larger surface area and hence in an increase in surface energy. In the second step, part of the liquid-vapor and liquid-solid interfaces are replaced by solid-vapor interface. The above reasoning can be summarized as

$$W_{\text{attachment}} = W_{\text{deformation}} + \gamma_{SV} - \gamma_{SL} - \gamma_{LV}$$

For flotation to occur, the bubble-particle aggregate must be stable. In other words the energy gain of the detachment process must be high enough and must not be overcome by external forces. This leads to the following relation:

$$W_{\text{deformation}} + \gamma_{SV} - \gamma_{SL} - \gamma_{LV} + W_{\text{detachment}} < 0$$

The work done by attachment is negative, it should lead to a decrease in energy. Both the detachment work and the work of deformation are positive. This leads to the condition

$$\gamma_{SV} - \gamma_{SL} - \gamma_{LV} < 0$$

which states that for flotation to occur the surface tension of the solid-vapor interface is to be smaller than the sum of surface tensions of the solid-liquid and liquid-vapor interfaces. Using Young's equation, that relates the mentioned surface tensions in terms of a contact angle θ, see eq. 2.13, the *Zisman condition* for flotation can be formulated as

$$\gamma_{LV}(\cos\theta - 1) < 0 \tag{8.1}$$

This negative work of attachment depends on the contact angle, as can be seen from Zisman's condition: if the contact angle increases, the work needed for attachment increases too. At a vanishing contact angle, which means that complete wetting takes place, flotation cannot occur. In the graph 8.2 a summary of Zisman's experiments is shown involving

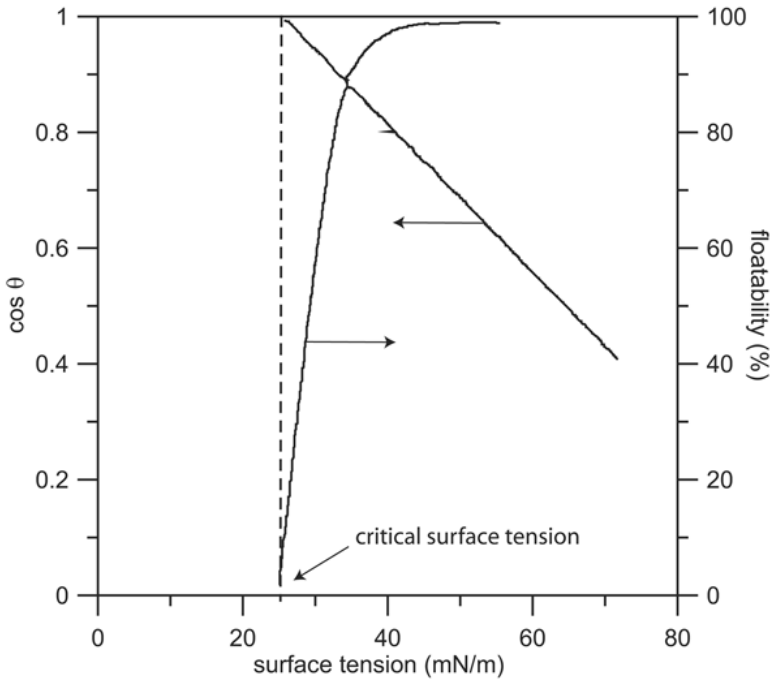

Figure 8.2 Summary of Zisman's experimental work on flotation in relation to surface tension.

floatability, contact angle and surface tension of various liquids. It demonstrates that the contact angle always decreases with decreasing liquid-vapor surface tension. Surfactants

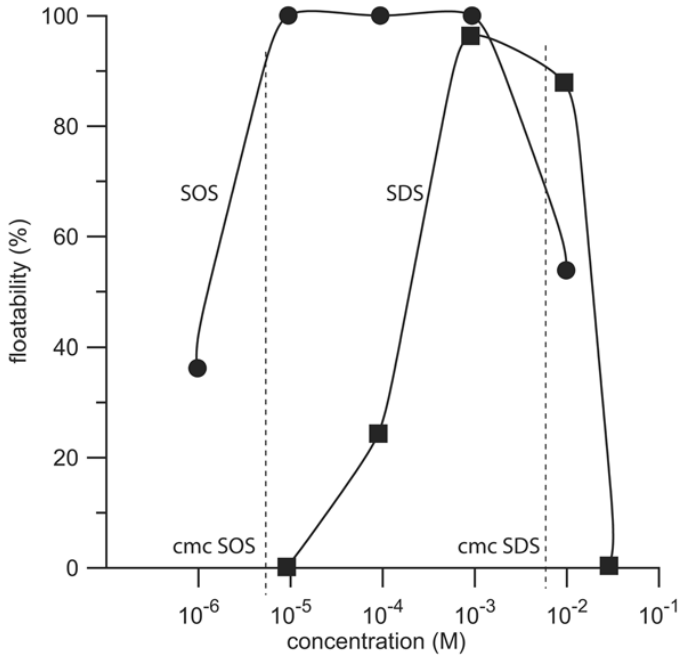

Figure 8.3 Effect of surfactant concentration on floatability of aluminum oxide on water. Surfactants are sodium dodecyl sulfate (SDS) and sodium octadecyl sulfate (SOS).

can be used to manipulate the surface tensions of the liquid-solid and the liquid-vapor interfaces in order to modify the contact angle. Then, the surfactant concentration can be used as a control on floatability. As an example the floatability of aluminum oxide in water is measured as a function of surfactant concentration. The results are depicted in figure 8.3 which demonstrates a competition between floatability and stability. At low surfactant concentration both the particle and the bubble surfaces are sparsely loaded with surfactant and the surfactant facilitates floatability. At very high surfactant concentrations both the particle and the bubble surfaces are saturated and there is maximum stability against particle-bubble aggregation so that there is no floatability. In between these two extremes is optimal floatability, this is when the surface tension is lowered by the adsorbed surfactant thereby minimizing the attachment energy but not loaded too much to prevent aggregation.

As in the case of emulsification, dynamical aspects may influence the behavior and things may be different on different timescales. The diffusivity of the surfactant molecules plays a dominant role there.

8.2 Flotation recovery

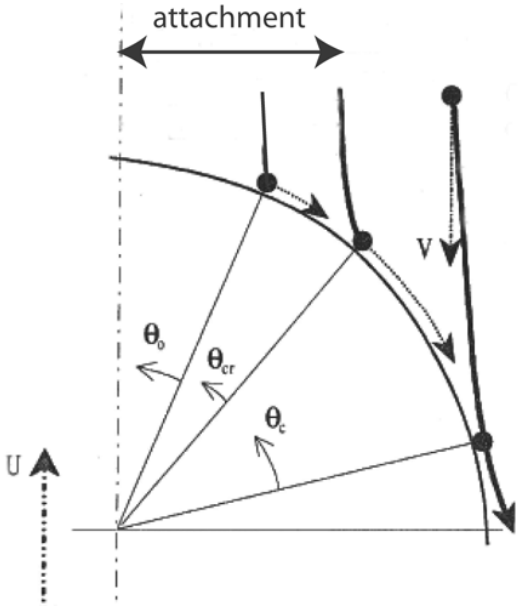

Figure 8.4 Analysis of bubble-particle interaction during flow.

Liquid flow around a bubble has an important effect on the bubble-particle interaction. Particles follow their trajectory around the bubble, can collide, attach or be pushed away from the bubble again, see figure 8.4. A maximum angle exists, the collision angle θ_c, beyond which no collision takes place: the particles are pushed away from the surface of the gas bubble by the liquid. Below this collision angle, the particles collide with the gas bubble, but do not necessarily become attached to the bubble. Another angle exists, the critical attachment angle θ_{cr} which is smaller than the collision angle, below which the particles collide and attach to the gas bubble and beyond which the particles collide with the gas bubble, slide along the surface and move away again. Due to the liquid flow only a small fraction of the particles are able to attach to the gas bubble. In addition, a minimum sliding time exist which is needed for the particles to attach. The angle which corresponds to this minimal sliding time is represented by θ_0 in the figure.

8.2.1 Probability of collision

The probability of a bubble-particle collision depends on the size of the particle d_p and the size of the gas bubble d_b and also on the liquid flow conditions[1]. Theoretical calculations for some well-defined flow types, Stokes or laminar flow and potential flow, yield the

[1] See R.-H Yoon, Int. J. Mineral. Proc. 58 (2000) 129-143.

following relation for the collision probability

$$P_c = A\left(\frac{d_p}{d_b}\right)^n \tag{8.2}$$

where the coefficients A and n are given in table 8.1. The condition for using the tab-

Flow type	Reynolds number	A	n
Stokes	$0 < \mathrm{Re} < 300$	3/2	2
Intermediate	$300 < \mathrm{Re} < 10^4 \cdots 10^5$	$\frac{3}{2}\left[1+\frac{(3/16)(\mathrm{Re}-300)}{1+0.249\mathrm{Re}^{0.56}}\right]$	2
Potential	$10^5 < \mathrm{Re}$	3	1

Table 8.1 Parameters acting in the collision probability eq. 8.2

ulated values for A and n is that the flow around the bubble is symmetric. In practice flow around bubbles is always asymmetric, but the values will give an indication of the collision probability.

8.2.2 Probability of attachment

Bubble-particle attachment depends largely on the hydrophobicity of particles, which means the ability of particles to adhere to the surface of the bubble. When the particles are sufficiently hydrophobic to attach to the surface, there is also still the possibility of particle to collide with the bubble surface and slide along the surface away from the bubble again.

The probability of attachment – the probability that particles collides with the bubble, slides along its surface and attaches – depends on the induction time and the sliding time of the particle, i.e.

$$P_c = \frac{t_{\text{induction}}}{t_{\text{sliding, min}}} \tag{8.3}$$

The induction time is the minimum time needed to thin and disrupt the liquid film between bubble and particle. The minimum sliding time is the minimum contact time of particles sliding along the surface of a gas bubble. The probability of attachment thus depends on the induction time compared to the time in which particles minimally slide along the surface before actually attaching. Logically if the induction time is greater than the sliding time, particles will never be able to attach to the bubble surface.

8.2.3 Flotation recovery

Probabilities of collision and attachment are important quantities to determine the collection efficiency of a flotation process. The quantity describing the efficiency of the process is called flotation recovery and is denoted by R. Flotation recovery is defined as the number of particles collected by the gas bubble divided by the number of particles in

the slurry passing by the bubble. It is a quantification of the efficiency of the flotation process. Flotation recovery is defined as

$$R = \frac{N_c}{\frac{\pi}{4}(d_p + d_b)^2 H c_p} \tag{8.4}$$

in which d_p and d_b are diameters of the particle and the bubble respectively, c_p is the particle concentration, H is a given height within which the flotation recovery is calculated. N_c is the amount of collected particles during the traversal of the distance H. It can be calculated by multiplying the probability of a particle being collected with the number of possible particle collisions

$$N_c = PN_{ci}$$

The probability of particle collection by a bubble is dependent on the probabilities of bubble-particle collision P_c, adhesion P_a, and attachment efficiency $1 - P_d$ in which P_d is the detachment probability, as

$$P = P_c P_a (1 - P_d)$$

The number of possible collisions, which is the ideal maximum number of collected particles depends on the diameters of bubble and droplet, and also on the rising velocity of the bubble u and the particle setting velocity v as

$$N_{ci} = \frac{\pi}{4}(d_p + d_b)^2 (u + v) c_p$$

in which c_p is the concentration of particles in solution. After some algebra, which is worked out in detail by Yoon[1] the following expression for flotation recovery is found

$$R = P_c P_a (1 - P_d) \left(1 + \frac{u}{v}\right) \tag{8.5}$$

8.3 Flotation micro-processes

If a particle indeed becomes attached to a bubble, a series of steps takes place from the first particle-bubble contact until final attachment. These "micro-processes" can be summarized as follows

1. Thinning of the intervening liquid film on the bubble surface
2. Rupture of the liquid film
3. Formation of a three phase contact line and attachment

These processes will be discussed in the following subsections.

8.3.1 Thinning of liquid film

Flotation can only take place when the thin liquid film between particle and bubble is unstable. If both particle and bubble have charges of the same sign, the layers are stable. A reverse charge can be created by selective adsorption of surfactant at either the surface of the particle or bubble.

When the two interfaces of particle and bubble approach one another, two forces play a role in a possible liquid film thinning process. On the one hand the electrostatic double layer force is repulsive and becomes stronger as the distance between particle and bubble decreases. On the other hand there is the omnipresent Van der Waals force between particle and bubble, which gives rise to attraction. Superposition of the electrostatic repulsive

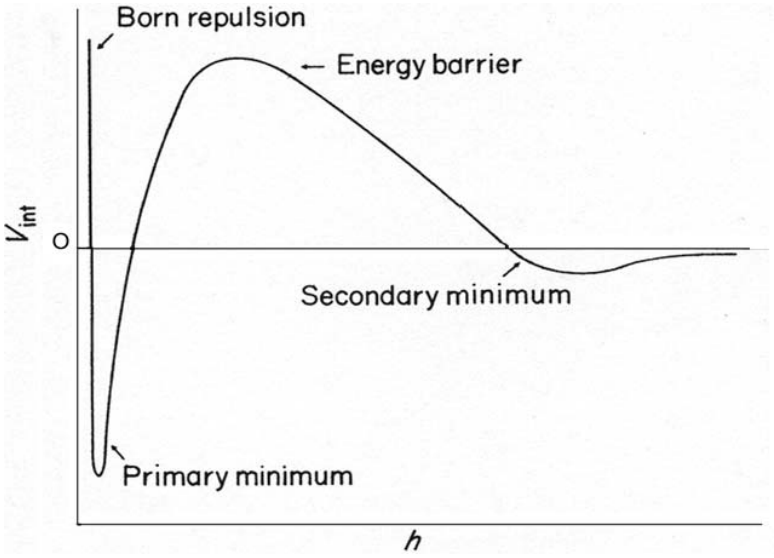

Figure 8.5 Sketch of interaction energy between charged surfaces.

forces and the Van der Waals attraction leads to an energy-distance function as sketched in figure 8.5 (this graph is very much the same as figure 4.6). The function shows an energy barrier, a primary and a secondary energy minimum. Particles which have enough kinetic energy to overcome the energy barrier, can attach to the bubble in the primary energy minimum. Fine particles may not have enough kinetic energy and can then be stabilized at the bubble in the secondary energy minimum.

8.3.2 Rupture of liquid film

Unstable films can rupture spontaneously at a certain critical thickness. The rupture mechanism is described by Kaišev's theory[2]. It assumes that a thinning film which thins by an

[2]D. Kaišev and D. Exerowa, J. Colloid Interf. Sci. 77 (1980) 501

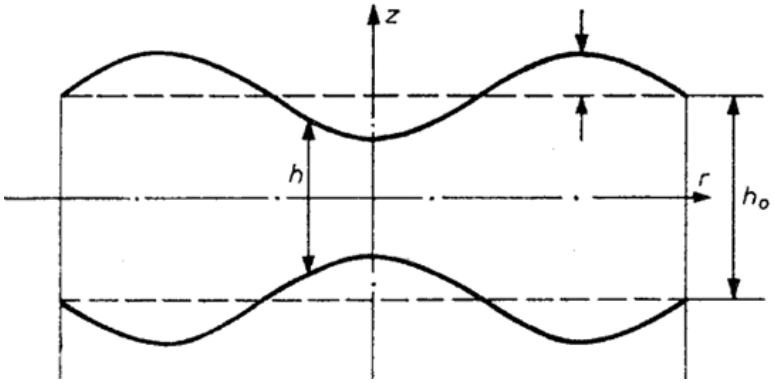

Figure 8.6 Undulations in a thinning film.

external driving force — gravitational or capillary — undergoes surface fluctuations; the film thickness varies wave-like. The amplitudes of these surface waves gradually increase under the influence of the interaction forces between particle and bubble. If the particle and bubble approach each other, the amplitudes of their fluctuations become higher. They keep on growing until the amplitude of one film is large enough to touch the other film and a hole is formed at this point. The film is then immediately destroyed. The thickness at which the film is destroyed is defined as the critical film thickness.

The hydrodynamic theory of Kaišev is extended by Ivanov et al.[3] and includes a theory about the process of drainage of the liquid film. The drainage process consists of two parallel processes which superimpose each other: the efflux of liquid flowing out of the film and the flow of liquid within the film, caused by the film fluctuations and growing amplitudes. The rate of decrease in thickness during drainage thus consists of two velocities: the film velocity and the wave velocity.

8.3.3 Formation of three phase contact line

The primary hole formed by the touching of the different waves is the first three-phase contact and work for its creation is provided by the kinetic energy of the particles. This amount of work can be seen as the minimal energy needed for flotation to occur. It is needed to remove the molecules of the boundary layers in order to create the first three-phase-contact.

The three-phase-contact line which is formed after attachment of the particle to the bubble gives rise to the formation free energy. The formation free energy per unit length of contact line is the "line tension"

$$\kappa = \left(\frac{\partial F}{\partial L}\right)_{T,V,A}$$

[3]I.B. Ivanov *et al* Trans. Faraday Soc. 569 (1970) 66.

It has typically a value of the order of 10^{-10} J/m. With this, the change in surface excess free energy, dF, can be described as

$$dF = \gamma_{SV} dA_{SV} - \gamma_{LV} dA_{LV} - \gamma_{SL} dA_{SL} + \kappa dL \tag{8.6}$$

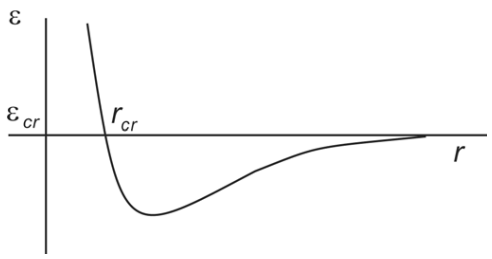

Figure 8.7 Capillary force at contact line.

A solid-vapor surface is formed whereas a liquid-vapor and solid-liquid surface are removed and a three phase contact line is formed. The capillary force at this line is

$$\varepsilon = -\gamma_{LV}(\cos\theta_r - \cos\theta_0) + \frac{\kappa}{r}\sqrt{1-\left(\frac{2r}{d_p}\right)^2} \tag{8.7}$$

and a sketch is given in figure 8.7.

This equation is arrived at from equation 8.6 by taking the derivative versus area as

$$\varepsilon = \frac{d\Delta F}{dA} = \gamma_{SV} - \gamma_{SL} - \gamma_{LV}\cos\theta + \kappa\frac{dL}{dA}$$

By realising that $dL = 2\pi dr$ and $dA = 2\pi r dr\cos\alpha$, see figure 8.7, the following relation is obtained

$$\varepsilon = \gamma_{SV} - \gamma_{SL} - \gamma_{LV}\cos\theta + \frac{\kappa}{r}\cos\alpha$$

in which r represents the instantaneous radius obtained when a three-phase-contact is formed. Using Young's equation

$$\gamma_{LV}\cos\theta = \gamma_{SV} - \gamma_{SL}$$

and the geometrical relation (see figure 8.7)

$$\cos\alpha = \sqrt{1-\left(\frac{2r}{d_p}\right)^2}$$

we obtain equation 8.7.

For the contact angle one may use the *dynamical contact angle* which is experimentally found to be different from the equilibrium contact angle and varying with contact line motion. The contact angle θ changes with the instantaneous radius r. When r becomes very small, the capillary force becomes indefinitely large. Therefore a certain radius r_{cr} is needed to make three-phase contact line expansion possible. This radius r_{cr} is called the critical radius with the critical amount of energy. This means that there is a minimal pore opening needed to give rise to three phase contact line expansion.

8.3.4 Detachment

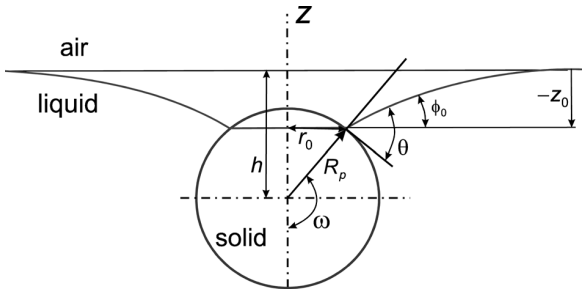

Figure 8.8 Geometry of particle attached to bubble.

When a particle is attached to a bubble, different forces are acting on the particle, see figure 8.8. They are balanced by the buoyancy of the displaced, surrounding liquid. The forces which are acting on the particle are the gravity force, the capillary force in the bubble on the three-phase-contact area, the capillary force outside bubble on the three-phase-contact, the hydrostatic pressure of the liquid column on the contact area and possible additional hydrodynamic forces, due to the motion and mass of the particle. In figure 8.9 is an example of the force on a 1 mm particle of relative density 2.5 adsorbed at the air-water interface in the absence of additional hydrodynamic forces for various values of the contact angle. It is very clear that before detachment first a repulsive force needs to be overcome.

8.4 Example: deinking in the paper industry

In the developed countries paper recycling is common practice nowadays and one of the main processes associated with recycling is deinking. This process[4] involves two steps of which the first step is the repulping, see figure 8.10, and mixing with chemicals. The deinking chemicals are sodium hydroxide, fatty acids, detergents or soap. In addition, to prevent yellowing, hydrogen peroxide, silicates and chelating agents are added. The action of the surfactant is to wrap around the ink particle and remove it from the fiber.

[4]This description is taken from O. Drabek *et al*, J. Pulp Paper Sci. 24 (1998) 116-120.

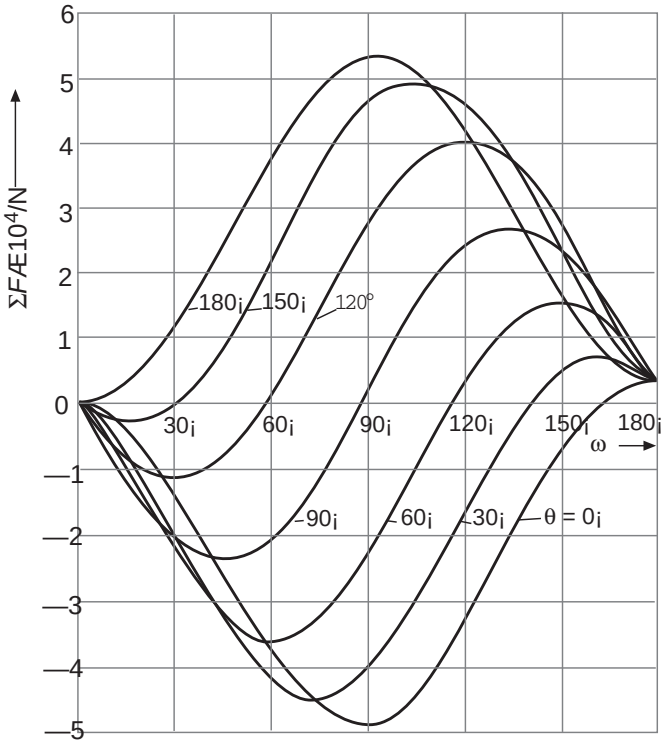

Figure 8.9 Example of force on a particle attached to a bubble as a function of its immersion.

Both the fibers and the anionic surfactant carry a negative charge and hence repel each other. This part of the process is sketched in figure 8.11.

In the repulper the fatty acids react with calcium ions to form small charged colloidal particles. Figure 8.12 shows electron microscope images where these particles have deposited on fibers. At low concentrations the calcium oleate particles remain sufficiently dispersed but at higher concentrations they become unstable because despite the charge the particles are sticky as well.

The second step of the process is the flotation where air is led through the suspension. The ink particles in themselves would be too small to adhere efficiently to the air bubbles. Due to the floc formation by means of the small charged colloidal particles this problem is overcome and the flocs attach efficiently to the air bubbles to be carried upwards and away by the froth. The main function is to flocculate the ink particles once they are released from the fibers. The disadvantage is, however, that it also advocates deposition on the fibers itself which leads to deposits as shown in figure 8.13.

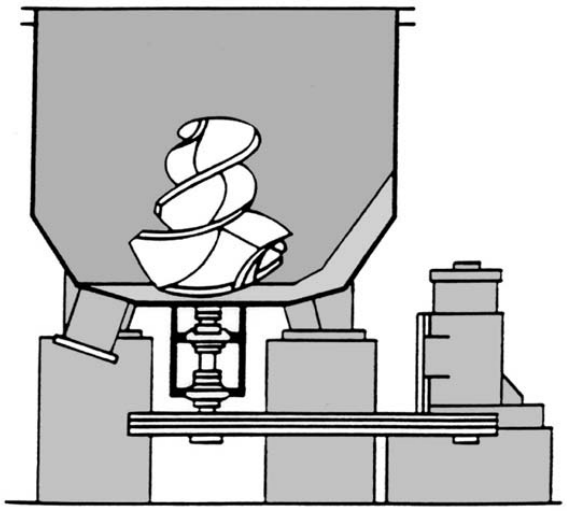

Figure 8.10 Repulper.

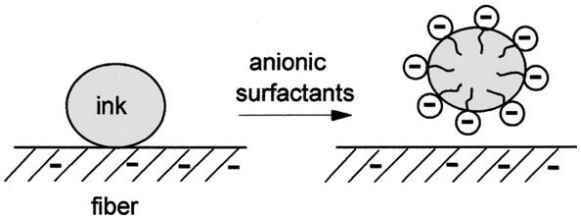

Figure 8.11 Removal of ink particles from fiber surfaces by means of anionic surfactant.

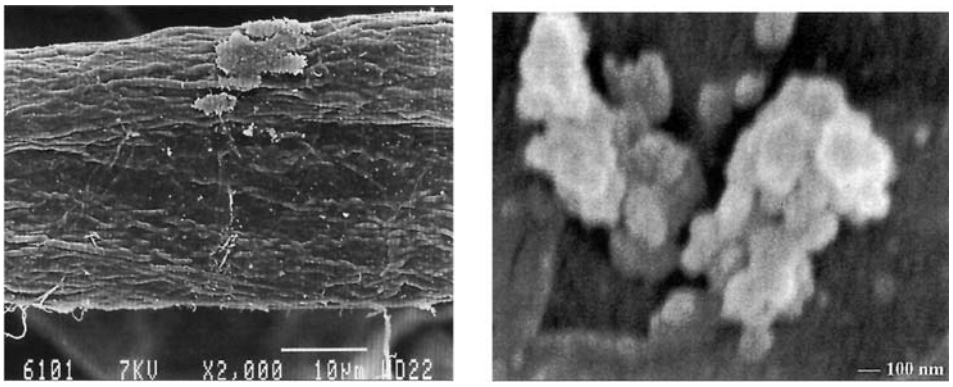

Figure 8.12 Electron microscope images of deposition of ink flocs on air bubbles.

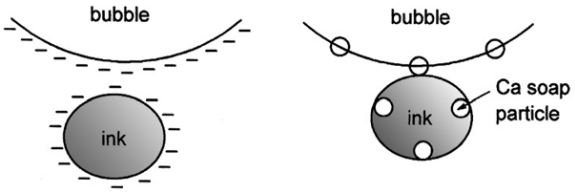

Figure 8.13 Deposition of calcium oleate on fibers.

Index